INFORMATION TO USERS

This material was produced from a microfilm copy of the original document. While the most advanced technological means to photograph and reproduce this document have been used, the quality is heavily dependent upon the quality of the original submitted.

The following explanation of techniques is provided to help you understand markings or patterns which may appear on this reproduction.

1. The sign or "target" for pages apparently lacking from the document photographed is "Missing Page(s)". If it was possible to obtain the missing page(s) or section, they are spliced into the film along with adjacent pages. This may have necessitated cutting thru an image and duplicating adjacent pages to insure you complete continuity.

2. When an image on the film is obliterated with a large round black mark, it is an indication that the photographer suspected that the copy may have moved during exposure and thus cause a blurred image. You will find a good image of the page in the adjacent frame.

3. When a map, drawing or chart, etc., was part of the material being photographed the photographer followed a definite method in "sectioning" the material. It is customary to begin photoing at the upper left hand corner of a large sheet and to continue photoing from left to right in equal sections with a small overlap. If necessary, sectioning is continued again – beginning below the first row and continuing on until complete.

4. The majority of users indicate that the textual content is of greatest value, however, a somewhat higher quality reproduction could be made from "photographs" if essential to the understanding of the dissertation. Silver prints of "photographs" may be ordered at additional charge by writing the Order Department, giving the catalog number, title, author and specific pages you wish reproduced.

5. PLEASE NOTE: Some pages may have indistinct print. Filmed as received.

Xerox University Microfilms

300 North Zeeb Road
Ann Arbor, Michigan 48106

77-26,960

OCHOA, Agustin Jr., 1949-
COMPOSITE BIPOLAR AND FIELD EFFECT CARRIER DOMAIN DEVICES.

The University of Arizona, Ph.D., 1977
Engineering, electronics and electrical

Xerox University Microfilms, Ann Arbor, Michigan 48106

COMPOSITE BIPOLAR AND FIELD EFFECT CARRIER DOMAIN DEVICES

by

Agustin Ochoa, Jr.

A Dissertation Submitted to the Faculty of the

DEPARTMENT OF ELECTRICAL ENGINEERING

In Partial Fulfillment of the Requirements
For the Degree of

DOCTOR OF PHILOSOPHY

In the Graduate College

THE UNIVERSITY OF ARIZONA

1 9 7 7

THE UNIVERSITY OF ARIZONA

GRADUATE COLLEGE

I hereby recommend that this dissertation prepared under my direction by AGUSTIN OCHOA, Jr.

entitled Composite Bipolar and Field Effect Carrier Domain Devices

be accepted as fulfilling the dissertation requirement for the degree of Doctor of Philosophy

Douglas J Hamilton — 5/27/77

Dissertation Director — Date

As members of the Final Examination Committee, we certify that we have read this dissertation and agree that it may be presented for final defense.

Douglas J Hamilton — 5/27/77

William J Harris — 5/27/77

James N. Gordenwalt — 5/27/77

Final approval and acceptance of this dissertation is contingent on the candidate's adequate performance and defense thereof at the final oral examination.

STATEMENT BY AUTHOR

This dissertation has been submitted in partial fulfillment of requirements for an advanced degree at The University of Arizona and is deposited in the University Library to be made available to borrowers under rules of the Library.

Brief quotations from this dissertation are allowable without special permission, provided that accurate acknowledgment of source is made. Requests for permission for extended quotation from or reproduction of this manuscript in whole or in part may be granted by the head of the major department or the Dean of the Graduate College when in his judgment the proposed use of the material is in the interests of scholarship. In all other instances, however, permission must be obtained from the author.

SIGNED: [signature]

ACKNOWLEDGMENTS

It is a pleasure to acknowledge some of the many people who aided and encouraged me in the preparation of this dissertation. Dr. Douglas J. Hamilton, my major professor and advisor, performed exceptionally in these roles. Major guidance was also received from Dr. Donald G. Dudley who was always available for discussions of the analysis. Mr. James A. Homoki, Laboratory Engineer, who was instrumental in the production of the device prototype described herein, and Mrs. Freida H. Long who prepared, commented on, and typed this work deserve a very grateful acknowledgment.

This dissertation would never have been attempted but for the efforts of my parents, Mr. and Mrs. Agustin M. Ochoa, and my family who all deserve to be recognized here, in particular, my brother Jesse. The cheerful support and understanding my wife, Norma, offered was deeply appreciated.

This work was supported by the Energy Research and Development Administration. The Motorola Foundation is also gratefully acknowledged for their assistance.

TABLE OF CONTENTS

		Page
LIST OF ILLUSTRATIONS		vi
LIST OF TABLES		ix
ABSTRACT		x
CHAPTER		
1	INTRODUCTION	1
2	A DISTRIBUTED MODEL FOR CDD'S	12
	Assumptions for the Distributed Model	12
	The Distributed-Kirchoff Equation	20
3	CDD BASE POTENTIAL ANALYSIS	27
	The Method of Finite Differences	27
	The Method of Green's Functions	30
	A One-Dimensional CDD	39
	Potential Distribution within the Base	43
	Summary of Methods of Analysis	46
4	CDD CHARACTERISTICS	50
	Emitter Current Density	51
	The Collector Currents	65
	The Composite Model	69
	The Two-Quadrant Multiplier	71
	A Comment on Temperature Effects	76
5	CDD APPLICATIONS	81
	A Four-Quadrant Multiplier	81
	An AGC Amplifier	85
	Spatial Effects	89
	CDD Logic	98
	Conclusions	99

TABLE OF CONTENTS (Continued)

Page

6 ANALYSIS OF GENERAL STRUCTURES 102

Definition of the Problem 102
Method of Solution of the d-KPDE 105
Summary of Analysis Procedure 117

7 SUMMARY AND CONCLUSIONS 119

Summary 119
Recommendations for Further Work 122

APPENDIX A: ANALYSIS OF TWO-REGION BASE STRUCTURE 124

APPENDIX B: NONDIMENSIONALIZING THE d-KPDE 129

APPENDIX C: DERIVATION OF GREEN'S FUNCTION 132

APPENDIX D: LISTING OF CDD BASE ANALYSIS PROGRAM 135

LIST OF REFERENCES 144

LIST OF ILLUSTRATIONS

Figure		Page
1.1	A Simple CDD Structure and Emitter Current Density Showing Domain Action	2
1.2	The Gilbert CDD Structure	4
1.3	Idealized Half Structure of Base Region of the Gilbert CDD	5
1.4	Rectangular Structure Having a Quadratic Potential Distribution	6
1.5	Three-Collector CDD Structure	9
1.6	Composite MOS Bipolar CDD Structure	10
2.1	Typical Dimensions of CDD Prototype	13
2.2	Photomicrograph of the MOS-CDD Prototype	15
2.3	Block Diagram Showing the Unilateral Dependence of the Responses of the Base, Emitter and Collector of a CDD	18
2.4	Base Morphology for Idealized CDD Prototype	21
2.5	Base Region of CDD Showing Arbitrary Region R Bounded by Surface S	22
3.1	Lumped Model for the Subregion (m,n) Defined by the Method of Finite Differences	31
3.2	Transformed Base Region in Normalized Form, Excited by an Arbitrary Source Distribution	33
3.3	One-Dimensional CDD Base Structure	41
3.4	Normalized Potential Distribution for One-Half of the Base Region of CDD Structure	44
3.5	Normalized Potential Profile Along Constant y Showing Parabolic Distribution	45

LIST OF ILLUSTRATIONS (Continued)

Figure		Page
3.6	Potential Profiles Along Constant y for Different Base End Potentials	47
3.7	Normalized Potential Maximum Location versus Normalized Base Drive Voltage	48
4.1	Normalized Emitter Current Density as a Function of Normalized Distance x/a for $\ell_o = a$	58
4.2	Normalized Emitter Current Density versus Normalized x/a for $\ell_o = a/2$	59
4.3	Normalized Emitter Current Density versus Normalized Distance x/a for $\ell_o = .2a$	60
4.4	Normalized Emitter Current Density versus Normalized Distance x/a for $\ell_o = .06a$	61
4.5	Emitter Terminal Voltage as a Function of Applied Base Voltage V_a	63
4.6	Idealized Collector Structure Used to Determine the Current Division Law for a Point Source Excitation Located at (x_o,y_o)	66
4.7	Domain Centroid Normalized by $\ell_o \sqrt{\pi}$ as a Function of the Base Potential Maxima Expressed in Units of ℓ_o . . .	68
4.8	CDD Model -- Potentiometer with an Electronically Positionable Wiper Contact.	70
4.9	CDD Transfer Characteristics $(I_{C2}-I_{C1})$ R_C versus $2V_a$ for $V_G = 0$	72
4.10	CDD Transfer Characteristics for V_G = -10 Volts	73
4.11	CDD Characteristics for V_G = -15 Volts	74
4.12	CDD Characteristics for V_G = -25 Volts	75
4.13	Output of CDD Two-Quadrant Multiplier	77
4.14	Bias and Drive Circuitry to Obtain Two-Quadrant Multiplication	78

LIST OF ILLUSTRATIONS (Continued)

Figure		Page
4.15	Normalized Deviation of x_m from $\langle x \rangle$ as a Function of Potential Maxima	80
5.1	Important CDD Parameters and Structure	82
5.2	Two CDD's Cross-Coupled to Produce Four-Quadrant Multiplication	84
5.3	Four-Quadrant Multiplication of a Sine Wave with a Triangle Wave	86
5.4	Output of Four-Quadrant Multiplier	87
5.5	Drive Circuit to Produce Four-Quadrant Multiplication . .	88
5.6	Block Diagram of AGC System	90
5.7	CDD Realization of AGC Circuit	91
5.8	Output versus Input of AGC Realization of Fig. 5.7 . . .	92
5.9	Localized Base Bias Injection	94
5.10	CDD Structure Producing D/A Conversion	95
5.11	Multiple Collector Structure that Produces A/D Behavior .	97
5.12	Threshold Logic Gates	100
6.1	Arbitrary Two-Dimensional Region for CDD Base Region . .	103
6.2	Systems Analogous to the Base Region of CDD's	106
6.3	Simple Geometry Used to Formulate Analysis Methodology Based Upon Green's Function of Rectangular Structure . .	109
A.1	Base Structure Composed of Two Conductivity Regions . . .	125

LIST OF TABLES

Table		Page
2.1	Typical Dimensions and Resistivities of the CDD Prototype Fabricated in The University of Arizona Solid State Laboratory	14

ABSTRACT

This dissertation presents an investigation and analysis of a new concept in electronic function generation: The Carrier Domain Device (CDD). Distributed and proximity effects are used to produce a CDD which is an elongated bipolar structure made to inject emitter current preferentially in localized, movable domains. Device characterization, analysis and applications are presented.

A distributed device model is derived for the base region of rectangular CDD's. The partial differential equation and its associated boundary condition account for the effects of distributed current sources and for voltage boundary excitations.

The potential distribution of the base region is obtained by two methods, Finite Differences and Green's Function Analysis. A set of network-like models is obtained by the application of the first technique while the latter generates an infinite series solution.

A monolithic structure, a composite of Metal-Oxide-Semiconductor (MOS) and bipolar technologies, was fabricated to demonstrate domain action. The CDD prototype is used to obtain two and four quadrant multiplication. Other applications of domain devices are presented.

The analysis methodology applied to the rectangular structure of the CDD prototype is extended to cover arbitrary geometrical designs. Frequency effects are included and a discussion of the isomorphic

systems, electrothermal circuits and distributed RC structures, is given. From the analysis, with little additional computation, the indefinite admittance parameters can be obtained.

CHAPTER 1

INTRODUCTION

The distributed nature of devices has generally not been advantageously utilized by integrated circuit designers. Such effects have been regarded as parasitic and efforts to minimize their presence have allowed I.C. designers to proceed along design rules and philosophies little modified from those established for discrete circuits. One area fully employing the distributed properties of the structure is that of Carrier Domain Devices (CDD's). Operation of a CDD relies upon localized injection along an elongated emitter-base structure of a bipolar transistor. The limited spatial injection (referred to as a current or carrier domain) arises in response to the distributed properties of the appropriately biased base region. Figure 1.1(a) shows a simple CDD structure and Fig. 1.1(b) shows the resulting emitter current distribution. A potential profile exhibiting an extrema is created and, since the emitter is an exponential function of the base voltage, the resultant emitter current is confined to that region near the maxima (npn structure). This effect has long been observed in transistor operation and has been known as "current crowding". The current domain can be made to move along the extent of the emitter making CDD's, in essence, mobile element transistors. Collector design and bias along with domain location and shape define the transfer characteristics of the device.

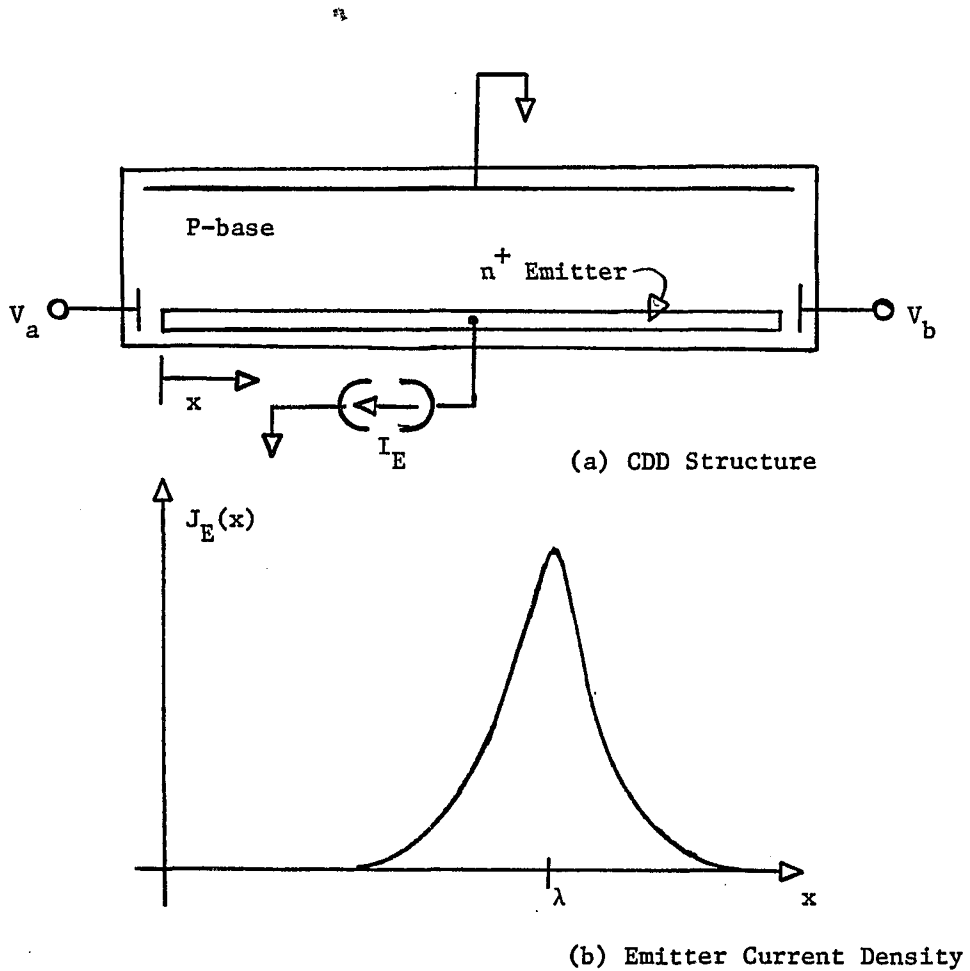

Fig. 1.1 A Simple CDD Structure and Emitter Current Density Showing Domain Action

Carrier Domain Devices have been used as multipliers. Other possible applications of the CDD concept are logic functions, automatic gain control, analog to digital and digital to analog converters, and special function generators.

Analysis of CDD behavior requires complete knowledge of the voltage distribution of the base region. Previous work on the CDD concept by Gilbert [1975b] and Smith [1974, 1975] examined only circular bipolar geometries. Symmetry greatly simplified the analysis of the Gilbert structure shown in Fig. 1.2, but the results are not applicable to other shapes.

Smith [1974] analyzed the circular CDD of Fig. 1.2 by using conformal transformation techniques on the idealized half structure pictured in Fig. 1.3. When driven by complementary current sources as indicated, the domain is centered about the point at

$$\theta_m = \cos^{-1} (1 - 2\alpha) \tag{1.1}$$

along the emitter strip [Smith, 1974]. A four quadrant multiplier and an arc-cosine generator were produced by Gilbert and Smith using this design. While demonstrating domain action, because of the extreme symmetry of the device, the analysis using conformal mapping is not readily applied to a generalized geometry.

The structure of Fig. 1.4 also exhibits domain action. Injected edge current $J_y^{\ell}(x)$, in conjunction with base end voltages, $\pm V_b$, sets up a potential distribution in the base that can be made approximately quadratic in distance along the emitter. If the emitter is driven by a

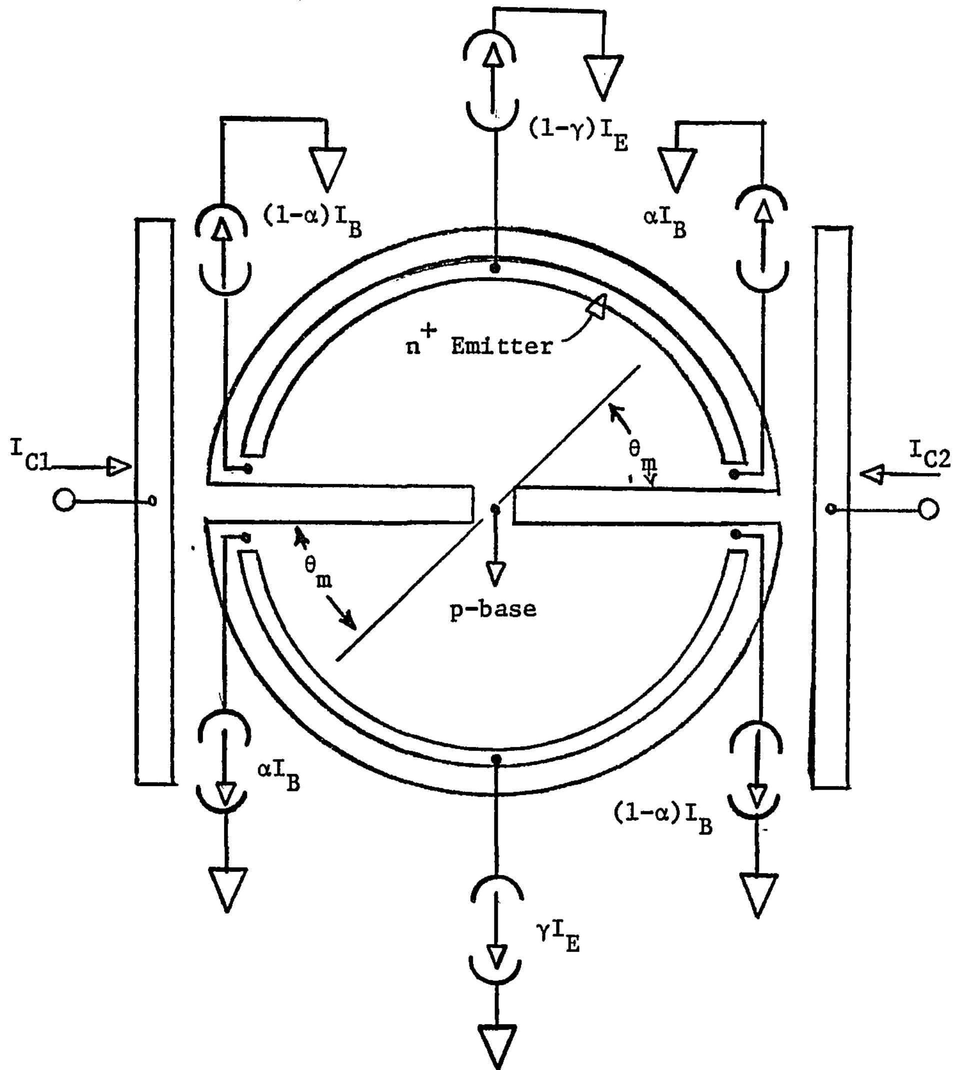

Fig. 1.2 The Gilbert CDD Structure

θ_m is the location of the potential maxima along the emitter.

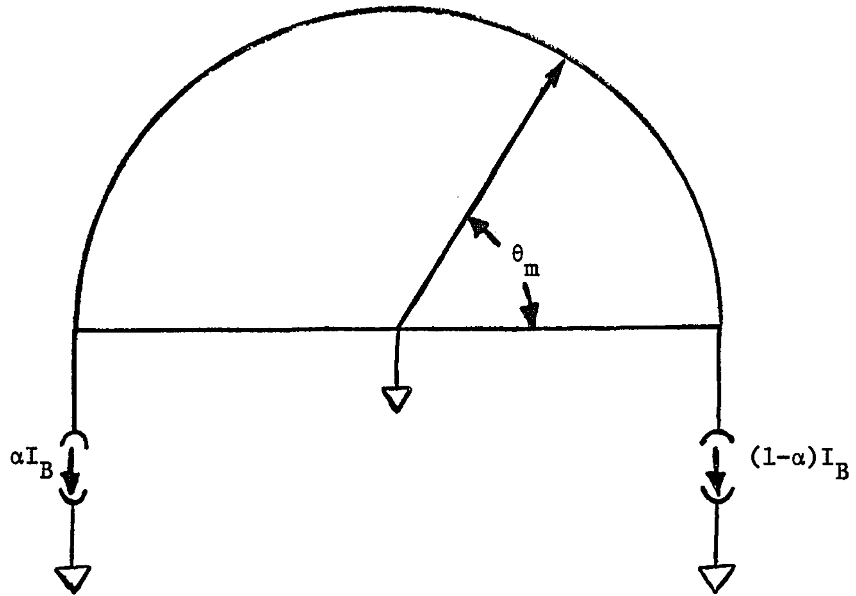

Fig. 1.3 Idealized Half Structure of Base Region of the Gilbert CDD

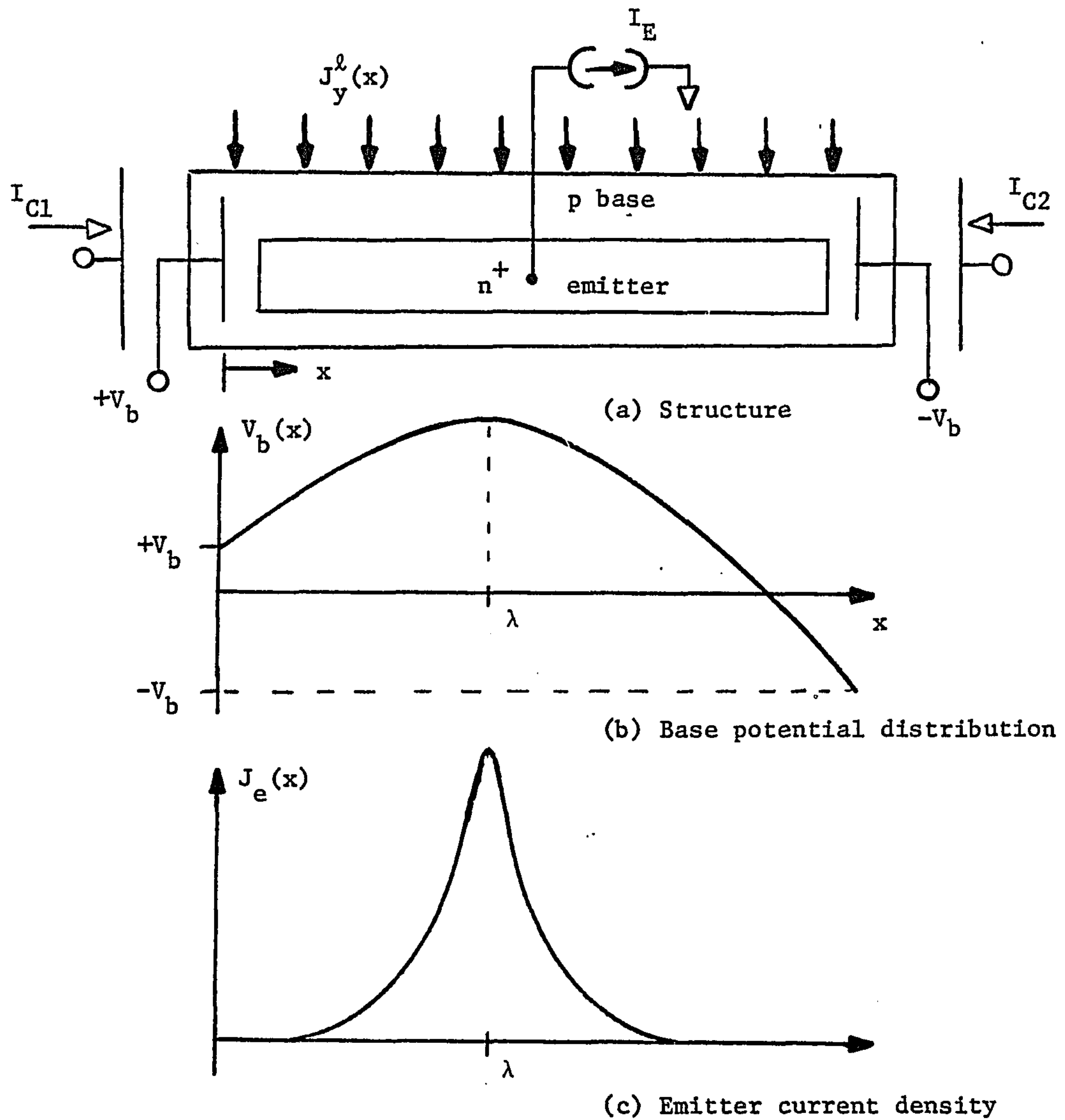

Fig. 1.4 Rectangular Structure Having a Quadratic Potential Distribution

current source, the emitter voltage tracks the base extrema, always being .5 to .7 volts below the base maxima (for npn CDD). The current injected into the collector divides resistively among the multiple collector contacts. Each collector receives a portion of current dependent upon relative placement of the collector contacts and the domain location and shape. For the arrangement shown in Fig. 1.4, current division is linear with respect to domain centroid (λ) resulting in the transfer relations:

$$I_{C1} = I_E\ (1/2 - \lambda) \qquad (1.2a)$$

$$I_{C2} = I_E\ (1/2 + \lambda) \qquad (1.2b)$$

The quadratic distribution is important as the extrema is then linearly related to the base complementary voltage, V_b.

$$\lambda = k\ V_b \qquad (1.3)$$

This yields an overall transadmittance relation that is linear.

$$I_{C1} = I_E\ (1/2 - g\ V_b) \qquad (1.4a)$$

$$I_{C2} = I_E\ (1/2 + g\ V_b) \qquad (1.4b)$$

An important distinction between CDD's and conventional devices lies in the fact that CDD transfer relations are defined primarily by device geometry. Since planar technology exhibits its greatest control

of this process parameter, CDD's are easily mass-produced and promise good matching of characteristics.

Another promising distinction is the ability to create devices with arbitrary transfer functions. For example, in Fig. 1.5(a) the collector current of contact 3 will have the qualitative shape shown in Fig. 1.5(b) as a function of domain centroid location, λ. Responses that would otherwise require complex circuitry could possibly be achieved by changing geometry only.

The basic MOS bipolar CDD is pictured in Fig. 1.6. The MOS portion supplies the edge bias current $J_y^{\ell}(x)$ indicated in Fig. 1.4. Devices of this morphology were fabricated in the Solid State Engineering Laboratory of The University of Arizona as test and study vehicles. Confirmation of domain action was observed and a four quadrant multiplier using two devices was designed.

The distributed properties of solid state devices make possible a new approach to electronic function generation. The broad objective of this dissertation is to investigate a new device representative of this approach: the Carrier Domain Device. Specific goals are the following:

1. To obtain a distributed model for the base region of a rectangular CDD structure. This will consist of a Distributed-Kirchoff Partial Differential Equation (d-KPDE) and a set of boundary conditions.

2. To obtain a solution to the d-KPDE of the base region. This will be done using Green's Function techniques and Finite Differences.

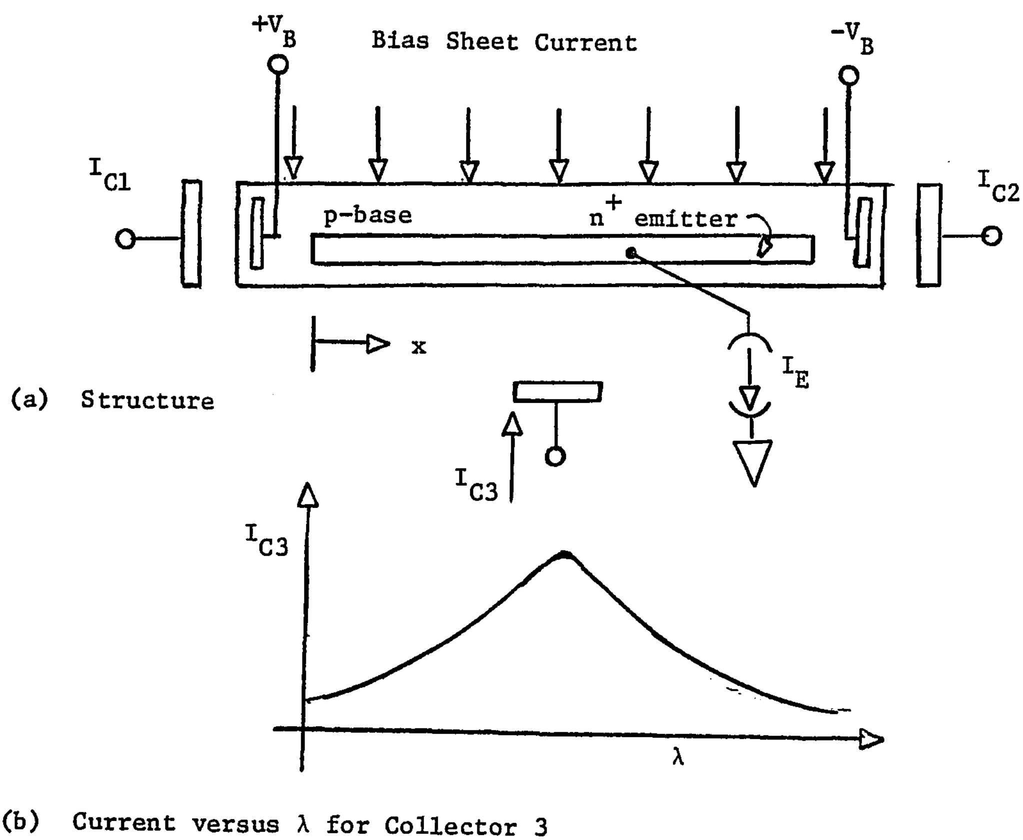

Fig. 1.5 Three-Collector CDD Structure

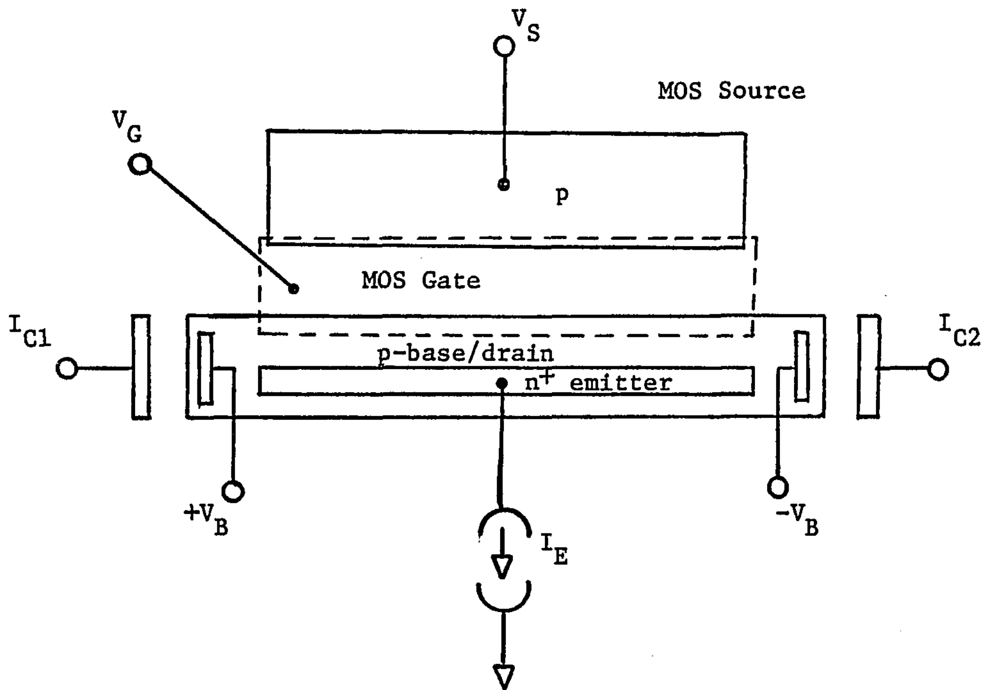

Fig. 1.6 Composite MOS Bipolar CDD Structure

3. To design appropriate bias techniques to produce controlled domain action.

4. To obtain information regarding the shape and extent of the current domain.

5. To generalize the analysis to arbitrary structure shapes. This will be done by defining an Integral Equation to be used in a Green's Function solution to the potential distribution.

6. To investigate possible applications of CDD phenomena.

The generalization of CDD analysis to rectangular structures of composite MOS (Metal-Oxide-Semiconductor) and bipolar transistors was a major objective of this dissertation.

CHAPTER 2

A DISTRIBUTED MODEL FOR CDD'S

Many different structures and bias methods will produce a distributed potential conductive to domain formation. In Chapter 1, three possible geometries were discussed. The specific morphology of Fig. 1.6, in addition to demonstrating the essential features of domain action, possesses a transfer function that is approximately linear. Since techniques used for analysis will be applicable to all rectangular structures, this particular morphology was selected to serve as the study model. Figure 2.1 shows typical dimensions of the CDD prototype. For easy reference, these and typical resistivities are given in Table 2.1. A photomicrograph of the CDD prototype fabricated in The University of Arizona Solid State Engineering Laboratory is shown in Fig. 2.2.

Assumptions for the Distributed Model

The transfer characteristics of Carrier Domain Devices are obtained by specifying the distributed behavior of the base region, defining the functional dependence of the emitter injection current to the base voltage, and finding the current division mode of the collector. This chapter develops the distributed model for the base region: a differential equation detailing the voltage distribution of the structure, a set of boundary conditions, and a specification of the drive sources and their distribution.

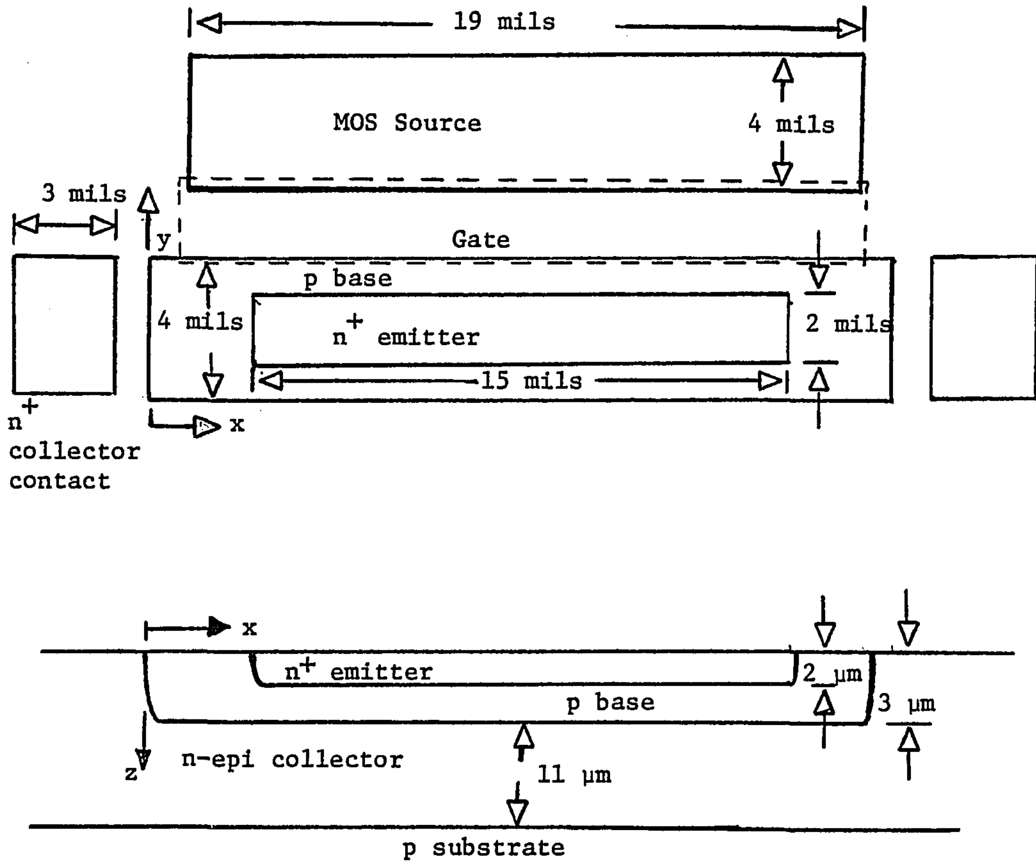

Fig. 2.1 Typical Dimensions of CDD Prototype

[Not to Scale]

Table 2.1 Typical Dimensions and Resistivities of the CDD Prototype Fabricated in The University of Arizona Solid State Laboratory

Region	Surface Dimensions	Thickness	Sheet Resistivity
Emitter	2 x 15 mils	2 μm	4 Ω/□
Base	4 x 21 mils	3.5 μ	200 Ω/□
Collector	~6 x 25 mils	11 μm	1 Ω-cm
MOS-Source	4 x 19 mils	3.5 μm	200 Ω/□
MOS-Channel	2 mils long		
MOS-Drain	Physically, the Base Region		

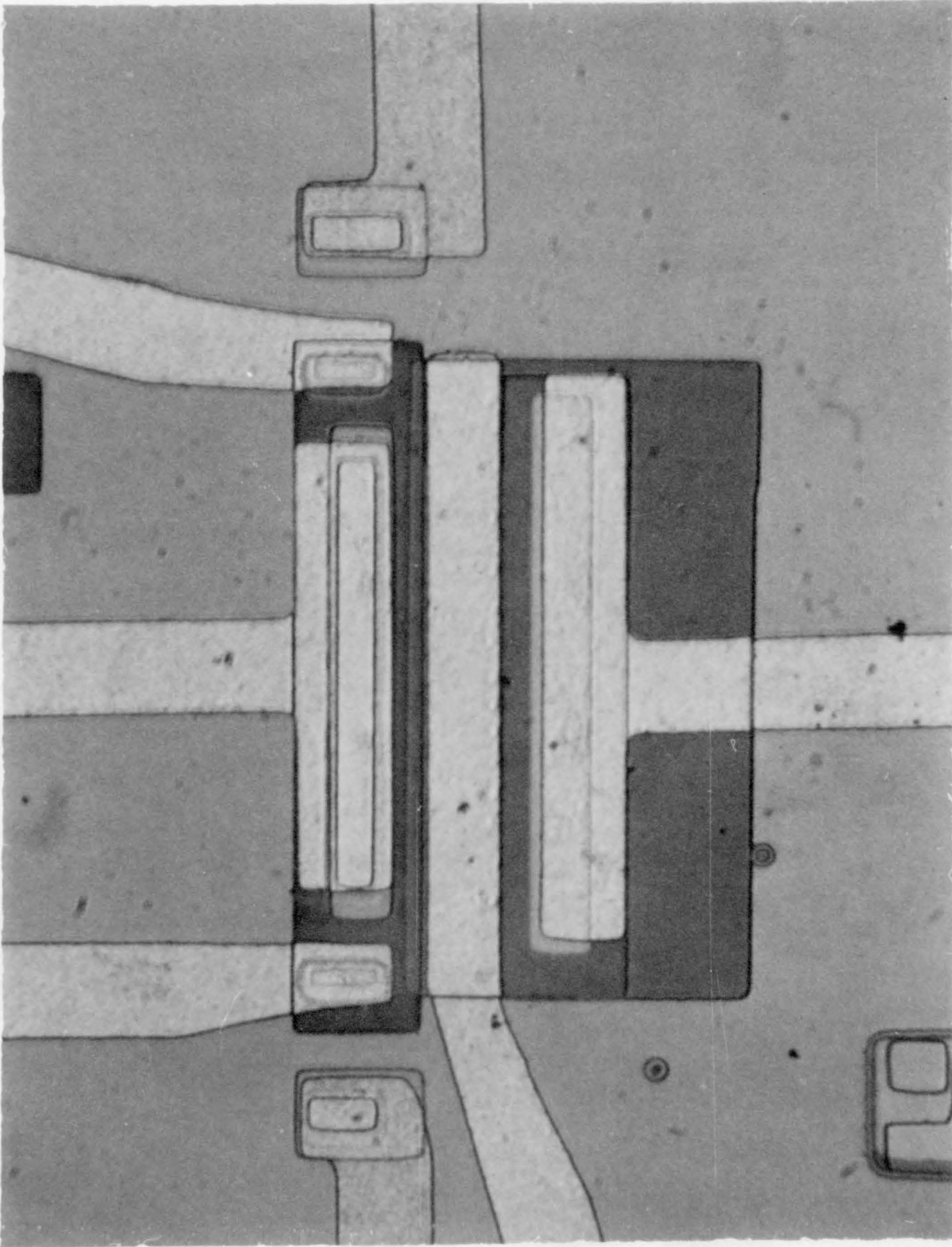

Fig. 2.2 Photomicrograph of the MOS CDD Prototype

A statement of the unilateral behavior of bipolar structures provides the first assumption required for facilitating CDD analysis. A unilateral device is one that exhibits strong directionality; the output response does not significantly influence the state of the input port. This behavior decouples the collector response from that of the base and emitter, thus allowing the design and analysis of the collector to be considered independent of the base-emitter morphology.

If we also assume that the base-emitter current is small, the base region behavior will become independent of the emitter. This greatly simplifies the analysis as now the base, emitter, and collector form three regions with only unilateral dependence. If we do not assume small base transistor current, the analysis is complicated by a feedback effect. Analysis then requires solving an integral equation as was shown by Hauser [1964]. However, this effect for moderate current levels is small and can be incorporated in the analysis.

Once the base voltage is known, as a consequence of the assumptions of unilateral behavior and small base-emitter current, the total response is easily obtained. The emitter current density, $J_E(x,y)$, is a function of the base potential, $\phi(x,y)$.

$$J_E(x,y) = J_o \exp\left[q\phi(x,y)/kT\right] \tag{2.1}$$

The term subtracting the saturation current has been neglected in the classical diode equation as the forward-biased junction current is orders of magnitude larger, and the constant, J_o, is selected to satisfy the continuity of emitter terminal current, I_E.

$$J_o = \frac{I_E}{\iint_{\text{Emitter}} \exp\,[q\phi(x,y)/kT]\,dxdy} \tag{2.2}$$

Knowledge of the emitter current density in conjunction with collector morphology specifies the collector currents.

$$I_{Ci} = \iint_{\text{Emitter}} J_E(x,y)\; K_i(x,y)\; dx\; dy \tag{2.3}$$

I_{Ci} = Terminal current at i^{th} collector contact

The function, $K_i(x,y)$, is the response at the ith collector to a delta function emitter current excitation at the point, $P(x,y)$. The complete CDD model is shown schematically in Fig. 2.3, where the block diagram transfer relations T_B, T_C, and T_E are yet to be specified.

Having indicated the major partitions in the analysis, we now restrict consideration to the base response. The following assumptions are used in the development:

1. The unilateral character of bipolar structures is assumed to apply to CDD structures.

2. Base current resulting in transistor action is assumed to be small compared to the total current entering the base region. These first two assumptions allow the decomposition indicated in Fig. 2.3 as already discussed.

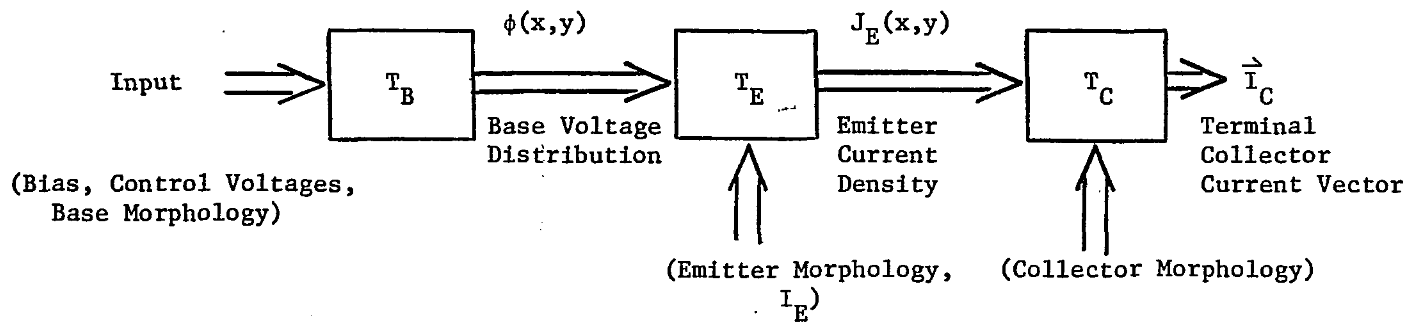

Fig. 2.3 Block Diagram Showing the Unilateral Dependence of the Responses of the Base, Emitter and Collector of a CDD

3. The base region is homogeneous. By this assumption, the analysis of the base potential distribution proceeds as though the emitter were not present. The perturbation caused by the emitter can be empirically accounted for by using an effective base width. The presence requires, in general, the assumption that the base is composed of two regions: One region defined where the emitter does not overlap; the other, that region constricted by the emitter and resulting in a higher resistivity. Correction due to this "pinch effect" is discussed in Appendix A.

4. Only majority current due to drift mechanism is significant. The relation between current flow and the resulting distributed potential is given by Ohm's point law:

$$\vec{J}(x,y) = \sigma \, \vec{\xi} \, (x,y) = - \sigma \, \vec{\nabla} \, \phi \, (x,y) \qquad (2.4)$$

where

σ = conductivity

ϕ = potential function

$\vec{\xi}$ = electric field

5. The MOS device is biased in the saturation region throughout its length. The bias injection current, $J_y^{\ell}(x)$, becomes a constant sheet current.

6. All contacts are ohmic.

7. The emitter, due to its low resistivity and full length metalization, is an equipotential region.

8. All junction isolations have negligible leakage currents.

9. All variations in the z-direction are small. Spatial derivities with respect to this variable are approximately zero, making the structure essentially two dimensional.

10. Time varying magnetic field effects are negligible.

The resultant base morphology is as shown in Fig. 2.4.

The Distributed-Kirchoff Equation

The model equation we seek is the distributed analog to Kirchoff's current-node law. For convenience, it is called the distributed-Kirchoff equation, or simply the d-K equation [Lindholm and Hamilton, 1964]. We now derive the d-K equation based upon the assumptions enumerated.

Arbitrarily selecting a closed region, R, as shown in Fig. 2.5, we see that the total current crossing the region's boundary, S, is equal to the enclosed source current.

$$\oint_S \vec{J}(x,y) \cdot d\vec{S} = I_f \tag{2.5}$$

$\vec{J}(x,y)$ = Current density in enclosed region crossing the boundary

$d\vec{S}$ = Surface differential area element in direction of normal, $\hat{n}$

I_f = Total source current within S

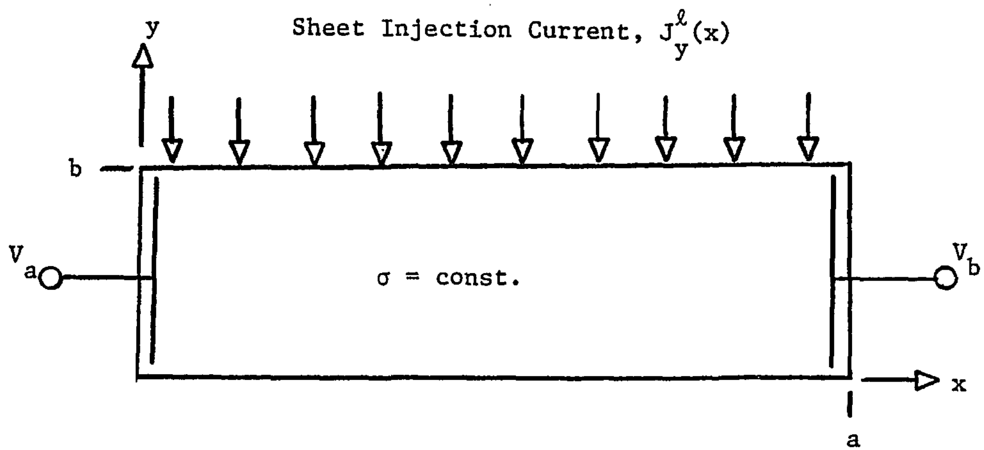

Fig. 2.4 Base Morphology for Idealized CDD Prototype

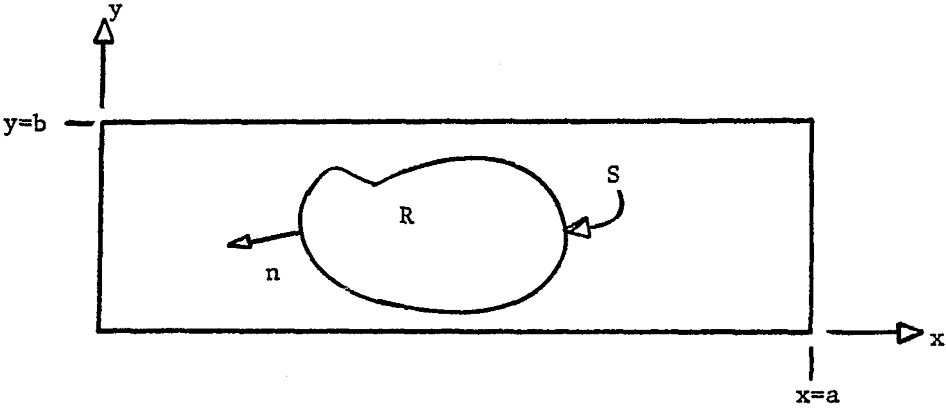

Fig. 2.5 Base Region of CDD Showing Arbitrary Region R Bounded by Surface S

By assumption 4, the current density, $\vec{J}(x,y)$, as a function of base potential, $\phi(x,y)$, is

$$\vec{J}(x,y) = -\sigma \vec{\nabla} \phi(x,y) \tag{2.6}$$

Substitution of Eq. (2.6) into Eq. (2.5) yields:

$$-\sigma \oint_S \vec{\nabla} \phi \cdot d\vec{S} = I_f \tag{2.7}$$

Applying Gauss's divergence theorem to Eq. (2.7), we obtain

$$-\sigma \iiint_R \nabla \cdot \nabla \phi(x,y) \, dxdydz = I_f \tag{2.8}$$

The source current can be expressed in terms of the current density, $\vec{J}_f(x,y,z)$, as

$$I_f = \iint_S J_{f_x} \, dydz + \iint_S J_{f_y} \, dxdz + \iint_S J_{f_z} \, dxdy \tag{2.9}$$

Since the integrals in Eq. (2.9) are over the surface, introduction of delta functions allow the integrals to be taken over the whole volume.

$$I_f = \iiint_R \left[J_{f_x} \, \delta(x-x_s) + J_{f_y} \, \delta(y-y_s) + J_{f_z} \, \delta(z-z_s) \right] dxdydz \tag{2.10}$$

x_s, y_s, z_s = coordinates along the surface, S

Substitution of Eq. (2.10) into Eq. (2.8) yields the d-K equation.

$$- \sigma \iiint_R \nabla^2 \phi(x,y)\,dxdydz = \iiint_R \left\{ J_{f_x}\, \delta(x-x_s) + J_{f_y}\, \delta(y-y_s) + J_{f_z}\, \delta(z-z_s) \right\} dxdydz \tag{2.11}$$

Since the integration region is arbitrary, the integrands must be equal. The resultant equation is the distributed-Kirchoff partial differential equation (d-KPDE) which is the analog to Kirchoff's current law expressed for a differential volume.

$$\nabla^2 \phi(x,y) = - \frac{1}{\sigma} \left\{ J_{f_x} \delta(x-x_s) + J_{f_y} \delta(y-y_s) + J_{f_z} \delta(z-z_s) \right\} \tag{2.12}$$

This equation is another representation of Poisson's equation in terms of the source current density over the surface.

Imposing assumption 9, which requires no variation in the z-direction, makes J_{f_z} in Eq. (2.12) equal to zero. Assumption 5 stating the mode of operation of the MOS transistor makes J_{f_x} zero and J_{f_y} a constant current density over the side where y = b. Thus, Eq. (2.12) simplifies to the d-KPDE of the base region.

$$\nabla^2 \phi(x,y) = - \rho_s' \, J_y^{\ell}(x) \, \delta(y-b) \tag{2.13}$$

where

$J_y^{\ell}(x) = t\, J_{f_y}$ = line current density injected by the MOS transistor

t = thickness in the z-direction

$\rho = \frac{1}{\sigma}$ = resistivity (Ω-cm)

$\rho_s' = \frac{\rho}{t}$ = sheet resistivity (Ω/□)

To complete the distributed model, the boundary conditions the system satisfies must be specified. Referring to Fig. 2.3, we see that the sides x=o and x=a are equipotential surfaces. This requires

$$\phi(o,y) = V_A \tag{2.14a}$$

$$\phi(a,y) = V_B \tag{2.14b}$$

$$o \leq y \leq b$$

V_A, V_B = external voltage sources

We also assumed perfect isolation along the sides y=o and y=b (assumption 5). This forces the condition on the derivative of the potential function

$$\left.\frac{\partial\phi(x,y)}{\partial y}\right|_{y=o} = 0 = \left.\frac{\partial\phi(x,y)}{\partial y}\right|_{y=b} \tag{2.15}$$

The d-KPDE (Eq. 2.13) and the specified boundary conditions (Equations 2.14 and 2.15) model the idealized structure of Fig. 2.1. The validity of this representation for the base region of CDD structures depends upon the extent to which the assumptions in its derivation represent the actual device.

CHAPTER 3

CDD BASE POTENTIAL ANALYSIS

This chapter presents the solution to the distributed model for the base region of Carrier Domain Devices (CDD). Two methods of analysis are used: The Finite Difference Technique and the Method of Green's Functions. The former method has the advantage of generating a lumped network representation, the elements of which maintain a close physical correspondence to the base structure being modeled. The Green's Function method results in a series solution easily programmed for high accuracy computer resolution.

The Method of Finite Differences

If the distributed Kirchoff equation (Eq. 2.11) is approximated directly by replacing integrals by finite sums and derivatives by ratios of finite differences [Lindholm and Hamilton, 1964], we obtain a system of algebraic equations that correspond to a lumped network representation.

We first subdivide the distributed base region by superimposing upon it a grid of equi-spaced planes in both x and y directions. Let the perpendicular distance between adjacent, parallel planes be h. For the subregion formed by the intersection of the planes $x = mh$, $x = (m+1)h$, and $y = (n+1)h$, the d-K equation becomes

$$(\phi_{m+1,n} - 2\phi_{m,n} + \phi_{m-1,n}) + (\phi_{m,n+1} - 2\phi_{m,n} + \phi_{m,n-1})$$

$$= - \rho_s' \bar{I}_{m,n} \qquad (3.1)$$

$1 \leq m \leq M$ (= a/h)

$1 \leq n \leq N$ (= b/h)

$\bar{I}_{m,n}$ = average source current entering subregion (m,n)

The continuous spatial variables have been replaced by the discrete set of (M+1) • (N+1) points representing the grid intersections, and the dependent continuous variable has been approximated by a vector of this many dimensions.

Equation (3.1) is identical to the Kirchoff node equation for the network shown in Fig. 3.1. The subregion under study is represented by this network; the total structure is modeled by a two dimensional lattice repetition of the subregion model. The network is terminated along its four sides to satisfy the system boundary conditions. Analysis of the resulting total model is accomplished by using classical nodal techniques and the superposition principle to separate the sources. The solution is

$$\left.\phi_{mn}\right] = \left[g_{(mn),(jk)}\right]^{-1} \left.\bar{I}_{mn}\right] + \left[\left(V_a - \frac{V_a - V_b}{M} \cdot m\right)_{(mn)}\right] \qquad (3.2)$$

where the elements of the g matrix are

$$g_{(mn),(mn)} = \sum_{P} [\text{conductances attached between node (mn) and all other nodes, P}]$$

$$g_{(mn),(jk)} = -\sum_{P} [\text{conductances between nodes (mn) and all other nodes } P = (j,k) \text{ with } (m,n) \neq (j,k)]$$

and the double subscripts have been retained to indicate the two-dimensional nature of the problem.

While this dissertation concentrates on the static characteristics of carrier domain phenomena, the analysis can be extended to the time varying response. This is done by introducing a charge storage term in the d-K equation to account for the dominant effect; the distributed capacitive coupling of the resistive base layer to the collector and substrate [Hamilton, Lindholm and Marshak, 1971]. The d-K equation becomes

$$-\sigma \iiint_R \nabla^2\phi\ (x,y,t)dxdydz = \iiint_R \left\{ J_{fx}\delta(x-x_s) + J_{fy}\delta(y-y_s) + J_{fz}\delta(z-z_s) + \frac{\partial\rho(x,y,t)}{\partial t} \right\} dxdydz \tag{3.3}$$

where

$$\rho(x,y,t) = \text{charge density} = \frac{c\ \phi(x,y,t)}{\text{subregion volume}}$$

and

c = total capacitance of the subregion

Application of the Finite Difference Method on Eq. (3.3) leads to a system of ordinary differential equations in time. The continuous space dependence once again is replaced by a discrete space representation. The subregion model of Fig. 3.1 is modified by a storage element, a capacitor of value c, attached from node (m,n) to the common node, and the solution is obtained by use of Laplace transforms which introduce a conductance, sc, to the elements along the main diagonal of the g-matrix of Eq. (3.2).

The method of Finite Differences does not require the partitioning of the region into a symmetrical rectangular lattice. Macneal [1953] describes the method for asymmetrical subdivision that may be applied to regions of arbitrary shapes or where a predetermined set of points are of particular importance [Gray, 1976]. In general, this method is easy to apply and, following Macneal, can be used to analyze arbitrary geometries, but suffers in accuracy. The solution is given only for the points on the grid. In the limit of zero grid spacing, the solution converges to the continuous case, but as the resolution is increased by decreasing h, larger matrices are generated.

The Method of Green's Functions

A more versatile solution is obtained by using the Method of Green's Functions [Friedman, 1956]. Since the operator of Eq. (2.13) is linear, the solution can be obtained as a superposition integral of the delta function response convolved with the forcing function plus the response due to the non-homogeneous boundary conditions.

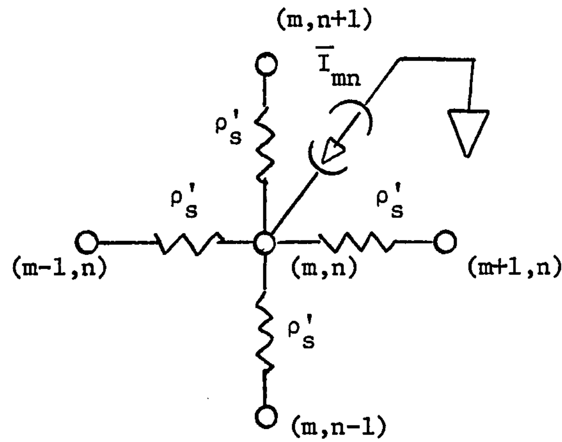

Fig. 3.1 Lumped Model for the Subregion (m,n) Defined by the Method of Finite Differences

To aid in scaling the solution and in recognizing dominant terms, the d-KPDE is cast into dimensionless form. This is carried out in detail in Appendix B. The base region is transformed to the dimensionless and now normalized region of Fig. 3.2, and the distributed model becomes

$$-\left(\frac{\partial^2}{\partial x^2} + R^2 \frac{\partial^2}{\partial y^2}\right) \phi(x,y) = \frac{R_{ab}\ I_b\ \delta(y-1)}{V_o} \tag{3.4}$$

$$\phi(o,y) = V_a/V_o \tag{3.5a}$$

$$\phi(1,y) = V_b/V_o \tag{3.5b}$$

$$\left.\frac{\partial\phi(x,y)}{\partial y}\right|_{y=o} = 0 \tag{3.5c}$$

$$\left.\frac{\partial\phi(x,y)}{\partial y}\right|_{y=1} = 0 \tag{3.5d}$$

where the dimensionless independent variables, x and y, are in the intervals

$$0 \leq x \leq 1$$

$$0 \leq y \leq 1$$

and

$R = a/b$, the aspect ratio

$R_{ab} = \frac{\rho a}{tb}$ = end-to-end base resistance

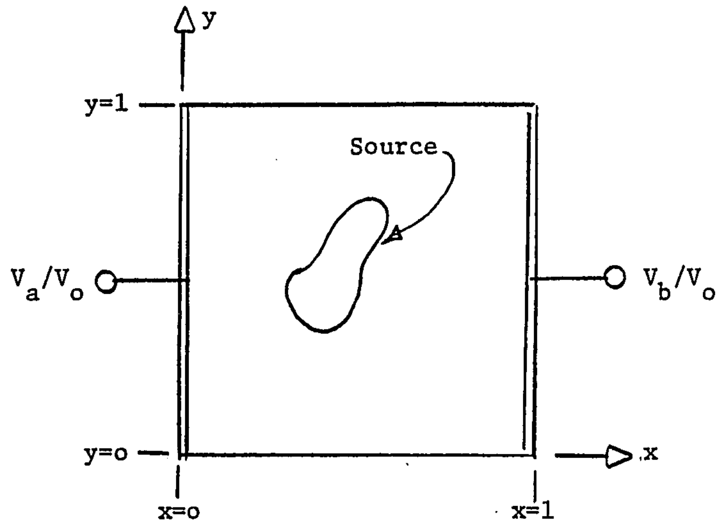

Fig. 3.2 Transformed Base Region in Normalized Form, Excited by an Arbitrary Source Distribution

$I_b = J_y^{\ell}(x) \cdot a$, total MOS bias current injected into the base

$V_o = \frac{KT}{q}$ the reference voltage used for normalization

Note that $\phi(x,y)$ is also a dimensionless variable. Multiplication of $\phi(x,y)$ by V_o yields the voltage distribution.

Since the operator in Eq. (3.4) is self adjoint, and the physical constraint on the real function, $\phi(x,y)$, satisfying the equation requires it to be bounded, a suitable inner product is

$$\langle \phi,\psi \rangle = \int_o^1 \int_o^1 \phi(x,y)\ \psi(x,y)\ dxdy \tag{3.6}$$

Taking the inner product of Eq. (3.3) with the adjoint Green's Function, $h(x,y|x'y')$, we obtain,

$$\int_o^1 \int_o^1 h(x,y|x'y') \left(- \frac{\partial^2}{\partial y^2} - R^2 \frac{\partial^2}{\partial y^2} \right) \phi(x,y)\ dxdy =$$

$$\int_o^1 \int_o^1 \phi(x,y) \left(- \frac{\partial^2}{\partial x^2} - R^2 \frac{\partial^2}{\partial y^2} \right) h(x,y|x',y')\ dx'dy'$$

$$- \int_s \left\{ h(x,y|x'y') \frac{\partial \phi(x,y)}{\partial n} - \phi(x,y) \frac{\partial h}{\partial n}(x,y|x'y') \right\} ds' \tag{3.7}$$

where the right hand side of Eq. (3.6) is obtained by integrating twice by parts, and $\partial/\partial n$ represents the partial derivative with respect to the outward normal along the boundary.

The adjoint Green's Function must satisfy

$$-\left(\frac{\partial^2}{\partial x^2} + R^2 \frac{\partial^2}{\partial y^2}\right) h(x,y|x',y') = \delta(x-x')\delta(y-y') \tag{3.8}$$

and the following boundary conditions:

$$h(o,y|x',y') = 0 \tag{3.9a}$$

$$h(1,y|x',y') = 0 \tag{3.9b}$$

$$\left.\frac{\partial h(x,y|x',y')}{\partial y}\right|_{y=0} = 0 \tag{3.9c}$$

$$\left.\frac{\partial h(x,y|x',y')}{\partial y}\right|_{y=1} = 0 \tag{3.9d}$$

The Dirac delta functions, $\delta(x-x')$ and $\delta(y-y')$, specify a point source located at the coordinates (x',y').

The derivation of the adjoint Green's Function is given in Appendix C. The result is

$$h(x,y|x',y') = \sum_{n=o}^{\infty} \frac{\varepsilon_n \cos(n\pi y') \cos(n\pi y) \sinh(n\pi R x_<) \sinh[n\pi R(1-x_>)]}{n\pi R \sinh(n\pi R)} \tag{3.10}$$

where

$$x_< = \min(x,x')$$

$$x_> = \max(x,x')$$

and

$$\varepsilon_n = \text{Neumann's number} = \begin{cases} 1 & \text{if } n=o \\ 2 & n \neq o \end{cases}$$

If at this point we invoke the superposition principle, the total response becomes the sum of the solution due to the forcing function with homogeneous boundary conditions

$$\phi(o,y) = \phi(1,y) = 0$$

$$\frac{\partial\phi(x,o)}{\partial y} = \frac{\partial\phi(x,1)}{\partial y} = 0 \tag{3.11}$$

and the homogeneous equation satisfying the boundary conditions given in Equations (3.5a, b, c, d).

The response due to the boundary conditions with the source term set to zero, $\phi_{b.c.}(x,y)$, is simplified by the rectangular geometry of the structure. This makes the partial response $\phi_{b.c.}(x,y)$ independent of the y-coordinate as was obtained by the Finite Difference Method.

$$\phi_{b.c.}(x,y) = \frac{V_a}{V_o} - \frac{V_a - V_b}{V_o}\, x \tag{3.12}$$

Equation (3.7) specialized to the homogeneous boundary conditions becomes

$$\int_o^1\int_o^1 g(x,y|x',y')\; J_y^{\ell}\,(x')\;\delta(y'-1)\; dx'dy' = \phi_s(x,y) \tag{3.13}$$

where we have interchanged the primed and unprimed coordinates and used the equality between the adjoint Green's Function and the Green's Function, $g(x,y|x',y')$,

$$g(x,y|x',y') = h(x',y'|x,y)$$

and the conjunct is identically zero. $\phi_s(x,y)$ is the partial response due to the current forcing function acting alone.

Performing the integration of Eq. (3.13) after substituting the derived expression for the Green's Function, and adding Eq. (3.12) yields the dimensionless distributed base potential

$$\phi(x,y) = \frac{V_a}{V_o} - \frac{V_a - V_b}{V_o} x$$

$$+ \left(\frac{R_{ab} I}{V_o}\right) \sum_{n=o}^{\infty} \frac{\varepsilon_n \cos (n\pi y) \ (-1)^n}{(Rn\pi)^2 \sinh Rn\pi} \left\{ \sinh [n\pi R(1-x)](\cosh(n\pi R\, x)-1) \right.$$

$$\left. + \sinh(n\pi Rx)[\cosh(n\pi R\,(1-x)) - 1] \right\} \tag{3.14}$$

where, in summary,

R_{ab} = end to end base resistance

I = total MOS bias current

V_o = KT/q, reference voltage

ε_n = Neumann's number

$$= \begin{cases} 1 \text{ if } n=o \\ 2 \text{ if } n\neq o \end{cases}$$

R = a/b = aspect ratio

The Green's Function analysis can also be extended to the time response. From Eq. (3.3), we obtain the d-KPDE

$$-\frac{1}{\rho_s'} \nabla^2 \phi(x,y,t) + k \frac{\partial \phi}{\partial t} = J_y^{\ell} (x,t) \ \delta(y-1) \tag{3.15}$$

$$\text{for } t \geq o$$

where k is proportional to the capacitance per unit area. We take the Laplace transform of Eq. (3.15) and assume zero initial conditions,

$$-\frac{1}{\rho_s'} \nabla^2 \ \Phi(x,y,s) + ks \ \Phi(x,y,x) = J_y^{\ell} \ (x,s) \ \delta(y-1) \tag{3.16}$$

and solve the resulting equation (Eq. 3.16) for the transformed function $\Phi(x,y,s)$ with the Laplace variable, s, a parameter assumed constant. This changes the eigenvalue of the x-operator from $+(n\pi R)^2$ to $[(n\pi R)^2 + \rho_s' \, ks]$. Thus, the solution to the time varying problem in the complex frequency space is found by replacing the quantity $(n\pi R)$ by $[(n\pi R)^2 + \rho_s' \, ks]^{1/2}$ in Eq. (3.10), and substituting the new Green's Function into Eq. (3.7) to obtain

$$\begin{aligned}\Phi(x,y,s) = \rho_s' \int_o^1\int_o^1 J_y^{\ell} \ (x's) \ \delta(y'-1) \ g(x,y;s|x',y') \ dx'dy' \\ + \int_o^1 \Bigg\{ \frac{V_a(s)}{V_o} \frac{\partial g}{\partial x'}(x,y;s|x',y') \Bigg|_{x'=o} \\ - \frac{V_b(s)}{V_o} \frac{\partial g}{\partial x'}(x,y;s|x',y') \Bigg|_{x'=1} \Bigg\} \, dy'\end{aligned}$$

If the function $J_y^{\ell}(x,t)$ is a constant as before but turned on at $t = 0$, the first integral is identical to the solution obtained for the forcing function response with homogeneous boundary conditions, $\phi_s(x,y)$, but with the change in eigenvalues as already discussed. The second integral of Eq. (3.17) represents the spectral response of the distributed base region to the now time varying potential sources at $x = 0$ and at $x = 1$.

Equation (3.17) is in a very useful form, familiar to electrical engineers. If we let $s = 0$, we revert to the static solution identically as is expected. More important, if we let $s = j\omega$, we obtain the steady state frequency response. This makes it unnecessary to perform the inverse Laplace transform as from the frequency response we can obtain magnitude and phase information required for performance characterization. Also, Eq. (3.17) is in a form from which the dominant pole locations can be obtained. This aids in estimating the behavior by ignoring poles reasonably removed from the frequencies of interest. Since the poles are defined by the geometry, judicious placement of the zeros controlled by the source locations can produce design information to obtain specified characteristics [Louw, 1975].

It should be noted that we have also solved the analogous problems of the two dimensional distributed RC system and the electrothermal filter. These areas will be discussed further in Chapter 6.

A One-Dimensional CDD

At this point it is easy to begin manipulating Eq. (3.14) on the computer and lose sight of the physics of the problem. If we

examine the solution for large aspect ratios, the equation simplifies considerably and can be seen to represent a one-dimensional CDD structure. Examination of this limiting case enhances our physical understanding of domain phenomena thereby aiding in interpreting the response for the more complicated structures.

Consider the one-dimensional structure shown in Fig. 3.3. The resistance is uniform of r ohms/unit length. Applying the Finite Difference Method we obtain the subregion model shown in Fig. 3.3b. Kirchoff's laws applied to the lumped subregion model yields

$$I_{m+1} = I_m + \frac{I_f}{a} \Delta x \tag{3.18}$$

$$V_m = V_{m+1} + r\Delta x \, I_{m+1} \tag{3.19}$$

In the limit as Δx approaches zero, the Finite difference solution becomes exact and we get the coupled equations

$$\frac{dI(x)}{dx} = \frac{I_f}{a} \tag{3.20a}$$

$$\frac{dV(x)}{dx} = - r \, I_f(x) \tag{3.20b}$$

These combine to give the voltage d-KPDE

$$\frac{d^2V(x)}{dx^2} = - \frac{rI_f}{a} \tag{3.21}$$

with the boundary condition

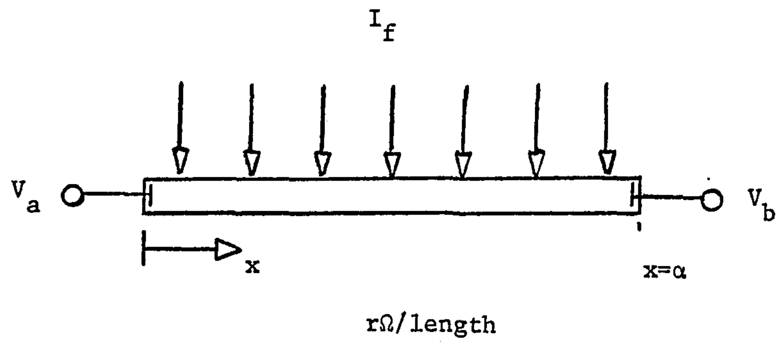

Fig. 3.3 One-Dimensional CDD Base Structure

$$V(o) = V_a \tag{3.22a}$$

$$V(a) = V_b \tag{3.22b}$$

and

I_f = total injected bias current

The solution to Eq. (3.21) satisfying the conditions (3.22) is

$$V(x) = -\frac{rI_f}{2a}(x-x_m)^2 + V_{max}(V_a, V_b, I_f) \tag{3.23}$$

where

$$x_m = \text{location of maximum voltage}$$

$$= \frac{V_b - V_a}{rI_f} + \frac{a}{2}$$

$$V_{max}(V_a, V_b, I) = \text{maximum voltage}$$

$$= V_a + \frac{x_m^2\, rI_f}{2a}$$

This solution can be obtained from the Green's Function solution, Eq. (3.14) by letting R become large. The significance of this distribution is that the location of maximum voltage, x_m, is a linear function of the applied base end voltages. Also of interest, is the factor multiplying the quadratic term. If we divide Eq. (3.23) by $V_o = \frac{KT}{q}$, we obtain the dimensionless voltage, $\phi(x)$, and this factor becomes

$$\frac{rI}{2aV_o} = \frac{R_{ab}I_f}{2a^2V_o} = \frac{1}{\left[a\sqrt{\frac{2V_o}{R_{ab}I_f}}\right]^2} = \frac{1}{\ell_o^2}$$

The parameter ℓ_o is a useful characteristic length and will be shown to be related to the width of the created current domain.

Potential Distribution within the Base

A computer program was written to obtain the distribution given in Eq. (3.14). A listing of the program is given in Appendix D. In the discussion that follows, we have assumed an effective base aspect ratio of 15 due to the emitters pinch effect. We did not attempt to predict exact behavior as too many parameters remained only approximately known. Instead we attempted to describe qualitative behavior and present a mathematical description suitable for performance prediction where essential parameters are well controlled. Thus, all data has been normalized suitable for scaling to desired levels within the limits of the device.

Figure 3.4 shows a normalized potential distribution for the case $V_a = V_b = 0$. Since the distribution for this bias is symmetrical about the line x = 1/2, only half of the distribution is indicated. Note that the gradients exist primarily in the x-direction while in the y-direction the potential is almost constant. The voltage profile for a constant value of y is very close to a parabola as was obtained for the one-dimensional CDD. This is shown in Fig. 3.5. Application of base end potentials of $\pm V_b$ introduces a linear bias to the distribution that

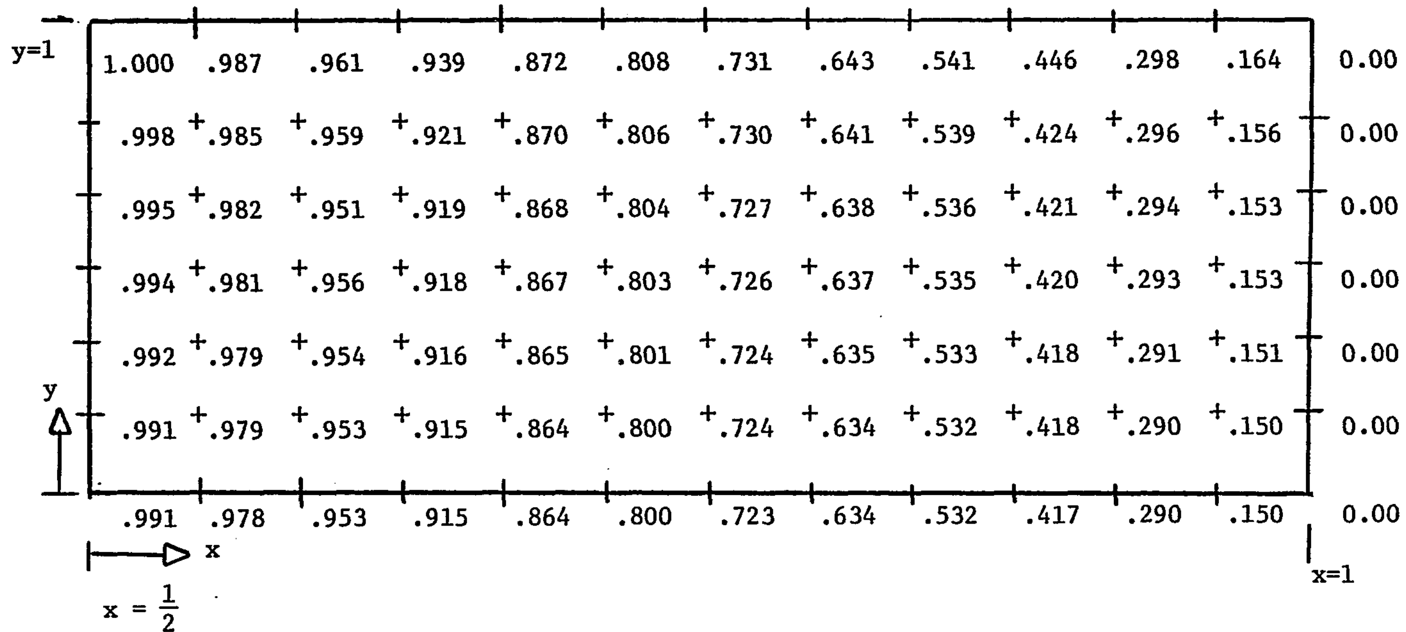

Aspect Ratio = 15

$V_a = V_b = 0$

Fig. 3.4 Normalized Potential Distribution for One-Half of the Base Region of CDD Structure

Note: Only half the structure is shown due to symmetry.

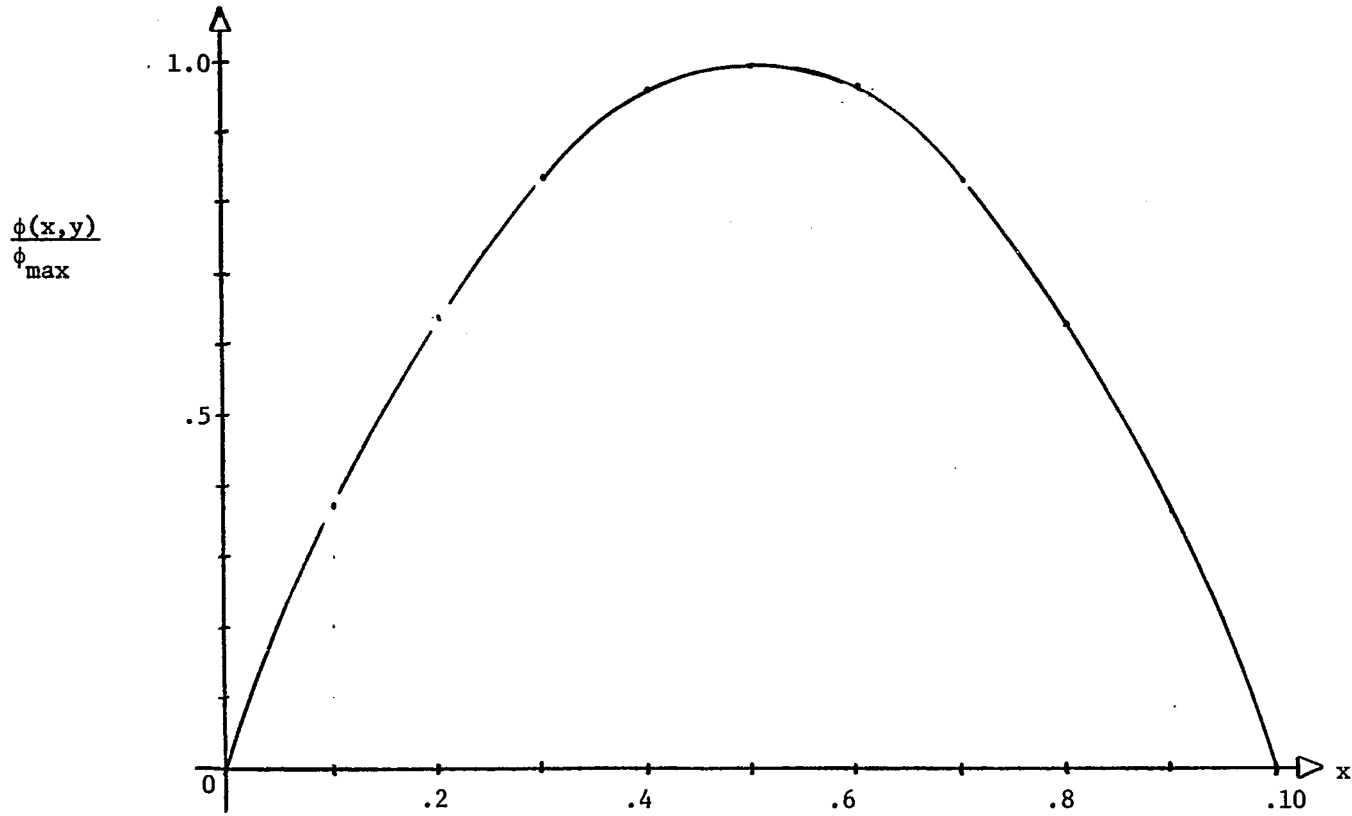

Fig. 3.5 Normalized Potential Profile Along Constant y Showing Parabolic Distribution

shifts the location and magnitude of the maxima, but the distribution remains quadratic in x. This effect is shown in Fig. 3.6 for three different normalized base drives of $V_b = 0, .5, 1.0$.

The location of the maximum potential, x_m, as a function of base drive voltage is shown in Fig. 3.7. The linear relation is expected as the obtained voltage distribution is approximately quadratic in x. This indicates that an aspect ratio of 15 produces an approximately one-dimensional structure.

Though the profiles obtained represent only the case of $R > 15$, the Green's Function solution and the computer program are valid for any aspect ratio. It is not necessary to recognize a spatial function that approximates the distribution as all calculations and integrations can remain in the numeric domain. However, since the quadratic relations obtained lead to simplified but interesting closed form relations, we will adopt this approximation in Chapter 4 where we complete the analysis of the CDD prototype of Fig. 1.6.

Summary of Methods of Analysis

The two methods used to solve for the base voltage distribution each have their respective merits. The Method of Finite Differences is easy to use and, if we use asymmetrical subdivision, can be used to describe the response of arbitrary geometries to arbitrary forcing functions and boundary conditions. Models having close correspondence to physical processes are obtained. Extension of the analysis to include time variations is easily done. A disadvantage is that large

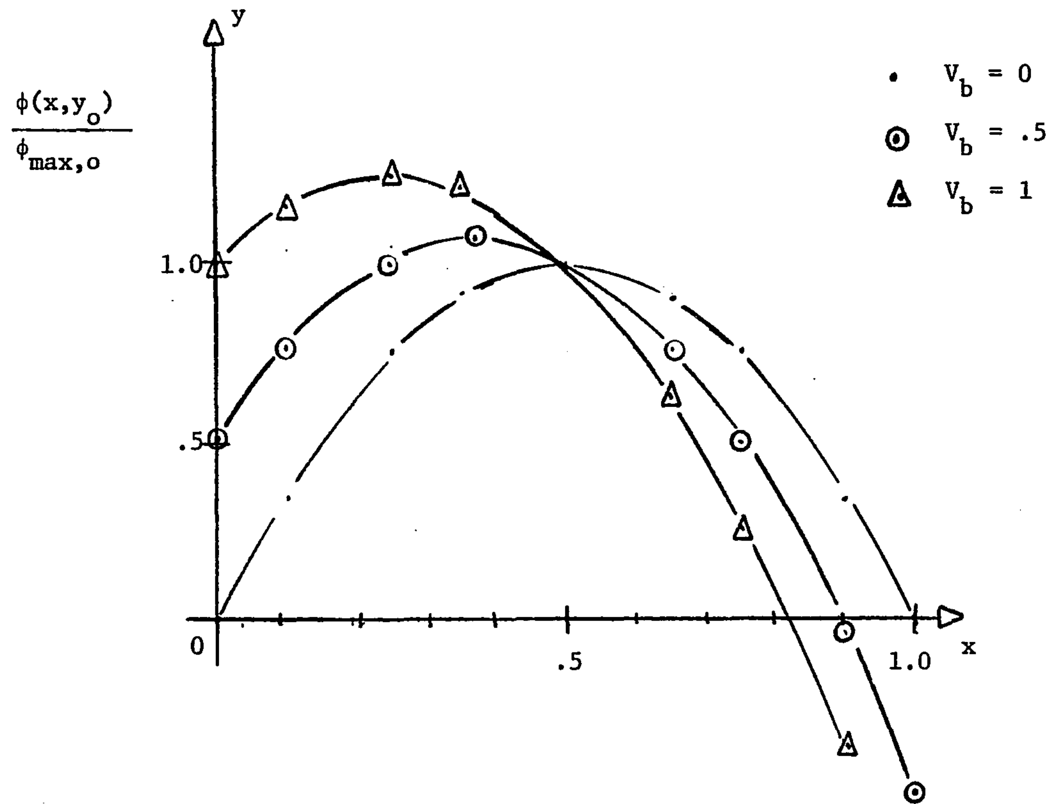

Fig. 3.6 Potential Profiles Along Constant y for Different Base End Potentials

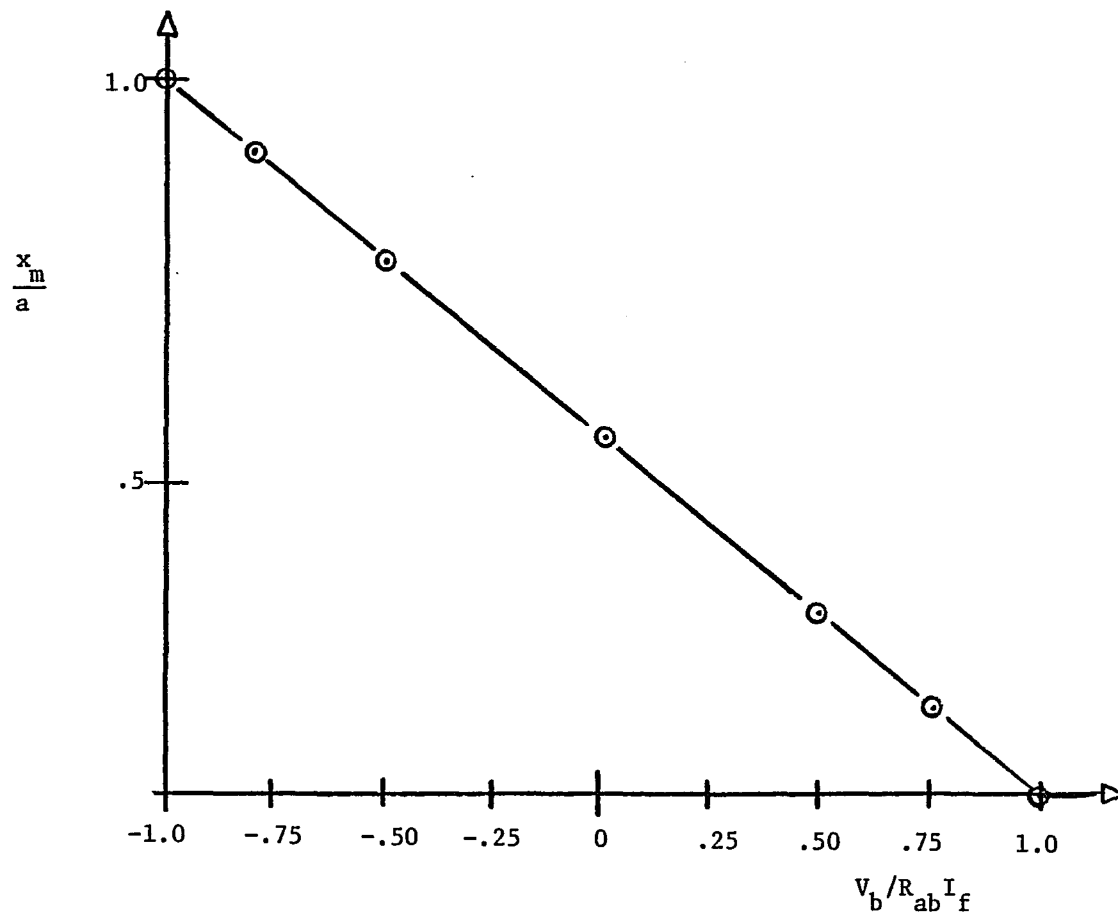

Fig. 3.7 Normalized Potential Maximum Location versus Normalized Base Drive Voltage

matrices result as we attempt to improve the resolution by reducing the size of the subregion.

The method of Green's Function is not as easily applied. Boundary conditions over only part of a side of the region require solution of a secondary problem, a Fredholm Integral equation, before the primary problem can be resolved. Generalization to other than rectangular structures requires a similar secondary solution. However, the resulting mathematical relations are easily programmed and high accuracy can be achieved. The form of the time varying problem in the transform space aids in analysis and design by facilitating the identification of the dominant poles. Direct frequency response is obtained easier than from the Finite Difference solution. In general, the Finite Difference method offers an advantage where a qualitative behavior is desired. The method of Green's Functions results in a more complete solution suitable for design as well as analysis.

CHAPTER 4

CDD CHARACTERISTICS

The transfer characteristics of a device relate the functional dependence of the output variable to the input signal. We have obtained the two-dimensional base voltage distribution as the solution to the d-KPDE and now will use this information to generate the remaining elements of the block diagram transfer relations of Fig. 2.3. In this chapter we develop the emitter and collector behaviors, then combine the partial responses to form the terminal characteristics of the CDD. Experimental measurements on the CDD prototype are given to demonstrate domain action and to confirm the analysis. Finally, a discussion of the dominant thermal effects is given.

It is a basic premise of this dissertation that the behavior of Carrier Domain Devices can be adequately represented by a two-dimensional analysis. This stems from the fact that the distributed interactions we seek to control require a relatively large planar geometry in order to manifest their nature. However, as was done in Chapter 3, we will apply the analysis to the one-dimensional structure whenever possible. Our interest in this limiting case is not based solely upon the simplicity of the resulting expressions, but more importantly upon the fact that, since large aspect ratios enhance the distributed effects, effective CDD design will exhibit elongated structures. Thus, specializing our results to the one-dimensional case does not represent

a serious limitation but rather the analysis of a large and useful class of Carrier Domain Devices.

Emitter Current Density

From the classical diode equation, as is shown for example by Sze [1969], we can write the emitter current density as

$$J_E(x,y) = J_S[\exp(V_{BE}(x,y)/V_o) - 1] \tag{4.1}$$

where

J_S = Junction saturation current / unit area

$V_{BE}(x,y)$ = Base-emitter forward bias

V_o = KT/q

Since the emitter is a low resistivity region and it is metallized along its entire length, it is everywhere at the same potential, allowing us to express the agrument in the exponential term as the difference between the spatial dependent base potential and the bias dependent terminal emitter voltage, V_E.

$$V_{BE}(x,y) = \phi_B(x,y) - V_E(V_a, V_b, I_E)/V_o \tag{4.2}$$

$V_E(V_a, V_b, I_E)$ is as yet, an unknown function.

Equation (4.1) is modified to

$$J_E(x,y) = J_S \exp [\phi_B(x,y) - \phi_{Bmax} - (V_E/V_o - \phi_{Bmax})] - J_S$$

$$= J_o \exp [\phi_B(x,y) - \phi_{Bmax}] - J_S \tag{4.3}$$

where

$$J_o = J_S \exp [\phi_{Bmax} - V_E/V_o]$$

ϕ_{Bmax} = the maximum of the dimensionless base potential

We have exchanged the unknown V_E for the new parameter J_o. If we require Eq. (4.3) to satisfy the conservation of current condition, we have

$$I_E = \iint_{\text{Emitter}} J_E(x,y)\ dxdy$$

$$I_E = J_o \iint_{\text{Emitter}} \exp [\phi_B(x,y) - \phi_{Bmax}]\ dxdy + J_S A_E \qquad (4.4)$$

In general, the saturation current $J_S \cdot A_E$ is orders of magnitude smaller than I_E and can be neglected. Since only J_o is unknown in Eq. (4.4), we can obtain

$$J_o = \frac{I_E}{\iint_{\text{Emitter}} \exp [\phi_B(x,y) - \phi_{Bmax}]\ dxdy} \qquad (4.5)$$

Substitution of Eq. (4.5) into Eq. (4.3) yields the emitter current density. If we let $\phi_B(x,y) = \phi_{Bmax}$ in Eq. (4.3), we identify J_o as being the maximum current density injected along the emitter. This new parameter serves as an indication of the extent of current crowding that is achieved. Larger ratios of the peak current density to the

average current density

$$\frac{J_o}{(I_E/A_E)}$$

correspond to a higher degree of current containment, that is, to more restricted domains.

Once the base distribution is known, Eq. (4.5) can be evaluated numerically for the parameter J_o which can then be used in Eq. (4.3) to yield the emitter response. For the limiting one-dimensional case, this response is especially simple. Equation (4.5) becomes

$$J_o = \frac{I_E}{a \cdot w \int_o^1 \exp \{\phi_B(x,\bar{y}) - \phi_{Bmax}\} \, dx} \tag{4.6}$$

where $\bar{y}$ is the average ordinate of the emitter, w is the width and a the length. Since the emitter is assumed narrow, there will be a negligible potential variation in the y-direction and the integration with respect to y introduced the factor w. We approximate the function in the integral remaining by its one-dimensional form

$$\phi_B(x,\bar{y}) = - \frac{R_{ab} \ I_f}{2V_o \ a^2} (x-x_m)^2 + \phi_{Bmax} \tag{4.7}$$

where

$R_{ab} = \rho_s' \ a/b$ = end-to-end base resistance

x_m = abscissa of the maximum potential

$$= a \left\{ \frac{V_B - V_A}{R_{ab}\ I_f} + \frac{1}{2} \right\}$$

ϕ_{Bmax} = maximum base potential along the ordinate $\overline{y}$

$$= \frac{V_a}{V_o} + \frac{R_{ab}\ I_f}{2V_o} \left[\frac{V_B - V_A}{R_{ab}\ I_f} + \frac{1}{2} \right]^2$$

I_f = total MOS bias current entering the base

Equation (4.7) is further simplified by introducing the characteristic length ℓ_o, discussed in Chapter 3, to

$$\phi_B(x,\overline{y}) = - (x-x_m)^2/\ell_o^2 + \phi_{Bmax} \tag{4.8}$$

where

$$\ell_o = a\sqrt{2V_o/R_{ab}I_f}$$

and the emitter current density, Eq. (4.3), becomes

$$J_E(x,\overline{y}) = J_o \exp \{- (x-x_m)^2/\ell_o^2 \} \tag{4.9}$$

where we have again neglected J_S. Since the distribution of Eq. (4.9) is Gaussian, the parameter ℓ_o is seen to be proportional to the standard deviation, σ.

$$\ell_o = \sqrt{2}\,\sigma$$

A measure of the domain width can now be given. At the coordinate points

$$x_{1/2} = x_m \pm \ell_o \sqrt{\ln(2)}$$

$$= x_m \pm \ell_o \ (.833)$$

The current density is half of its peak value. Since 76% of the current flows between these points, we define the effective domain width to be

$$w_d \approx 2\ \ell_o (.833)$$

The parameter ℓ_o, and therefore the domain width, cannot be made arbitrarily small. As the current is confined to a smaller portion of the emitter length, parts of the junction become reverse biased. If breakdown occurs at any part of the reverse biased junction, the domain signal will be lost. For a typical junction transistor a breakdown voltage of 7 volts can be expected and since the maximum reverse voltage, which occurs at one end when the domain is at the opposite end, is approximately $R_{ab} I_f / 2$ volts, the minimum ℓ_o is

$$\ell_{omin} = a \sqrt{V_o / V_{BKD}} = a \ (.061)$$

This results in a minimum domain width as defined by the 50% points of

$$w_{d,min} = 2\ \ell_o \sqrt{\ln 2}$$

$$= .1016\ a$$

corresponding to a confinement of the current to approximately 10% of the emitter length. Smaller domains can be obtained by reducing the base doping level which increases the breakdown voltage of the junction thereby reducing ℓ_{omin}. For example, assuming a one-sided step junction for which the breakdown voltage is inversely proportional to the base doping level [Grove, 1967], if we reduce the base impurity concentration by a factor of four, we halve ℓ_o making possible domains constrained to 5% of the emitter length.

Equation (4.6) is most easily solved by introducing a change of variables

$$U = \frac{x - x_m}{\ell_o} \cdot \sqrt{2} \tag{4.10}$$

transforming the integral to

$$J_o = \frac{I_E}{w\ell_o\sqrt{\pi} \displaystyle\int_{\frac{-x_m\sqrt{2}}{\ell_o}}^{\frac{a-x_m}{\ell_o}\sqrt{2}} \frac{\exp(-U^2/2)\ dU}{\sqrt{2\pi}}} \tag{4.11}$$

which casts it into the form of the normal probability distribution and can be obtained from mathematical tables. Note that for

$$\frac{x_m\sqrt{2}}{\ell_o} \gtrsim 3$$

The integral in Eq. (4.11) is approximately equal to 1.0 and the maximum current density is $(a/\ell_o\sqrt{\pi})$ times larger than the average current

density, that which would be obtained if the entire emitter were uniformly biased. When x_m does not satisfy the inequality, the tails of the distribution extend beyond the emitter region but the current must become zero and a truncated Gaussian distribution results. Requiring the total current to remain constant causes J_o to increase; when $x_m = 0$, the distribution is half Gaussian and J_o is increased by a factor of two over the full Gaussian distribution. This effect as well as the formation of current domains is demonstrated in Figures 4.1 through 4.4 where we have plotted the normalized current density

$$J_E(x,\overline{y})/(I_E/\omega\ \ell_o\ \sqrt{\pi})$$

as a function of normalized distance x/a for different values of ℓ_o/a.

The assumption of constant base-emitter potential along the y-direction, as demonstrated by the potential plot of Fig. 3.4, leads to a uniform current injection in this direction. Along the main axis, however, the potential can change significantly in units of V_o which results in enhanced injection about the maximum point. For $\ell_o = a$, Fig. 4.1, the domain is evident but is not well localized; as ℓ_o becomes smaller than a, the domain becomes more localized as shown in the succeeding figures. In any one figure, the area under each profile is constant and in each case equal to $\ell_o\sqrt{\pi}$. Thus the truncated distributions overlapping the emitter ends have greater maximum values as discussed earlier.

Although the analysis presented provides a complete description of the two-dimensional (and the limiting one-dimensional) behavior of

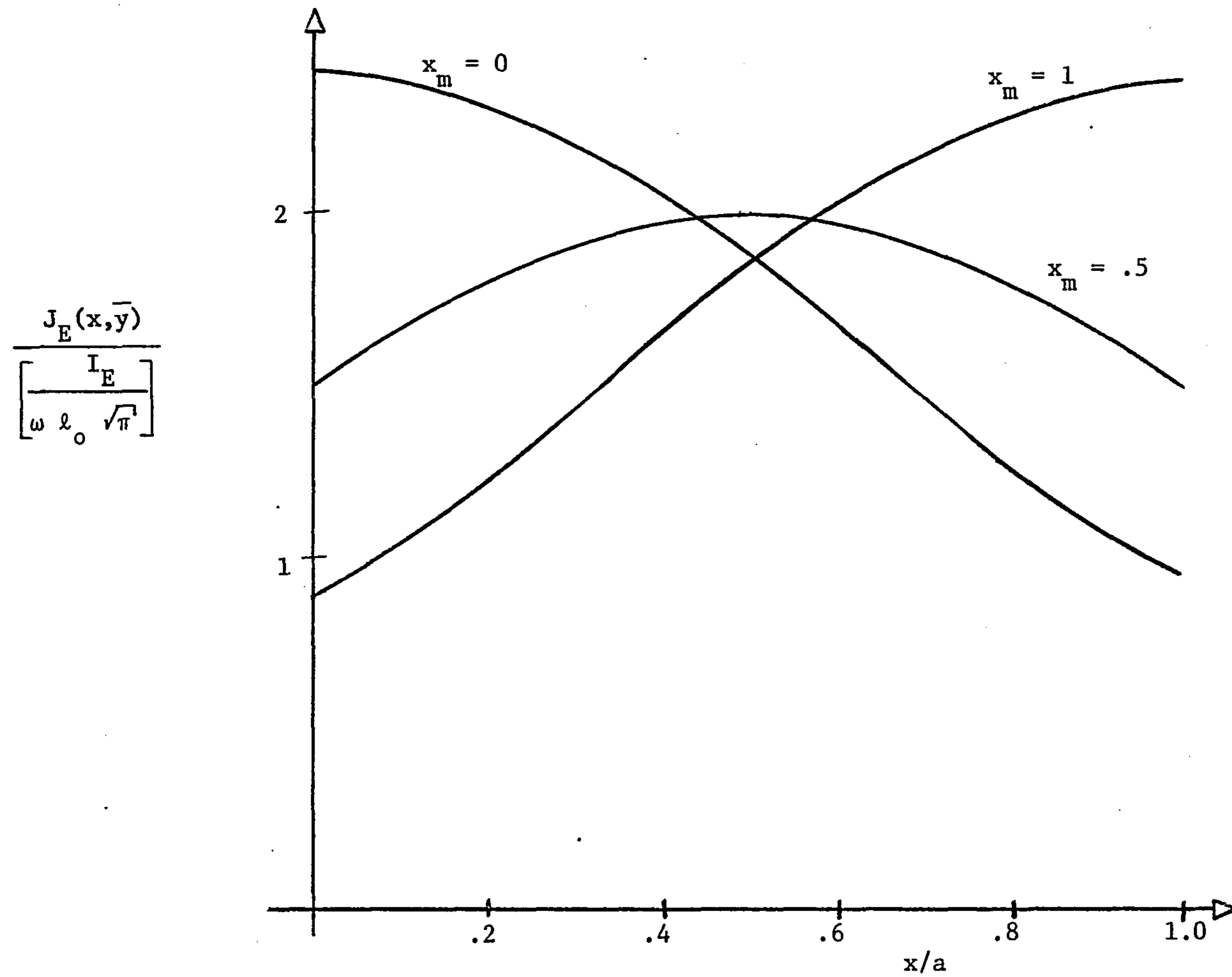

Fig. 4.1 Normalized Emitter Current Density as a Function of Normalized Distance x/a for $\ell_o = a$

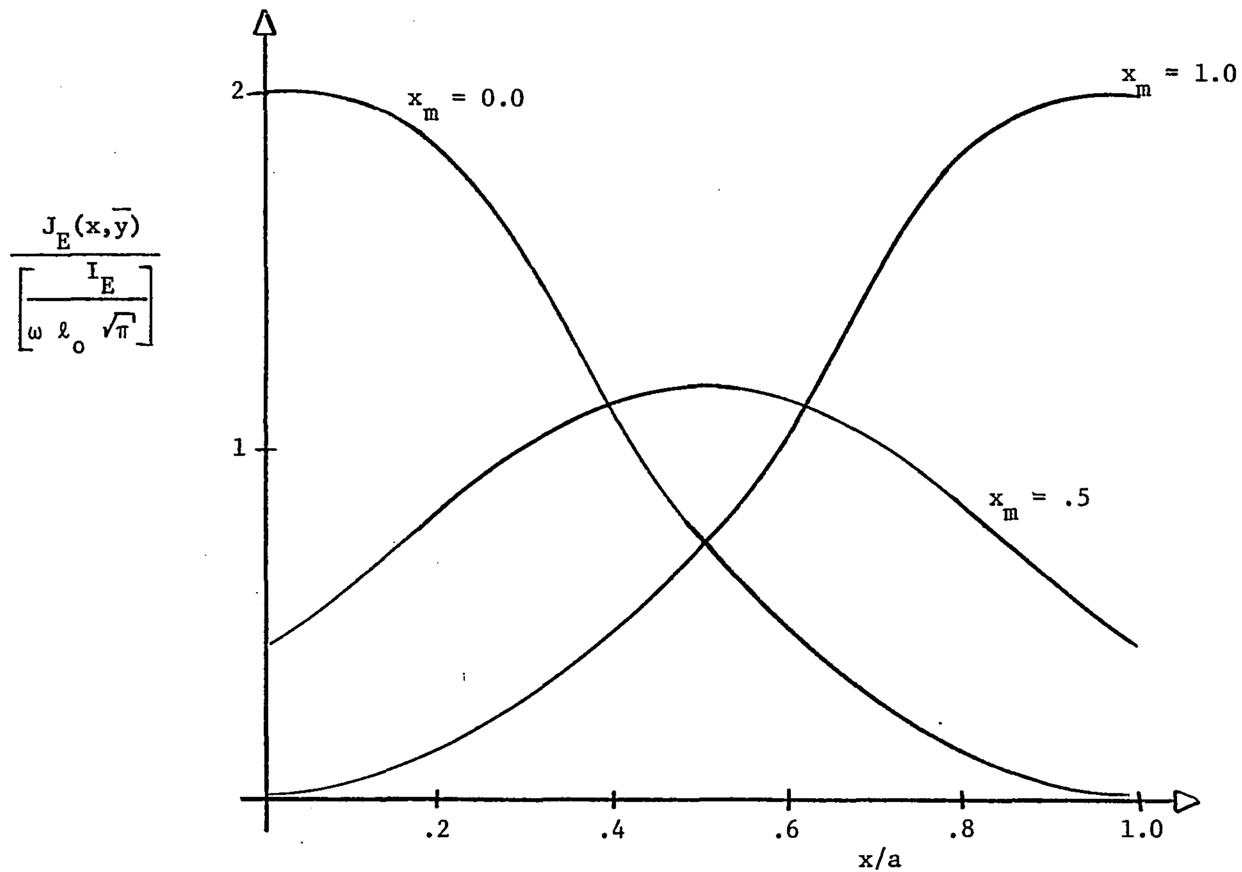

Fig. 4.2 Normalized Emitter Current Density versus Normalized x/a for $\ell_o = a/2$

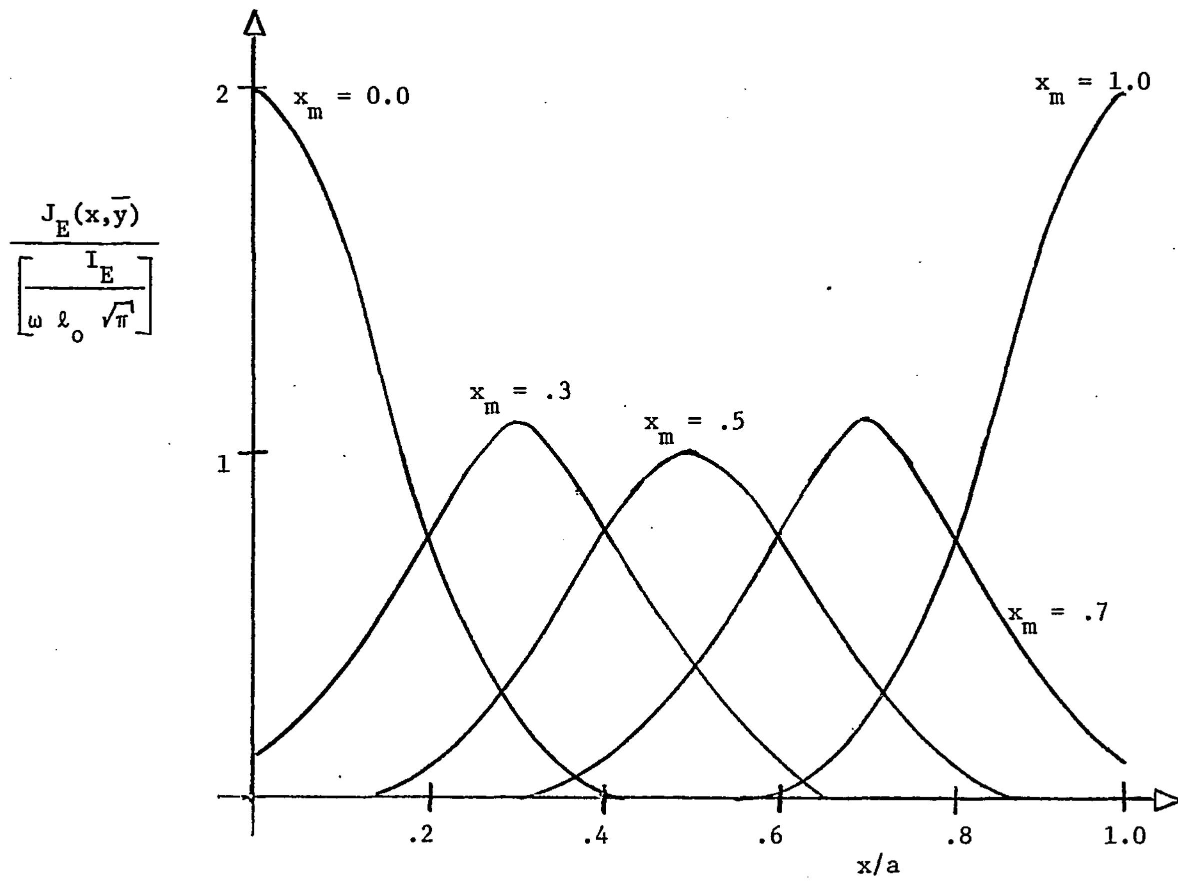

Fig. 4.3 Normalized Emitter Current Density versus Normalized Distance x/a for ℓ_o = .2a

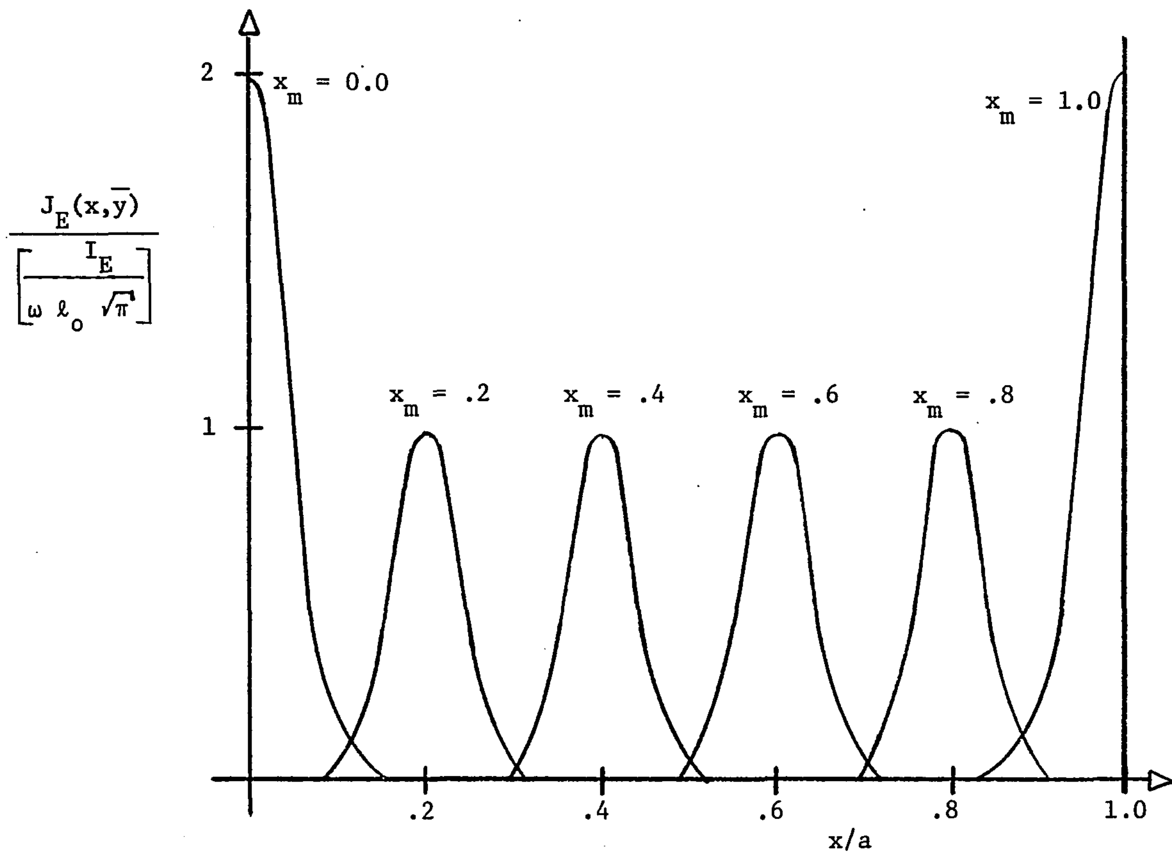

Fig. 4.4 Normalized Emitter Current Density versus Normalized Distance x/a for ℓ_o = .06a

the emitter-base structure of a CDD, the distribution are not observable as such since only terminal quantities are available. Partial verification is offered by the behavior of the emitter voltage. From Eq. (4.2), we see that the emitter voltage, V_E, is equal to the maximum base potential less the forward bias of the junction.

$$V_E = V_o \, \phi_{Bmax} - V_o \, \ell n \, J_o/J_s \tag{4.12}$$

The second term representing the forward bias of a junction having a current density J_o, is a weak function of the domain location and is in the range of .5 to .7 volts. This implies that V_E has the functional form of ϕ_{Bmax}

$$\phi_{Bmax} = \frac{a^2}{\ell_o^2} \left[\left(\frac{x_m}{a} - \frac{1}{2} \right)^2 + \frac{1}{4} \right]$$

$$= \frac{a^2}{\ell_o^2} \quad \frac{1}{4} + \frac{V_A^2}{V_o^2} \frac{\ell_o^2}{a^2} \tag{4.13}$$

That is, the emitter voltage is a quadratic function of V_A whose curvature decreases as ℓ_o^2 but whose minima increases as $1/\ell_o^2$. Figure 4.5 indicates V_E has this behavior; the plot indicated by circles has an effective ℓ_o/a of .11 while that denoted by triangles has $\ell_o/a \approx .063$.

Another important parameter relating to the emitter current distribution is its centroid $\langle x \rangle$.

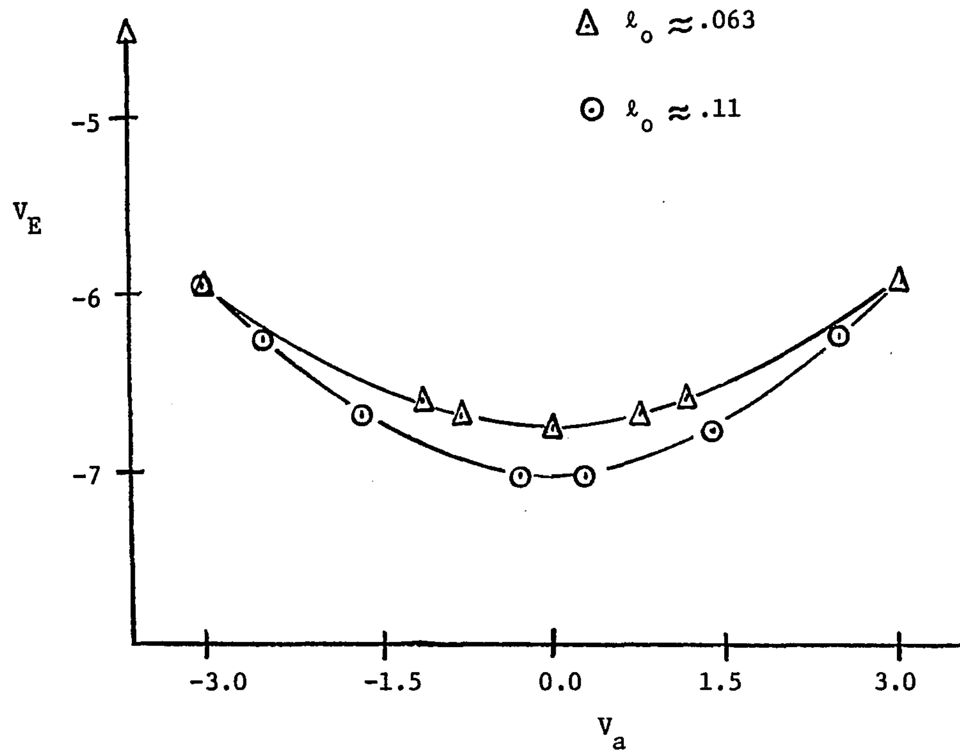

Fig. 4.5 Emitter Terminal Voltage as a Function of Applied Base Voltage V_a

$$\langle x \rangle = \frac{\int_{o}^{a} J_E(x,\bar{y})\ x\ dx}{I_E/\omega} \tag{4.14}$$

Substituting Eq. (4.9) into Eq. (4.14), we obtain

$$\langle x \rangle = \frac{J_o}{(I_E/\omega)} \int_{o}^{a} x \exp\ [-(x-x_m)^2/\ell_o^2]\ dx \tag{4.15}$$

which, after integrating by parts becomes

$$\langle x \rangle = x_m - \frac{\ell_o \left\{ \exp\left[-\left(\frac{a-x_m}{\ell_o} \right)^2 \right] - \exp\left[-(x_m/\ell_o)^2 \right] \right\}}{2\sqrt{\pi} \displaystyle\int_{\frac{-x_m\sqrt{2}}{\ell_o}}^{\frac{a-x_m}{\ell_o}\sqrt{2}} \frac{\exp\ [-\omega^2/2]\ d\omega}{\sqrt{2\pi}}} \tag{4.16}$$

and relates the deviation of the centroid from the position of maximum base potential. It is evident from Eq. (4.16) that the maximum deviation occurs when the domain is positioned at either extreme of the emitter and that it is symmetrical with respect to the midpoint. For $a/\ell_o \geq 2$, the integral is approximately .5 and the maximum deviation is

$$\langle x \rangle - x_m = \frac{\ell_o}{\sqrt{\pi}} \exp(-a^2/\ell_o^2)$$

$$\approx \frac{\ell_o}{\sqrt{\pi}}$$

For $\ell_o/a = .06$, the deviation is approximately 3% of full scale. Both the domain centroid and the characteristic length, ℓ_o, are discussed further in the following section.

The Collector Currents

The collector structure of our CDD prototype is similar to that used by Smith [1974]. He showed that the terminal collector currents due to a point current source as shown in Fig. 4.6 follow a resistive divider law that is independent of the y-coordinate. The terminal response is given by Equations (1.2a) and (1.2b), repeated here

$$I_{C1} = I(1/2 - \lambda) \tag{4.16a}$$

$$I_{C2} = I(1/2 + \lambda) \tag{4.16b}$$

For an arbitrary injection current distribution, since Equations (4.17) are linear, we can take a superposition integral over the distribution to obtain the total terminal collector currents.

$$I_{C1} = \iint_{\text{Emitter}} J_E(x,y)(1-x)\, dxdy \tag{4.17a}$$

$$I_{C2} = \iint_{\text{Emitter}} J_E(x,y)\, x\, dxdy \tag{4.17b}$$

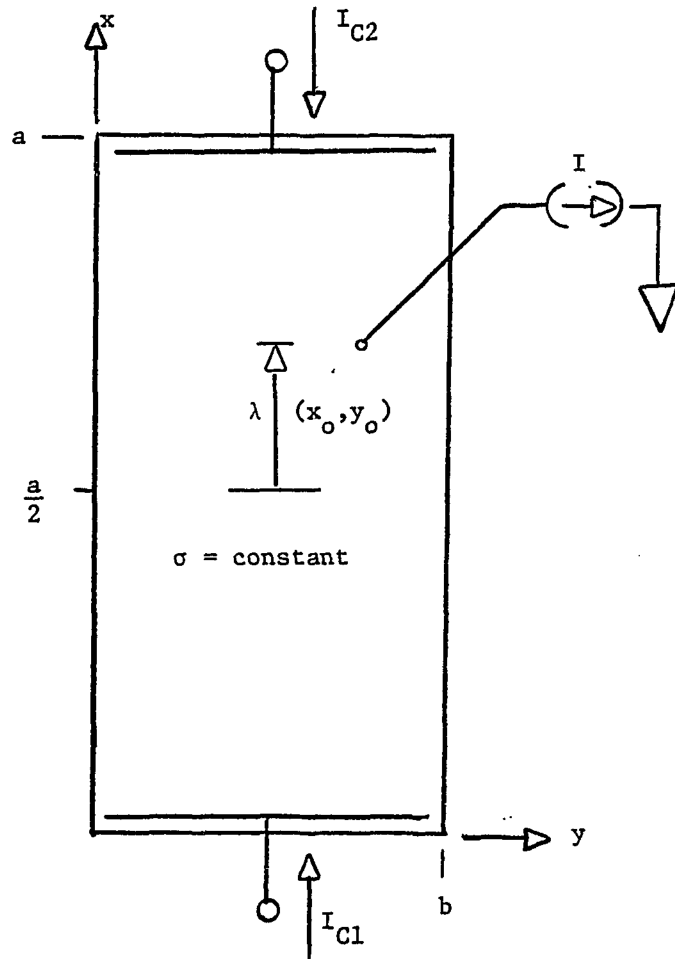

Fig. 4.6 Idealized Collector Structure Used to Determine the Current Division Law for a Point Source Excitation Located at (x_o,y_o)

If we divide Equations (4.17a and b) by I_E and again assume no variation in the y-direction, we obtain the distribution centroids referenced to each end of the emitter. Thus, the collector response is completely characterized by the first moment of the emitter current density distribution. λ in Equations (4.16a and b) for a general source distribution becomes

$$\lambda = \langle x \rangle - 1/2 \tag{4.18}$$

the center-reference centroid. We have shown, however, that the centroid and the location of the base potential maxima x_m, deviate significantly only when the domain approaches either end of the emitter. If we replace $\langle x \rangle$ by x_m in Eq. (4.18) an approximation is obtained whose greatest error can be reduced to 3% of full scale and becomes negligible when the domain is at least 2 ℓ_o from either end. However, the useful linear dynamic range coincides with the region where x_m is in good agreement with the domain centroid. This is due to the symmetry of the distribution about x_m when the distribution is not truncated at the emitter ends. Figure 4.7 shows the centroid normalized by $\ell_o/\sqrt{\pi}$ as a function of x_m/ℓ_o. The linear region extends over

$$2\ \ell_o \leq x_m \leq a - 2\ \ell_o$$

with a negligible error (< .009 a).

The terminal collector currents for a general structure are not obtained this easily. First, the kernel in the integrand of Eq. (2.3) must be obtained by solving a boundary value problem similar to the one solved for the base region in Chapter 3. Once this is done, the

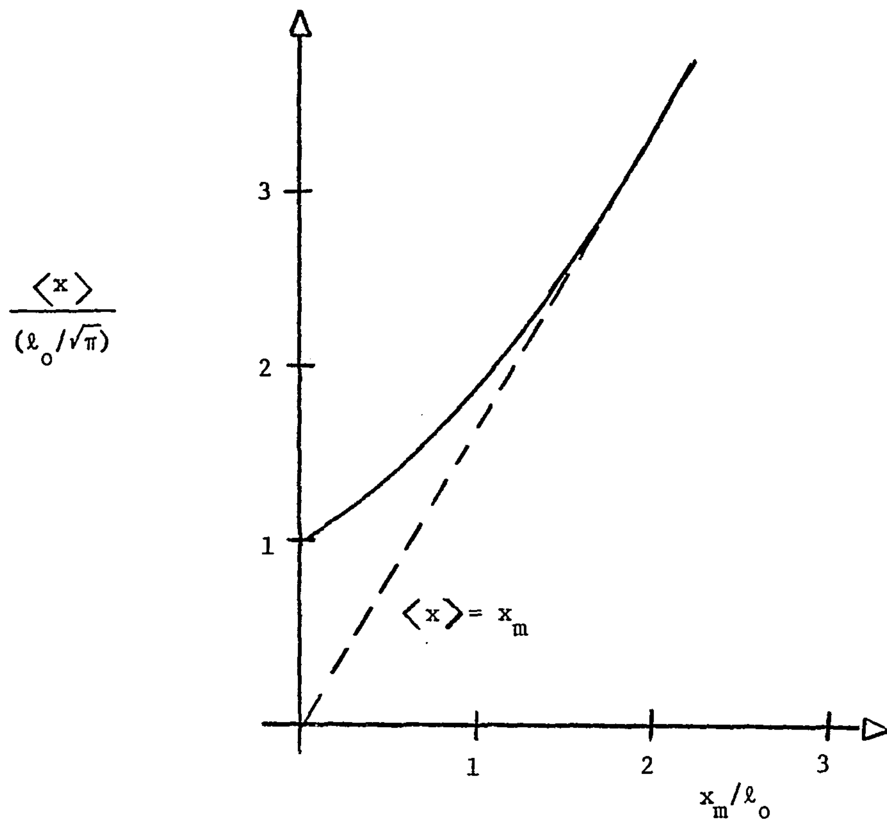

Fig. 4.7 Domain Centroid Normalized by $\ell_o \sqrt{\pi}$ as a Function of the Base Potential Maxima Expressed in Units of ℓ_o

procedure is identical to that for the above case. This generalization is discussed further in Chapter 6.

The Composite Model

Having discussed separately the dominant behavior of the base, emitter and collector regions, we can now synthesize the composite device characteristics. Briefly, the base is biased by its end contacts and the MOS transistor such that a non-uniform potential distribution is produced. The emitter, assumed to be a constant potential region, is caused to inject preferentially about the base potential maxima. Finally, the collector divides the injected current into terminal currents that are weighted functions of the centroid of the domain. For small characteristic lengths, Equations (4.16) are approximated adequately by replacing λ by $(1/2 - x_m/a)$, the location of the base potential maxima referred to the center of the emitter. This mobile element transistor behavior can be modeled as a potentiometer with an electronically adjustable wiper shown in Fig. 4.8.

Rather than process the individual collector currents, if we subtract one from the other we produce

$$I_{C2} - I_{C1} = 2I_E \lambda \qquad (4.19)$$

This represents two-quadrant multiplier behavior; λ can be positive or negative but I_E is strictly positive. Letting λ be

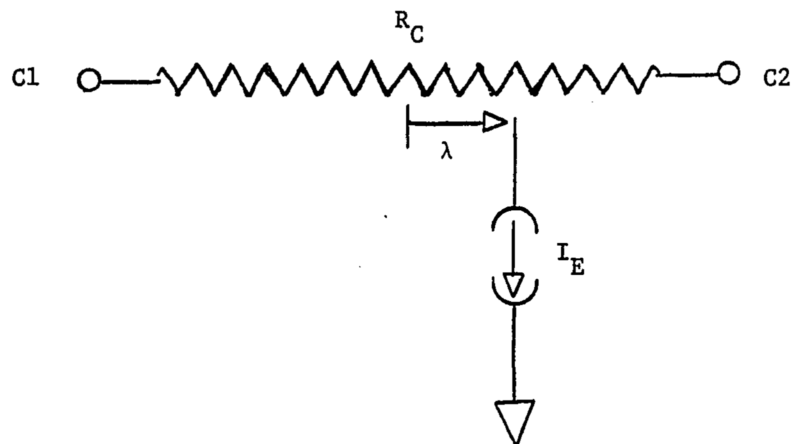

Fig. 4.8 CDD Model -- Potentiometer with an Electronically Positionable Wiper Contact

$$\lambda = \frac{1}{2} - x_m/a$$

$$\lambda = \frac{2V_a}{R_{ab} I_f} \tag{4.20}$$

We see that if we plot $(I_{C2} - I_{C1})$ versus $(2V_a)$, we should obtain a straight line over the range that Eq. (4.20) holds, that is, as long as the domain is sufficiently removed from the emitter ends. Also, the linear range should increase as ℓ_o is made smaller. This behavior is demonstrated in Figures 4.9 through 4.12, where we plot a voltage proportional to the difference of the collector currents against $2V_a$. In Fig. 4.10, the MOS device is cutoff. The emitter current crowds at either extreme except for small differences in base end voltages when the bias is almost uniform. The linear region is limited to $|2V_a| \leq$ .25 volts. Progressively, as we increase the MOS gate voltage to inject more bias current into the base region (making ℓ_o smaller), the linear region increase indicating smaller domains are being formed. The gain of the device (the slope at the origin) decreases in agreement with Eq. (4.20).

The Two-Quadrant Multiplier

We have already stated that a two-quadrant multiplier function is performed by our CDD prototype. If we express the terminal emitter current as

$$I_E = I_o(1 + \alpha) \tag{4.21}$$

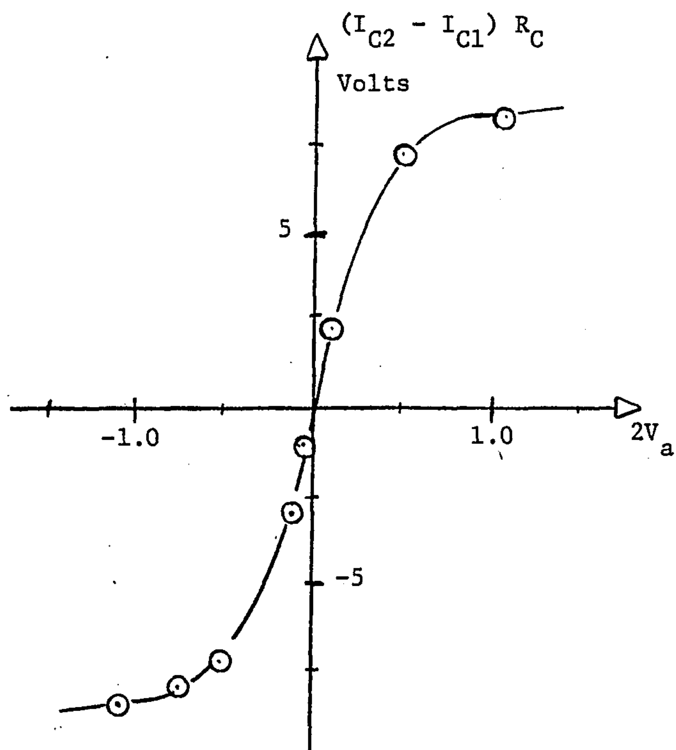

Fig. 4.9 CDD Transfer Characteristics $(I_{C2}-I_{C1})\ R_C$ versus $2V_a$ for $V_G = 0$

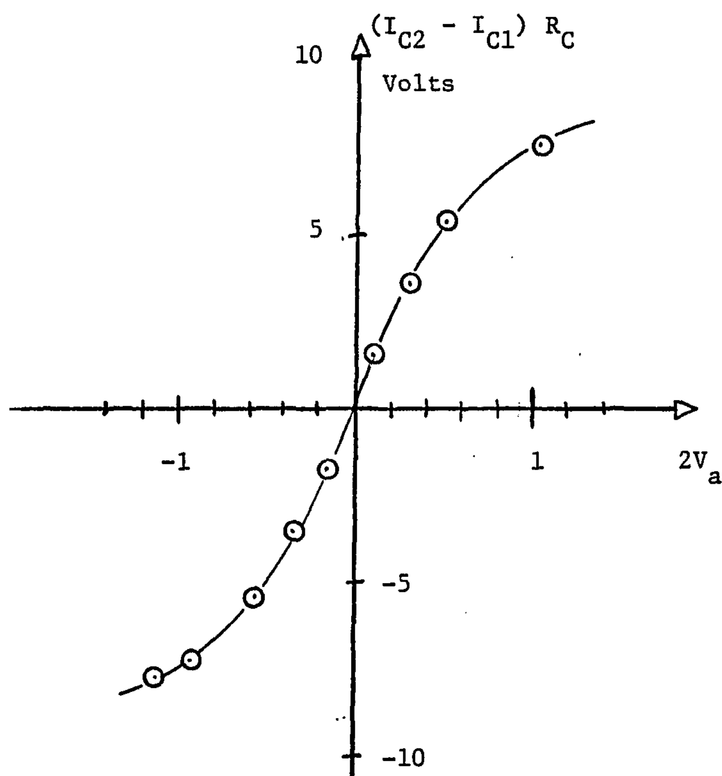

Fig. 4.10 CDD Transfer Characteristics for $V_G = -10$ Volts

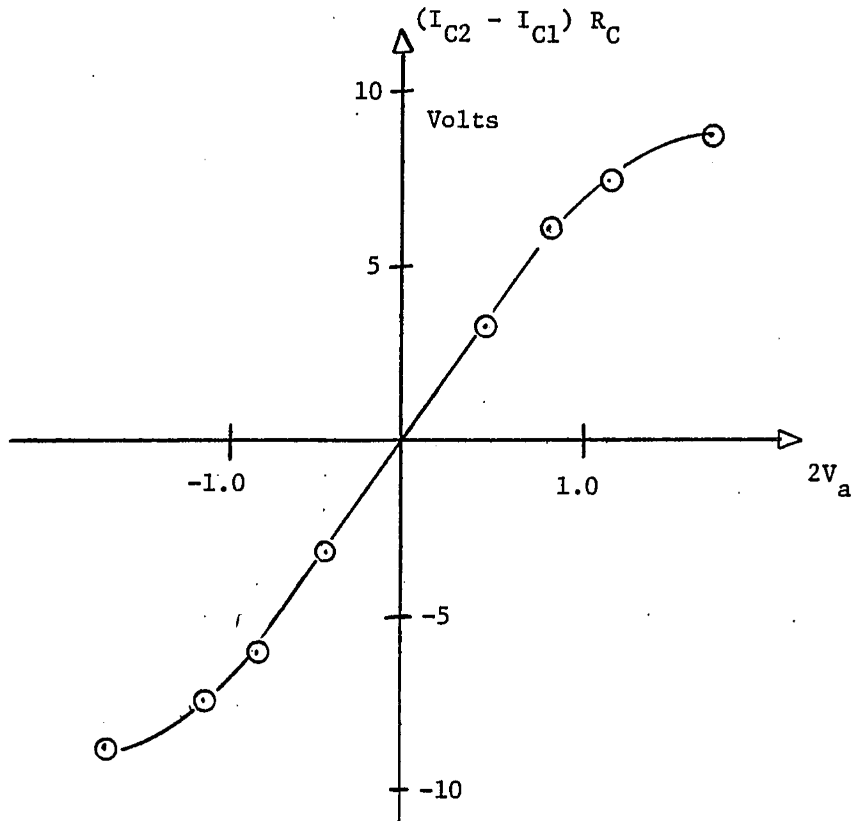

Fig. 4.11 CDD Characteristics for V_G = -15 Volts

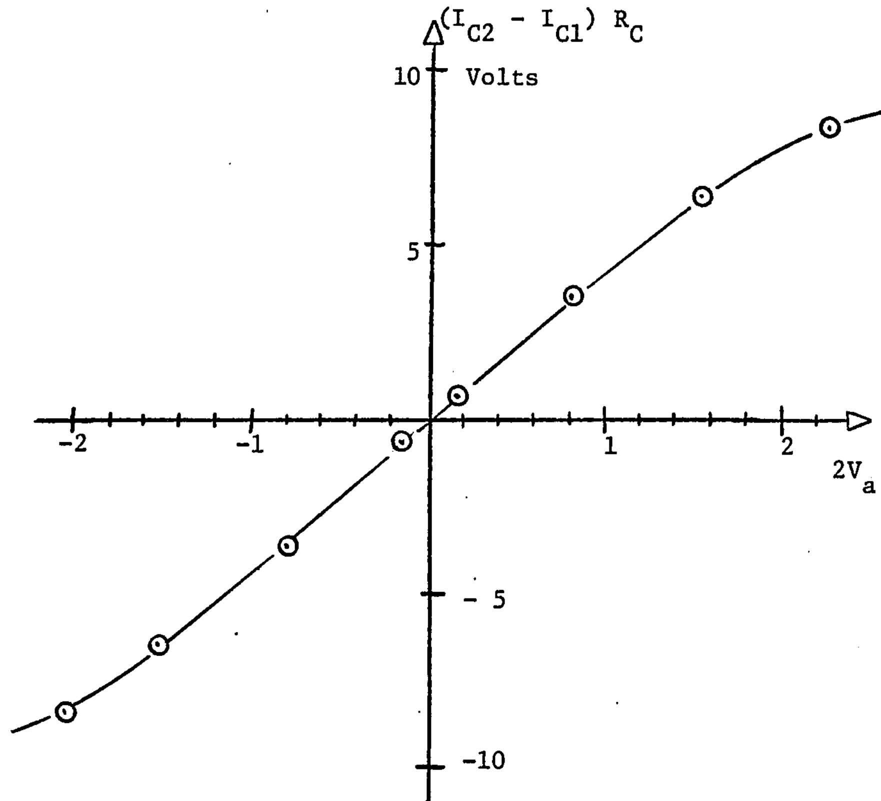

Fig. 4.12 CDD Characteristics for V_G = -25 Volts

I_o is the D.C. bias current and α, a small signal that may be a function of time and confined to the range $-1 \leq \alpha(t) \leq 1$. Then, substituting Equations (4.21) and (4.20) into Eq. (4.19), we get

$$I_{C2} - I_{C1} = \frac{4\ v_a(t)}{R_{ab}\ I_f}\ [1 + \alpha(t)]\ I_o = k\ v_a(t)\ \ [1 + \alpha(t)] \qquad (4.22)$$

where we replace the base drive voltage by $v_a(t)$ denoting it as a small signal function of time. In Fig. 4.13(a) we show an oscilloscope trace of the product of a sine wave and an offset square wave, and in Fig. 4.13(b), the product of a sine wave and an offset triangle function. The bias and drive circuitry is shown in Fig. 4.14. We indicate the CDD by its potentiometer model and hold the two collectors at the same voltage by employing the transistor pair Q_1 and Q_2. The circuit enclosed by the dashed box forms the complementary and offset base drive from the sine wave input. Other applications are discussed in Chapter 6.

A Comment on Temperature Effects

Carrier Domain Devices and their associated drive circuitry have low thermal sensitivity. The drive requirements are met by circuits exhibiting a balance of transistor placement, inherently a low sensitivity design [See Gilbert, 1971 and 1975a]; the balanced pair tract in their thermal response decreasing that of the circuit. The primary temperature sensitive parameter is ℓ_o which depends approximately on temperature as

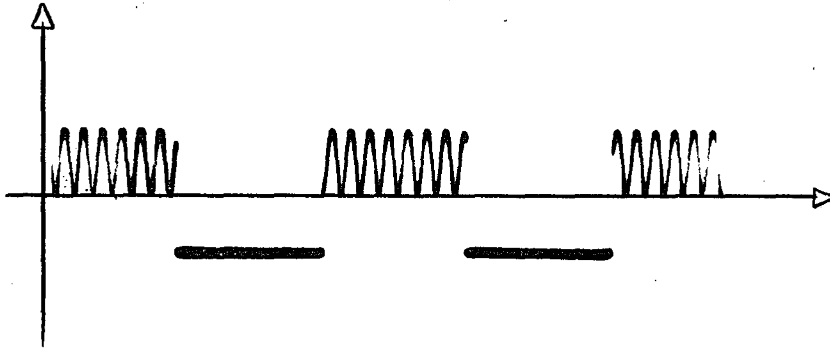

(a) 15 kHz sine x 1 kHz square wave

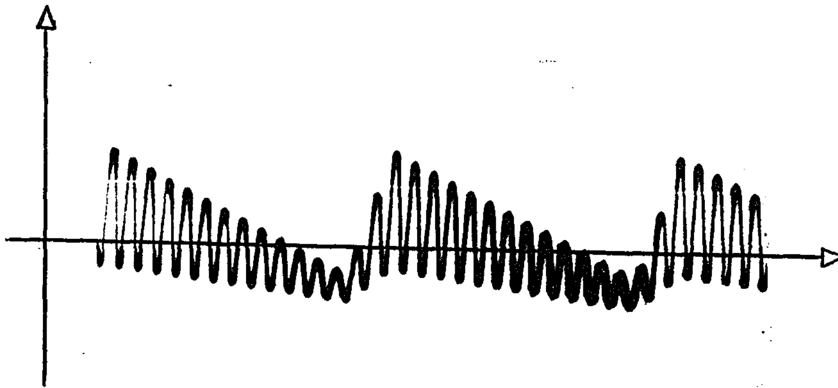

(b) 15 kHz sine x 1 kHz triangle function

Fig. 4.13 Output of CDD Two-Quadrant Multiplier

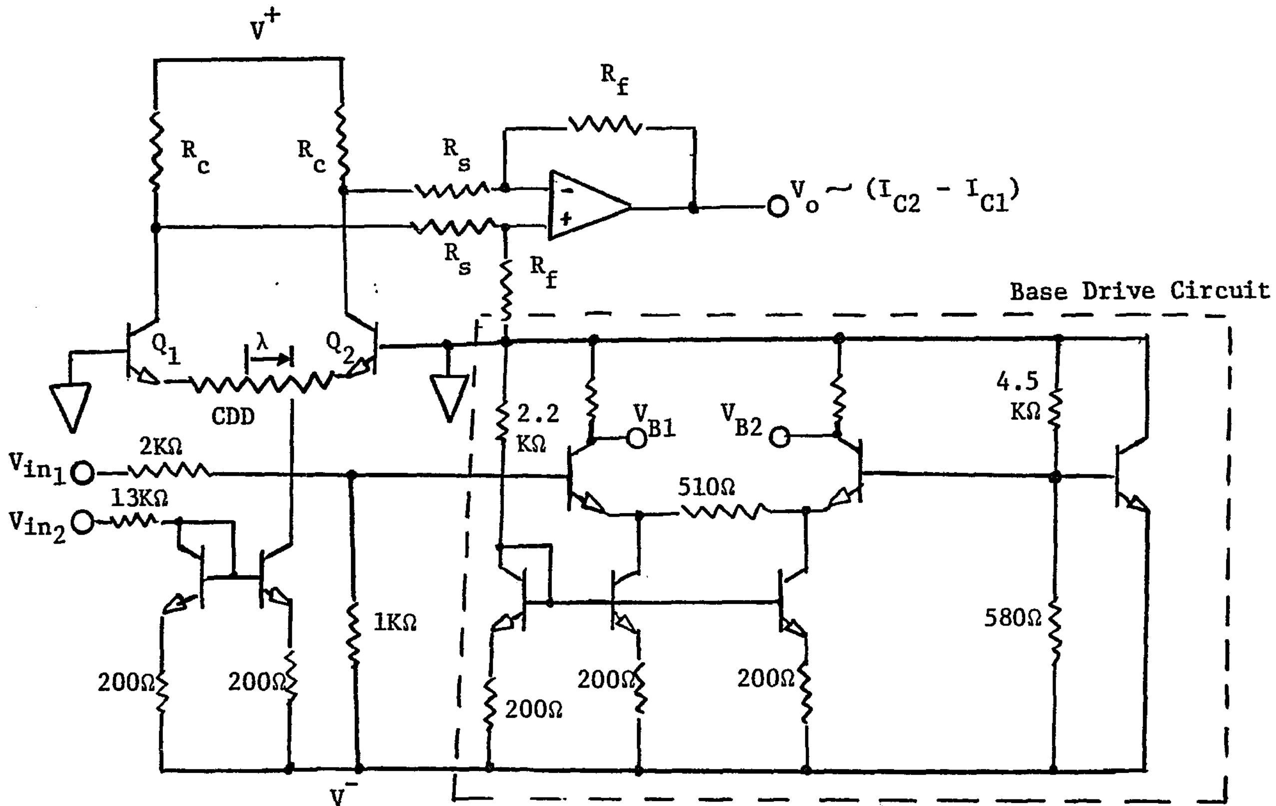

Fig. 4.14 Bias and Drive Circuitry to Obtain Two-Quadrant Multiplication

$$\ell_o(T) = \ell_o(T_o)\sqrt{1 + \delta T/T_o}$$

$$\approx \ell_o(T_o)\,(1 + \delta T/2T_o) \qquad (4.23)$$

T_o = Reference Temperature, 300°K

δT = change in temperature above $T_o << T_o$

with the net result is that ℓ_o increases as the temperature rises. For a 50°K rise in temperature from a reference point of 300°K, ℓ_o increases approximately 8%. This effect is demonstrated in Fig. 4.15, where we plot the error ($\langle x \rangle - x_m$) normalized by $\ell_o/\sqrt{\pi}$ for T = 300°K and T = 350°K.

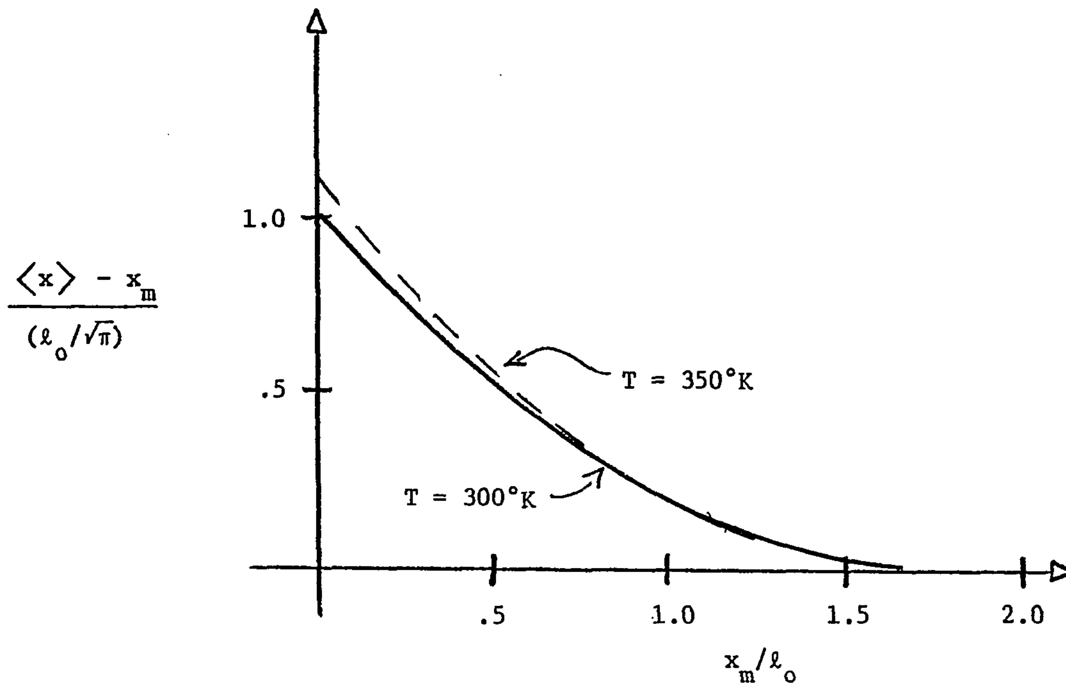

Fig. 4.15 Normalized Deviation of x_m from $\langle x \rangle$ as a Function of Potential Maxima
Note that the Deviation Becomes Negligible at $\sim 2\ \ell_o$ from the Emitter Ends.

CHAPTER 5

CDD APPLICATIONS

In this chapter we discuss particular applications of Carrier Domain Devices. The applications are intended to demonstrate the unique approach domain phenomena and spatial effects in general offer to electronic function design. As such, the means of achieving the transfer relations are not presented as optimum or even as having any particular advantage in this form over more conventional techniques, but for the expressed purpose of expanding the understanding of domain effects and its control. We concentrate on the rectangular bipolar design and its one-dimensional idealization. In Chapter 4 we presented a two-quadrant multiplier CDD realization. In this chapter we discuss a four-quadrant multiplier, an AGC amplifier, some spatial effects that produce A/D and D/A functions and some logic realizations.

A Four-Quadrant Multiplier

Electronic multiplication of two signals is used in communication systems and in processing signals in analog computers. In our discussion of the two-quadrant multiplier, we modeled the dominant effects as being functions of the domain centroid which is adequately represented by the location of the base potential maxima. We show the important parameters and geometry in Fig. 5.1. Subtraction of the terminal collector currents

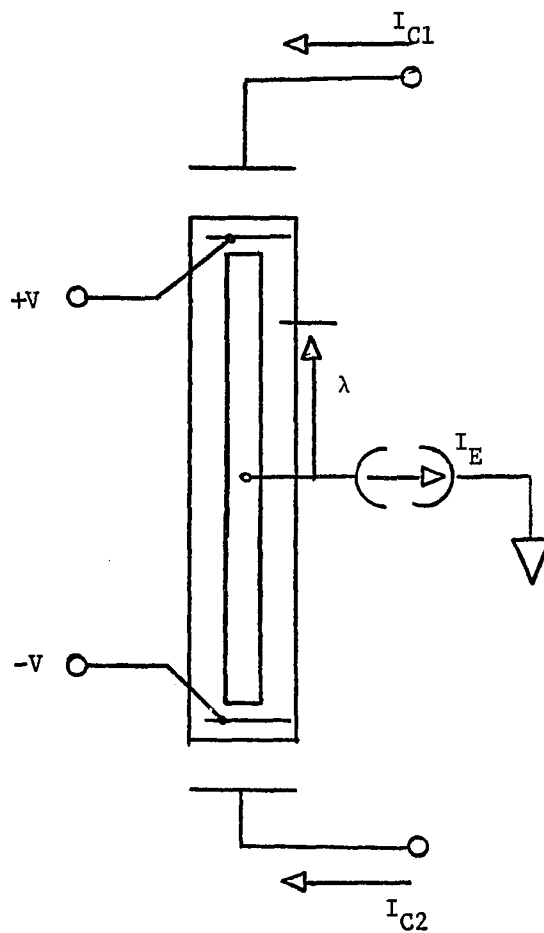

Fig. 5.1 Important CDD Parameters and Structure

yields an output that exhibits the features of two-quadrant multiplication. If, as shown in Fig. 5.2, two devices are cross-coupled, the individual collector currents become

$$I_{C1} = I_o(1 + \alpha)(1/2 + \lambda) \tag{5.1a}$$

$$I_{C2} = I_o(1 + \alpha)(1/2 - \lambda) \tag{5.1b}$$

$$I_{C3} = I_o(1 - \alpha)(1/2 - \lambda) \tag{5.1c}$$

$$I_{C4} = I_o(1 - \alpha)(1/2 + \lambda) \tag{5.1d}$$

Four-quadrant multiplication behavior is obtained by forming the linear combination

$$(I_{C1} + I_{C3}) - (I_{C2} + I_{C4}) = 4\ \alpha\ \lambda \tag{5.2}$$

The small signal parameter α is proportional to the complementary emitter current drives and is relatively device independent; λ is the centroid location referenced to the device center and is a function of device geometry and bias. This latter factor makes it essential to match the two devices; such matching can best be achieved by fabricating them side by side on the same substrate. For simplicity, however, we have used two independent MOS-bipolar CDD's to obtain the four-quadrant multiplier. Since λ is device dependent, Eq. (5.2) is changed to

$$(I_{C1} + I_{C3}) - (I_{C2} + I_{C4}) = 2\alpha(\lambda_1 + \lambda_2) + (\lambda_1 - \lambda_2) \tag{5.3}$$

For the matched condition $\lambda_1 = \lambda_2$, this reduces to Eq. (5.2). In

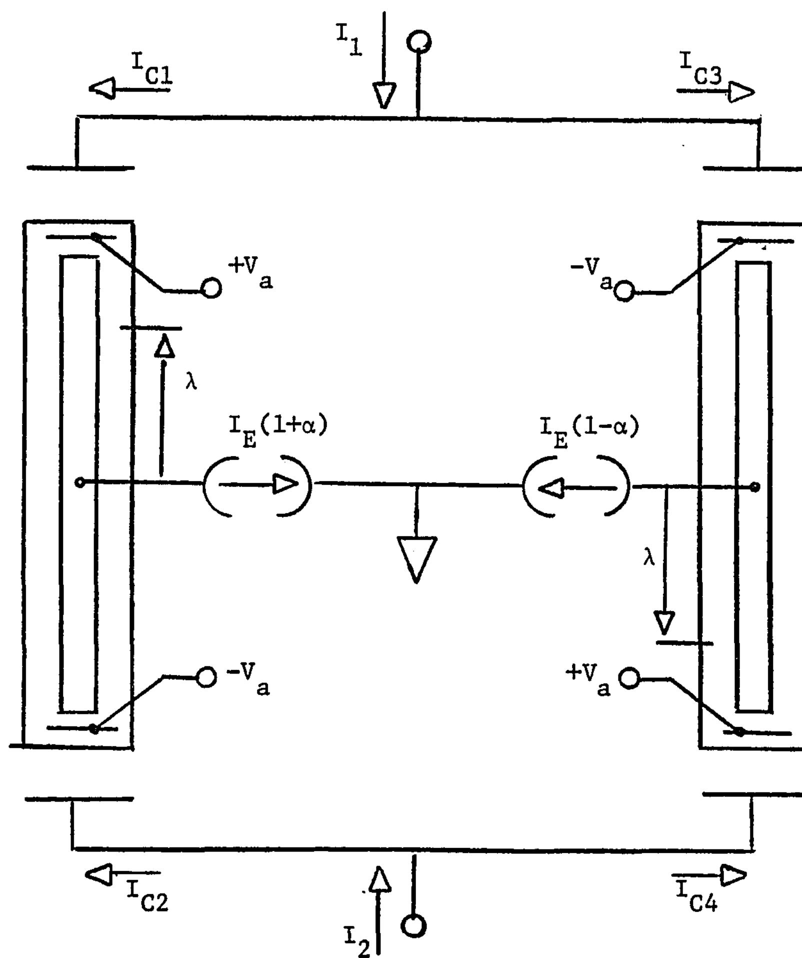

Fig. 5.2 Two CDD's Cross-Coupled to Produce Four-Quadrant Multiplication

Fig. 5.3 we show the output of a multiplier realization when the input signals are a 15 kHz sine wave and a triangle wave of 1 kHz. The products of a sine wave with a square wave and with a sine wave of another frequency are shown in Fig. 5.4a and b. Note that in Fig. 5.4a, the output does not become identically zero during the low portion of the square wave but rather that a residual output is observed. This is due to the mismatch between the devices used.

The drive requirements of the device demand special consideration. For the emitter, we must supply complementary current signal superimposed upon a quiescent bias level; the base requires a complementary voltage drive, also offset, and a constant sheet bias current supplied by the MOS transistor operated in its saturated region. The collectors, in order that the current division mode be primarily spatially defined, must both be maintained at the same voltage. These requirements are met by the circuit shown in Fig. 5.5. The current signals are converted to a voltage output by the resistors R_C and the subtraction operation is then performed by the op-amp circuit. Individual gate voltages can be used to match the dynamic responses of the devices but this adds a complication that should not be necessary if adjacent devices are used.

An AGC Amplifier

In many applications, the total linear gain that a signal undergoes in a processing system must be varied to account for changes in signal strengths in order to maintain a constant detected signal level. A good example of such a need is an audio system in which the broadcast

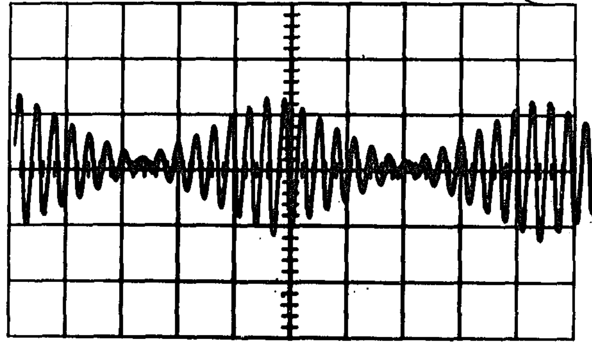

(a) 15 kHz sine x 1 kHz triangle

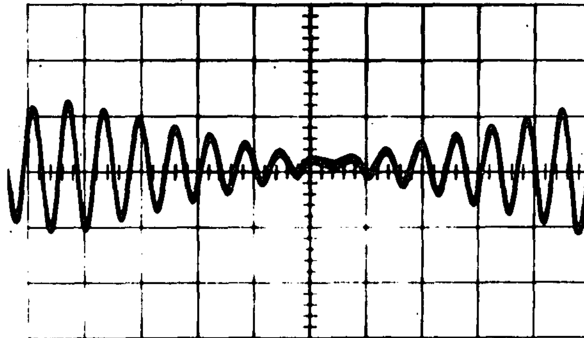

(b) Expansion of region near a zero

Fig. 5.3 Four Quadrant Multiplication of a Sine Wave with a Triangle Wave

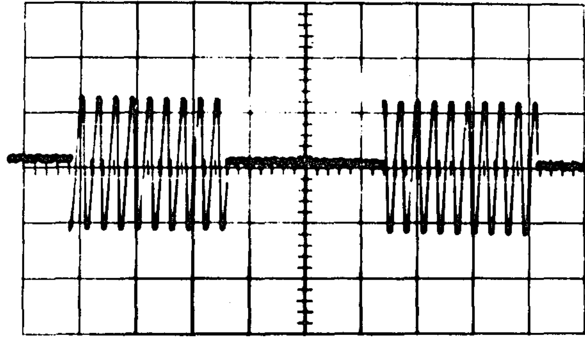

(a) 15 kHz sine x 1 kHz square wave

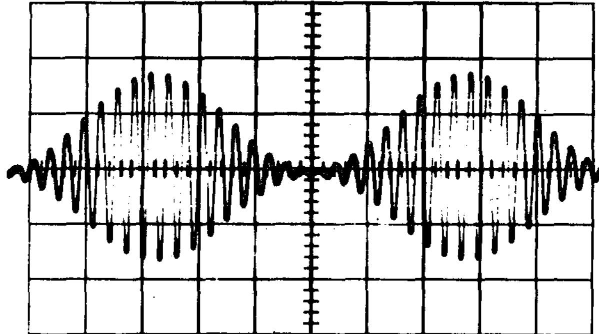

(b) 15 kHz sine x 1 kHz sine wave

Fig. 5.4 Output of Four-Quadrant Multiplier

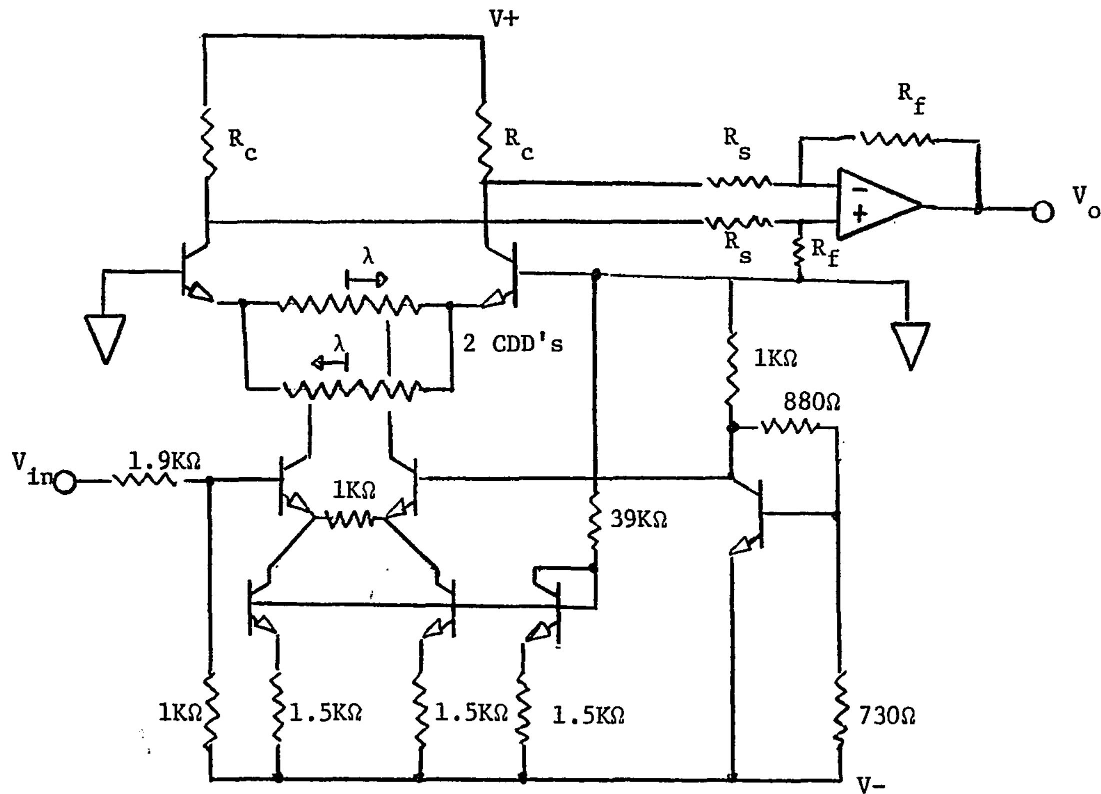

Fig. 5.5 Drive Circuit to Produce Four-Quadrant Multiplication

Note: Base Drive Not Shown.

signal may suffer amplitude changes over a period of time that, in a constant gain detector, would cause the volume to fluctuate. To prevent this, a stage is included in the amplification path whose gain is controlled by a feedback signal proportional to the output level. Figure 5.6 shows the block diagram of an Automatic Gain Control (AGC) circuit. The low pass filter is used to prevent cancellation of the signal and at the same time, respond to the slower drifts of the total signal level. Since the output of a CDD is directly proportional to the bias current I_E, it can serve as the gain controllable stage of Fig. 5.6. The AGC function is performed by the circuit shown in Fig. 5.7 with the response as shown in Fig. 5.8. The onset of distortion limits the range of the input level to less than four volts in this particular realization. A constant output is maintained for a one decade change in input level.

Spatial Effects

Our CDD prototype with two collector contacts and constant MOS bias current produces terminal characteristics that are porportional to the domain centroid, a totally analog process. By localizing the MOS bias current or by altering the collector design, a quasi-discrete operation can be obtained.

We first consider the effects of the bias current. The system Green's Function (Eq. 3.10), when taken to its one-dimensional asymptote by specifying the aspect ratio, R, to be large, becomes

$$g(x,y|x',y') = \begin{cases} x(1-x') & x < x' \\ x'(1-x) & x > x' \end{cases} \tag{5.4}$$

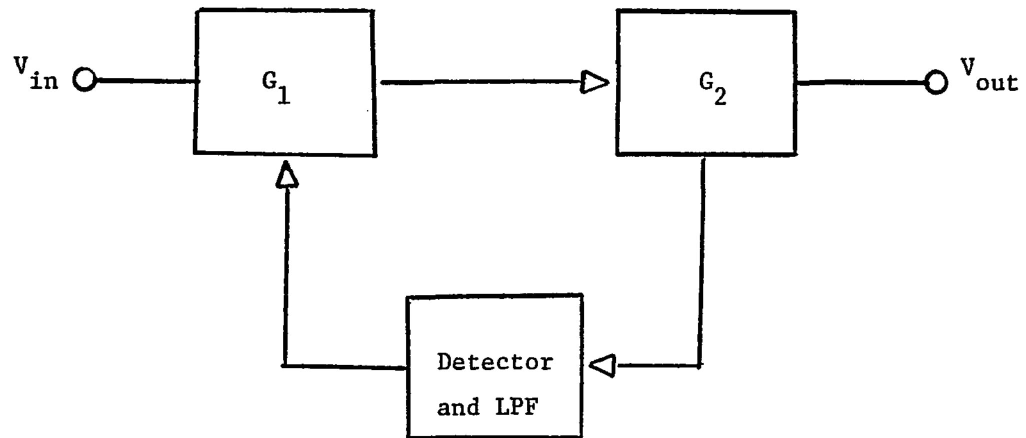

Fig. 5.6 Block Diagram of AGC System

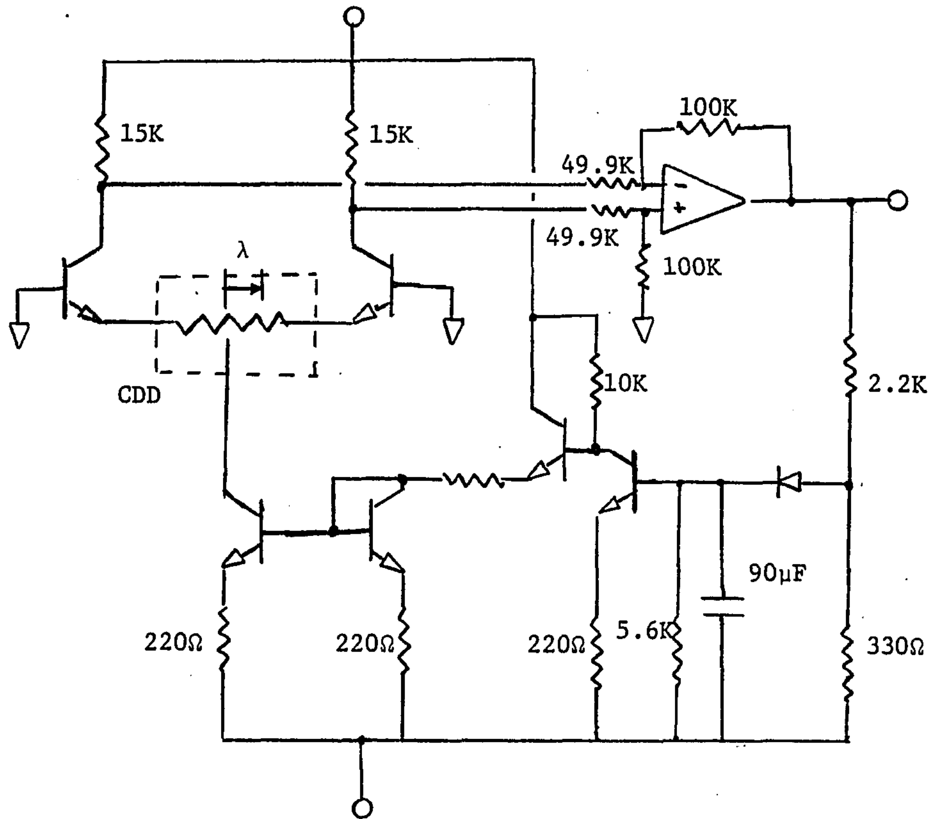

Fig. 5.7 CDD Realization of AGC Circuit

Note: The base drive circuit is not shown.

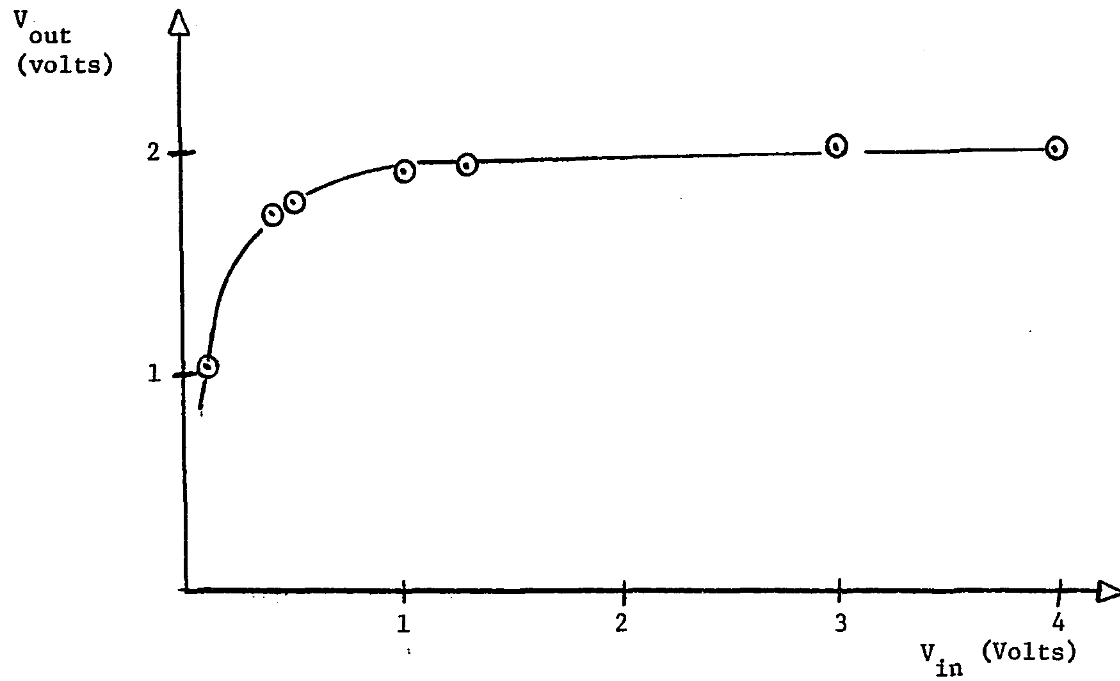

Fig. 5.8 Output versus Input of AGC Realization of Fig. 5.7

a distribution that is linearly decreasing as the field point x moves away from the source point x'. The distribution exhibits the required form for domain action, that is, a spatially positionable base potential extremum. In Fig. 5.9 we show an idealized structure with base current injected at a point x'. The terminal collector currents are now a direct function of x' and, although the emitter current density is no longer symmetrical about this point, the centroid is still approximated by this parameter since the domain is more localized than it was for the quadratic case as the potential initially falls off more rapidly. In any case, an effective domain location can be calculated to give as terminal collector currents

$$I_{C1} = x'_{eff} \, I_E \tag{5.5a}$$

$$I_{C2} = (1 - x'_{eff}) \, I_E \tag{5.5b}$$

The point source is simulated by a small MOS transistor injecting current over a small region as shown in Fig. 5.10a. If the dimensions of the source regions cannot adequately be approximated as points when compared to the entire length of the base, Eq. (3.13) can be used (with the limits of integration changed to correspond to those of the MOS source) to yield the potential distribution. For example, if only the ith MOS device is active, the normalized base potential is

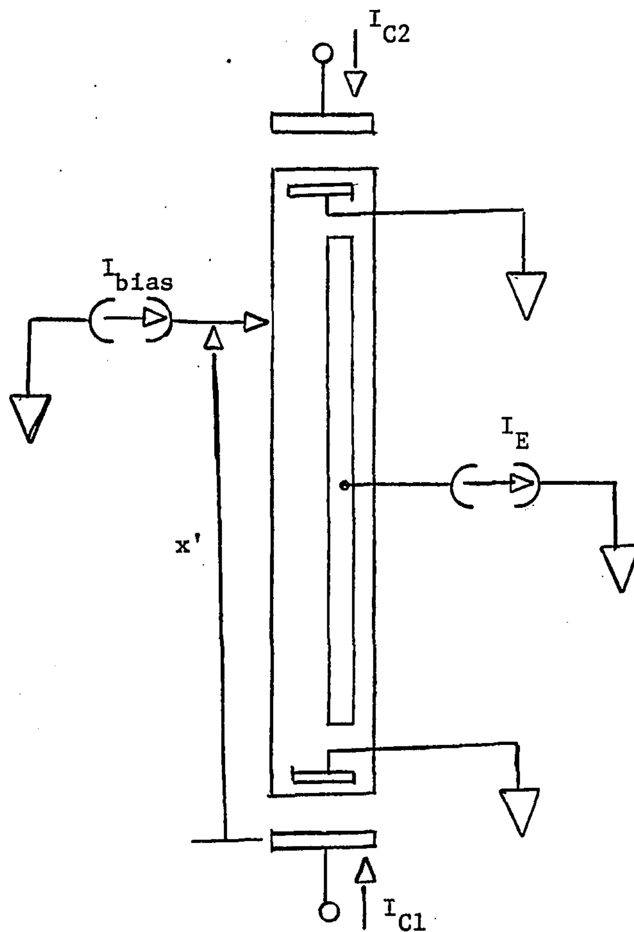

Fig. 5.9 Localized Base Bias Injection

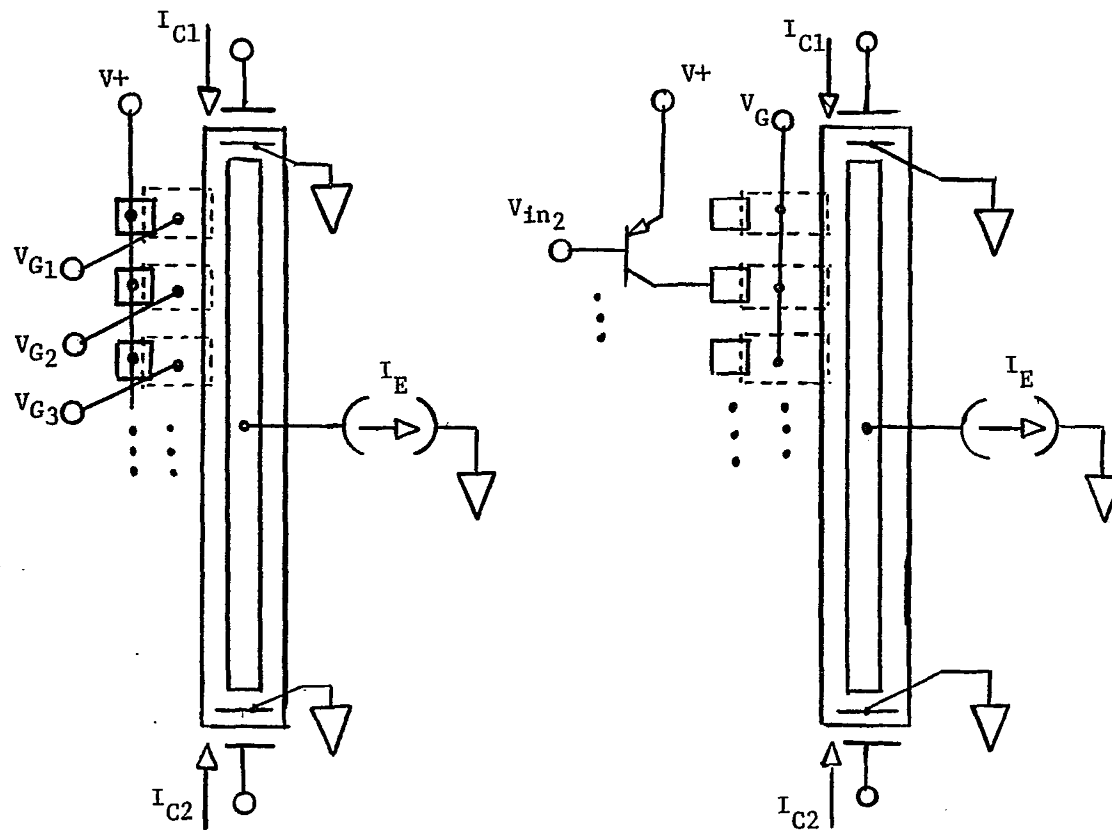

(a) Gate Controlled Input

(b) Source Controlled Input

Fig. 5.10 CDD Structure Producing D/A Conversion

$$\phi_s(x) = \frac{R_{ab}}{V_o} \int_{x_{i_\ell}}^{x} x(1 - x')\, H(x' - x)\, J^{\ell}_{y_i}(x')\, dx'$$

$$+ \frac{R_{ab}}{V_o} \int_{x'}^{x_{i_u}} x'(1 - x)\, H(x - x')\, J^{\ell}_{y_i}(x')dx' \qquad (5.6)$$

where

x_{i_ℓ} = lower coordinate of the ith MOS source

x_{i_u} = upper coordinate of the ith MOS source

$H(\alpha-\beta)$ = Heaviside step function

$$= \begin{cases} 1 & \alpha > \beta \\ 0 & \alpha < \beta \end{cases}$$

$J^{\ell}_{y_i}(x)$ = line current density supplied by the ith MOS source

The emitter current centroid can now be calculated by following the procedure outlined in detail in Chapter 4. Substituting this for x'_{eff} in Equations (5.5a and b) we obtain the terminal response which, since x'_{eff} is a discrete spatially defined quantity, is seen to provide a digital to analog conversion. The particular i^{th} MOS source can be excited by either controlling the individual gates as is shown in Fig. 5.10a with all the sources in common, or by placing a common voltage on the gates and driving the selected source as is indicated in Fig. 5.10b.

We now consider a different collector design. Figure 5.11 shows a multiple collector structure. As before, the centroid of the emitter

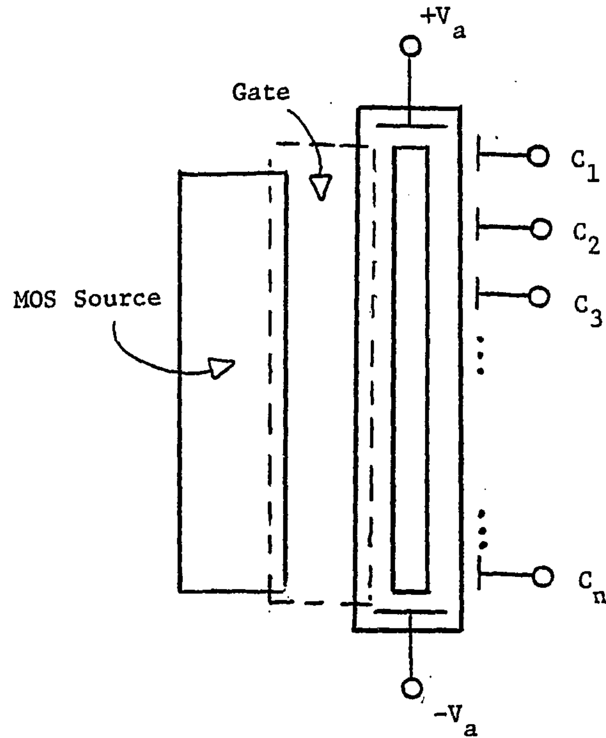

Fig. 5.11 Multiple Collector Structure that Produces A/D Behavior

current distribution is an analog function of the base drive voltage but now the collector current division is very different. As the domain is swept across the emitter length, the collector closest to it will collect a greater portion of the total current. If we process the collector signals with a threshold detector, we produce the analog to digital (A/D) converter function. Since the domain can be concentrated to 5% of the emitter extent, ten level A/D conversion should be easily achieved.

CDD Logic

A viable logic family can be obtained if a device or a combination of devices can assume recognizable states as unique functions of present inputs or, for memory devices, functions of present inputs and past states. The transfer characteristic of our CDD prototype with no MOS bias current shows it to form a two state logic element. The device has incompatible input and output requirements, however, and must be buffered for cascaded logic. Nevertheless, the essential features of a logic family are present although perhaps at too great an expense in complexity.

In Chapter 1, a structure was presented (Fig. 1.5) that can be identified as useful in tri-level logic. Our discussion of the A/D converter showed a multi-level discriminator. Domain phenomena then can produce multi-level logic functions. CDD's also have a second control port, the emitter current, that allows greater flexibility per device than may have originally been evident.

Since the collector current must be further processed and shaped, weighted combinations of these can be taken in an analog/digital merge to produce gates of a generalized threshold logic family. Such a function is indicated in Fig. 5.12. The variable weights are defined by pre-setting the base voltages to position the domain at a location that results in the desired positional attenuation factor, α. The presence or absence of the variable (1 or 0) is indicated by controlling the emitter current of a device. Note that the complementary signal is automatically generated. If all bases are set at the same level ($\alpha = 1/2$), setting the threshold of the level detector to $1/2\ I_E$, produces the two-input "OR" gate; a threshold of $1 \cdot I_E$ produces the two-input "AND" gate. Complicated threshold logic is obtained by controlling individual variable weights by domain positioning and independent threshold settings.

Conclusions

In this chapter we have shown domain phenomena to be useful in novel realization of various functions. Devices operating on the domain principle can form a merge of analog and digital signals that merits further consideration and study.

Realizable CDD functions go beyond that implied in this limited sketch as we have concentrated on those centered about a rectangular structure. The circular device of Smith [1974], for example, produced the arc-cosine transfer relation. Other output responses can be produced that are well defined functions of input parameters controlled

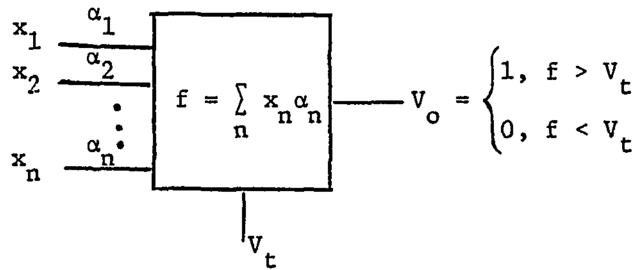

(a) General Threshold Logic

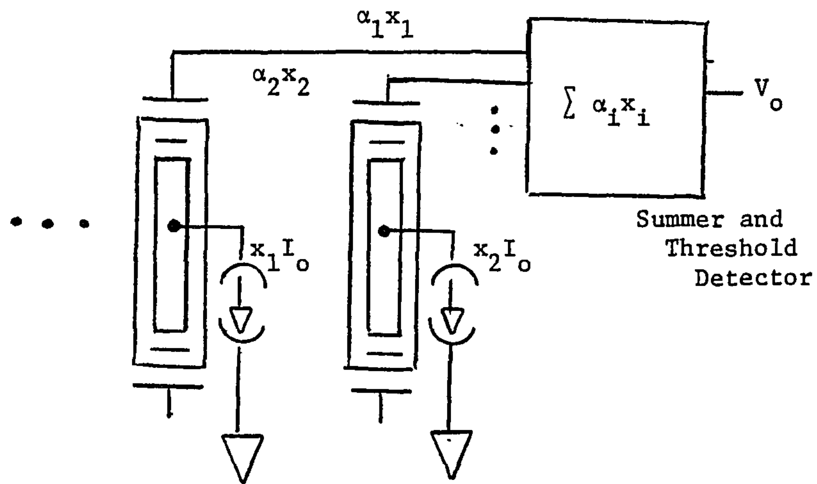

(b) CDD Realization

Fig. 5.12 Threshold Logic Gates

primarily by the device's planar geometry. In the next chapter we extend the analysis techniques to general base geometries.

CHAPTER 6

ANALYSIS OF GENERAL STRUCTURES

In the previous chapters we have confined our discussions to the rectangular structure of the CDD prototype and to the Gilbert circular design. It is of interest to formulate an analysis procedure that may be applied to general geometries in order to fully employ spatial phenomena in electronic function design. While we are primarily interested in describing domain effects, the distributed model is analogous to that of Electrothermal Circuits (ETC) [Louw, 1975] and also to that of distributed RC (d-RC) structures. Consequently, our formulations have direct applications to the analysis of these interesting distributed systems.

We now develop, by means of Green's Functions, the potential distribution for general geometrical regions.

Definition of the Problem

Consider the two-dimensional structure shown in Fig. 6.1. The interior region is of constant, finite conductivity with an arbitrary distribution of current sources. The boundary is formed by perfect isolation regions alternating with constant potential strips. Thus the boundary conditions are:

$$\frac{\partial \phi(x,y)}{\partial n} = 0 \tag{6.1}$$

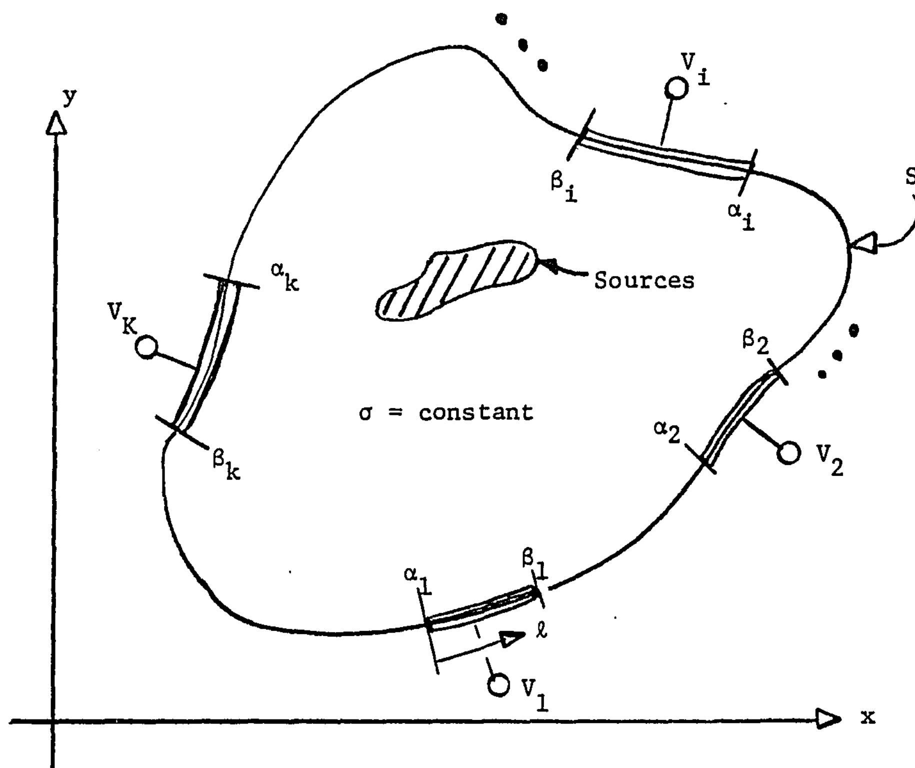

Fig. 6.1 Arbitrary Two-Dimensional Region for CDD Base Region

along the isolating arcs and on the ith metallized portion,

$$\phi(x,y)\Big|_{s_i} = V_i \tag{6.2}$$

The system d-KPDE is

$$\rho_s' \, J_f(x,y) = - \nabla^2\phi(x,y,t) + \rho_s' \, C \, \frac{\partial\phi}{\partial t} \tag{6.3}$$

with the parameters as defined in Chapter 3. This equation is the distributed model for a d-RC structure and for an electrothermal system if we identify the analogous quantities

$$\rho_s' \, J_f(x,y,t) \leftrightarrow P(x,y,t)$$

$$\phi(x,y,t) \leftrightarrow T(x,y,t)$$

$$\rho_s' \leftrightarrow \gamma$$

$$C \leftrightarrow k$$

where the quantities dual to the CDD system are: $P(x,z,t)$, the source power density; $T(x,y,t)$, the temperature distribution; γ, the thermal resistivity; and k the thermal capacitance per unit volume (= density × specific heat -- Louw, 1975). Replacing the variables of Eq. (6.3) by their Electrothermal duals produces the distributed model for an ETC.

$$P(x,y,t) = - \nabla^2 T(x,y,t) + \gamma \, k \, \frac{\partial T(x,y,t)}{\partial t} \tag{6.4}$$

Solution of any of the isomorphic systems automatically results in the

solution of the others by a simple transformation of variables. The two dual systems to the CDD base region are shown in Fig. 6.2.

Method of Solution of the d-KPDE

To solve Eq. (6.3), we first take its Laplace transform, thereby removing the time dependence. We indicate transformed quantities by the presence of the Laplace parameter, p, in the last position of the argument list where it replaces the temporal parameter t.

$$- \nabla^2 \phi(x,y,p) + C \rho_s' p \phi(x,y,p) = \rho_s' J_f(x,y,p) \tag{6.5}$$

$$[- \nabla^2 + k^2] \phi(x,y,p) = F(x,y,p) \tag{6.6}$$

where in Eq. (6.6) we have let

$$k^2 = C \rho_s' p$$

and

$$F(x,y,p) = \rho_s' J_f(x,y,p)$$

Again as in Chapter 3, since the operator of Eq. (6.6) is Hermetian and $\phi(x,y,p)$ is a physical quantity and can therefore represent only limited energy, a suitable inner product is the following:

$$\langle \phi, \psi \rangle = \iint_A \phi \psi \, dxdy \tag{6.7}$$

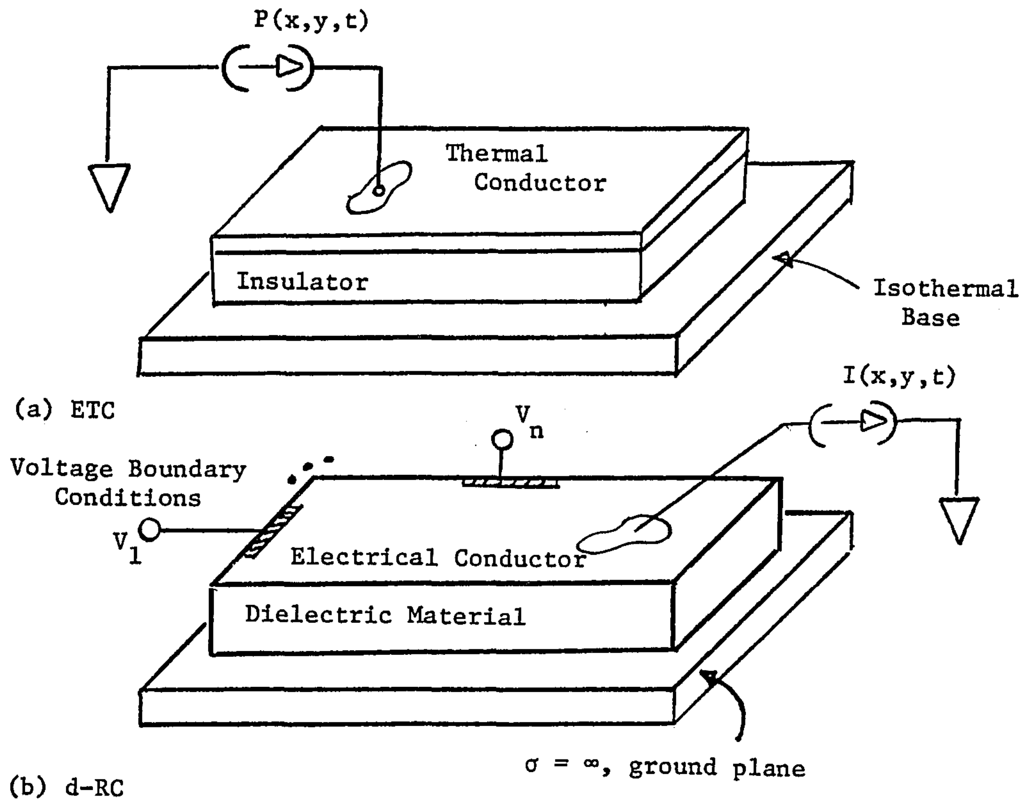

Fig. 6.2 Systems Analogous to the Base Region of CDD's

Letting $h(x,y;p|x';y')$ be the adjoint Green's Function that satisfies the operator equation

$$(-\nabla^2 + k^2)h = \delta(x - x')\,\delta(y - y') \tag{6.8}$$

and as yet an unspecified set of boundary conditions, we take the inner product of Eq. (6.6) with h and integrate by parts to obtain

$$\langle h,(-\nabla^2 + k^2)\phi\rangle = \langle h,F(x,y;p)\rangle$$

$$= \langle(-\nabla^2 + k^2)h,\phi\rangle - \int_S \left(h\,\frac{\partial\phi}{\partial n} - \phi\,\frac{\partial h}{\partial n}\right) dS \tag{6.9}$$

Substitution of Eq. (6.8) into Eq. (6.9) results in

$$\langle h,F(x,y;p)\rangle = \phi(x',y';p) - \int_S \left(h\,\frac{\partial\phi}{\partial n} - \phi\,\frac{\partial h}{\partial n}\right) dS \tag{6.10}$$

The quantity $\left.\frac{\partial\phi}{\partial n}\right|_S$ is proportional to the current density leaving the enclosed region at the boundaries and is unknown along the metallized contacts, zero along the insulated boundary portions; ϕ is the voltage function defined externally on the contacts, and unknown along the insulating arcs. If these two quantities can be determined, a sufficient set of information required for the total solution of the distribution potential function, Eq. (6.10), is obtained.

An integral equation for the solution of the quantities in the surface integral of Eq. (6.10) is formed by letting the field point

P(x,y) approach the boundary, interchanging the primed and unprimed coordinates, and using the equality between the Green's Function and its adjoint

$$g(x,y;p|x',y') = h(x',y';p|x,y) \tag{6.11}$$

This results in

$$\left\langle g,F(x',y';p)\right\rangle = \phi(x,y;p)\Big|_S - \operatorname*{Limit}_{(x,y)\to(x_S,y_S)} \left\{ \int_S g(x,y;p|x',y') \frac{\partial\phi}{\partial n'}(x',y';p)\, dS - \int_S \phi(x',y';p) \frac{\partial g}{\partial n'}(x,y;p|x',y')\, dS \right\} \tag{6.12}$$

Equation (6.12) may be solved approximtely by the Method of Moments [Harrington, 1968] as will now be outlined.

A judicious choice of boundary conditions the Green's Function is to satisfy results in a simplification of the problem. For example, consider the potential distribution for the structure shown in Fig. 6.3 where a corner of the rectangular geometry analyzed in Chapter 3 has been removed and replaced by an insulating boundary. If we use the same boundary conditions we used for that geometry, namely

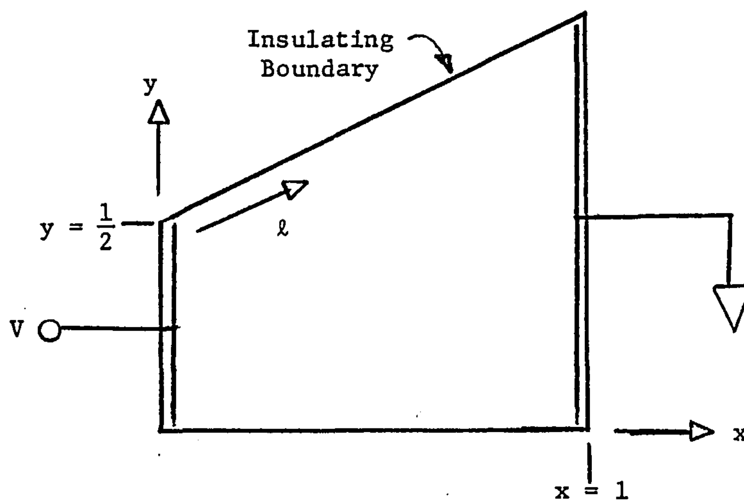

Fig. 6.3 Simple Geometry Used to Formulate Analysis Methodology Based Upon Green's Function of Rectangular Structure

$$g(x,y;p|x',y')\Big|_{\substack{x=o,\\ x=1}} = 0 \tag{6.13a}$$

$$\frac{\partial g}{\partial y}(x,y;p|x',y')\Big|_{\substack{y=o,\\ y=1}} = 0 \tag{6.13b}$$

Equation (6.12) is simplified to

$$- V \int_{o}^{1/2} \frac{\partial g}{\partial x'}(x,y;p|x',y')\Big|_{x'=0} dy' = \phi(x,y;p)\Big|_{S_1}$$

$$- \underset{(x,y)\to(x_{S_1},y_{S_1})}{\text{Limit}} \int_{S_1} \phi(x',y';p) \frac{\partial g}{\partial n'}(x,y;p|x'y')\, dS' \tag{6.14}$$

Since the Green's Function of Eq. (6.14) is that derived in Chapter 3, the integral on the left hand side is calculable, and the kernel in the integral on the right side is obtained by using the definition of a directional derivative

$$\frac{\partial g}{\partial n'} = \nabla_{x'y'}\, g \cdot \hat{n}' \tag{6.15}$$

with the normal $\hat{n}'$ defined by the geometry.

Following the Method of Moments, we express the potential along Side 1 as an expansion of a localized basis such as the set of pulse functions $P_n(\ell)$, so that

$$\phi(x,y;p)\Big|_{S_1} = \sum_{n=1}^{N} a_n(p)\, P_n(\ell) \tag{6.16}$$

where

$$P_n(\ell) = \begin{cases} 1 & \frac{n}{N+1} < \ell < \frac{n+1}{N+1} \\ 0 & \text{Otherwise} \end{cases}$$

ℓ = arc length along Side 1

N = Total number of pulses used to approximate ϕ along Side 1

It is clear from Eq. (6.16) that a step function approximation to the potential distribution along Side 1 is being made, and that using more pulses will result in a better representation.

Substituting Equations (6.16) and (6.15) into Eq. (6.14), we obtain

$$G(\ell;p) = \sum_{n=1}^{N} a_n(p)\, P_n(\ell) - \sum_{n=1}^{N} a_n(p) \int_{\alpha_n}^{\beta_n} \underset{(x,y)\to(x_S,y_S)}{\text{Limit}} \nabla' g \cdot \hat{n}' d\ell' \tag{6.17}$$

with

$$G(\ell;p) = G(x,y;p)$$

$$= -V \int_{o}^{1/2} \frac{\partial g}{\partial x'}(x_S,y_S;p|o,y')\, dy'$$

α_n = lower coordinate of nth pulse = $\frac{n}{N+1}$

β_n = upper coordinate of nth pulse = $\frac{n+1}{N+1}$

If we now use point matching by taking the inner product of Eq. (6.17) with a delta weight function located at the center of the mth pulse, we obtain

$$G\left(\frac{m+\frac{1}{2}}{N+1}\,;\,p\right) = a_m(p) - \sum_{n\neq m} a_n(p) \int_{\alpha_n}^{\beta_n} \nabla' g\left(\frac{m+\frac{1}{2}}{N+1}\,;\,p|\ell'\right)\cdot\hat{n}'d\ell'$$

$$- a_m(p) \int_{\alpha_m}^{\beta} \operatorname*{Limit}_{\ell \to \left(\frac{m+\frac{1}{2}}{N+1}\right)} \nabla' g(\ell;p|\ell')d\ell' \tag{6.18}$$

The integrand in the last integral is singular but of an integrable kind. For the two-dimensional operator ∇^2_{xy}, the singularity is logarithmic. In general, the small argument asymptote to the series can be used to remove the singularity and perform the integration. Equation (6.18) for the N values of m becomes a set of simultaneous equations

$$G_m = \sum_{n=1}^{N} K_{mn}\, a_n \tag{6.19}$$

which can be inverted to solve for the a_n by matrix manipulations. The resultant approximation to the potential along Side 1 is then used in Eq. (6.12) to generate the potential throughout the region.

For the general case depicted in Fig. 6.1, it is advantageous to use the free space Green's Function. For the static case, this is given by

$$g_F(\rho|\rho') = \frac{-1}{2\pi} \ln |\rho - \rho'| \tag{6.20}$$

while for the operator of Eq. (6.6) it is

$$g_F(\rho;p|\rho') = \frac{1}{2\pi} K_o(k|\rho - \rho'|) \tag{6.21}$$

where

$$k = \sqrt{C\rho' p}$$

and

$$\rho = \text{field point}$$

$$\rho' = \text{source point}$$

and K_o is the hyperbolic Bessel function of order zero [Arfken, 1970]. The integral equation (Eq. 6.12) defined over the entire bounding surface must be solved. To do this, we again use the arc length ℓ as the distance parameter. Dividing the perimeter into N equispaced regions, we use step function approximations for ϕ along the insulating arcs and for $\frac{\partial\phi}{\partial n}$ on the contact portions of the boundary

$$\phi(\ell;p) = \sum_{n=1}^{N} a_n(p)\, P_n(\ell) \tag{6.22a}$$

with $a_n(p) = V_i(p)$ for all n such that

$$\frac{\alpha_i}{N+1} < n < \frac{\beta_i}{N+1}$$

$$\frac{\partial\phi(\ell;p)}{\partial n} = \sum_{n=1}^{N} b_n(p)\ P_n(\ell) \tag{6.22b}$$

with $b_n(p) = 0$ for all n such that

$$\frac{\beta_j}{N+1} < n < \frac{\alpha_{j+1}}{N+1} \qquad j = 1, 2, \ldots, K$$

and

α_i = lower coordinate for the ith metal contact

β_i = upper coordinate for the ith metal contact where the coordinate is arc length, ℓ

Note that the sets $\{a_n\}$ and $\{b_n\}$ are unknown over complementary regions and that they are independent. Together they form a sufficient set of information necessary for the solution of Eq. (6.12) which becomes

$$\left\langle g_F, F(\ell';p)\right\rangle = \sum_{n=1}^{N} a_n(p)\ P_n(\ell) - \sum_{n=1}^{N} b_n(p) \underset{\ell \to \ell_S}{\text{Limit}} \left\{ \int_{\alpha_n}^{\beta_n} g(\ell;p|\ell')\,d\ell' \right\} + \sum_{n=1}^{N} a_n(p) \underset{\ell \to \ell_S}{\text{Limit}} \int_{\alpha_n}^{\beta_n} \nabla'\ g(\ell;p|\ell')\cdot \hat{n}'d\ell' \tag{6.23}$$

Again we must consider the singularity in the integrands that results as the field point approaches the source point. For the free space Green's Functions given in Equations (6.20) and (6.21), it is logarithmic and therefore integrable. Point matching is used to generate a matrix equation of the form of Eq. (6.19). Inverting this, we obtain $\{a_n\}$ and $\{b_n\}$ which can be substituted into Eq. (6.12) to solve for the potential throughout the region of interest.

An interesting consequence of this methodology is that we have obtained the means of producing the indefinite admittance parameters [y] for the n-port structure of Fig. 6.1. The current leaving the ith contact is given by

$$I_i = \int_{\alpha_i}^{\beta_i} J(\ell)\, d\ell$$

$$= -\sigma \int_{S_i} \frac{\partial\phi}{\partial n}(\ell)\, d\ell$$

$$\cong -\sigma \sum_{S_i} b_n \frac{1}{N+1} \qquad (6.24)$$

where the b_n are obtained from the solution of Eq. (6.23). Setting all metallized regions but the jth to zero volts, we can obtain the current at the ith port due to excitation at the jth port making

$$y_{ij} = - \sigma \sum_{S_i} b_n \frac{1}{N+1} \Bigg|_{\substack{V_i=o \\ V_j=1}} \qquad i \neq j \tag{6.25}$$

Cycling through j to obtain the complete set, we generate the matrix $[y_{ij}]$ such that

$$I_i] = [y_{ij}]\ V_j] \tag{6.26}$$

Such a formulation is extremely useful to the design engineer as it represents the total information necessary to obtain the terminal response for any excitation vector and load requirements compatible with the analysis. The indefinite admittance matrix allows the device to be replaced by an electronic "black box" and makes knowledge of the internal behavioral details unnecessary for the use of CDD's (or d-RC's or ETC's) in electronic systems.

We have presented an analysis methodology for the solution of the distributed potential within arbitrary regions and having arbitrary excitations. The time varying problem is resolved in the Laplace or frequency space and can be inverse transformed numerically or else kept in the frequency space representation. Electrical engineers have long used this space for system operation description as both magnitude of response and phase information easily obtained from this form are sufficient to characterize the system behavior completely. This formulation is also advantageous for the recognition of dominant pole locations, information that can be used for synthesis as shown by Louw [1975].

Similar problems have been solved by using these procedures (except for the indefinite admittance parameters) in the field of Electro-Magnetics where tractable, accurate and efficient solutions have been obtained. (See, for example, Seidel, 1977.)

Also of interest is the simultaneous solution of the isomorphic systems. Previous work in ETC characterization has considered only rectangular structures with insulating and impedance boundary conditions on the top surface [Ali, 1975]. With this formulation, we can specify regions having known temperature profiles as functions of time and use irregularly cut die to achieve greater flexibility in design of ETC's.

Summary of Analysis Procedure

The proposed analysis methodology consists of the following steps:

1. Obtain the Green's Function to be used in the analysis: either the free space one, or one for a rectangular structure that matches the geometry under consideration along as many sides as possible.
2. Formulate Green's identity consisting of an integral of a source term, a trivial integral with a factor in the integrand being the two-dimensional delta function, and a boundary integral.
3. Generate the integral equation by allowing the field point to approach the surface where the function is unknown.
4. Solve the integral equation by the Method of Moments.

5. With the potential function, and its normal derivative if applicable, approximated along the boundary, solve the Green's Function formulated in Step 2. Note that the procedure is an application of the equivalency principle used frequently in Electro-Magnetic problems.
6. Advantage should be taken of symmetry relations in order to solve only the necessary portions of the problem thereby using small matrices for a given resolution.

CHAPTER 7

SUMMARY AND CONCLUSIONS

The general objective of this dissertation was to examine a new concept in solid state devices: The Carrier Domain. More specifically, we sought to develop a device that functioned on the domain principle and possessed a linear input-output transfer relation, and to extend the analytical techniques to cover general planar structures.

Previous work in this area considered only the highly symmetrical circular base design in conjunction with a collector structure that produced current division linearly dependent upon a single spatial coordinate. The mathematical analysis used conformal mapping techniques that are not readily adopted to other structures and bias conditions.

Summary

A summary of the work reported in this dissertation follows. First, a general discussion of domain phenomena was presented. CDD's offer a novel approach to the design of linear and functional integrated circuits. Transfer characteristics are defined primarily by the device's planar geometry, the parameter most controllable in present day device fabrication. CDD's present the potential for function generation at a reduced complexity level over conventional designs.

Next, an idealized structure and bias mode were presented. The particular design was selected after preliminary investigations indicated

it would yield an approximately linear base-collector transadmittance relation. A physical realization, a monolithic structure that was a unique merge of MOS and bipolar technologies, was designed that adequately approximated the idealized design. Devices of this morphology were fabricated in the Solid State Engineering Laboratory at The University of Arizona.

The describing d-KPDE for the base region of the CDD prototype was developed. Limitations to the analysis that followed were explicitly stated in a list of assumptions made that served to keep the mathematics tractable and realistic.

A solution to the distributed base potential in the form of an infinite series was derived using the Method of Green's Functions. In parallel, a Finite Difference solution leading to a physically intuitive lumped model was presented. It was suggested that for qualitative device understanding, the latter method be applied; for accurate numerical solutions, that of Green's Functions is superior.

The solutions obtained by both analysis methods were extended to the time varying case.

Theoretical limits to the domain width were presented in terms of device parameters. For the particular collector design used, the domain centroid proved to be the parameter of greatest interest. Numerical formulation of its location and motion were presented. In cases of long, narrow design, the centroid was given in terms of the normal probability density function and obtained from mathematical tables.

A characteristic length for the approximate one-dimensional designs was defined mathematically as a function of device parameters and bias conditions. This parameter was shown to be proportional to the width of the domain.

Experimental correlation of theoretical results was obtained. Further, to demonstrate CDD versatility, the fabricated device was used to realize two and four quadrant multiplication and a gain controllable amplifier stage useful in AGC circuits. Designs that would produce A/D and D/A conversion and multilevel and threshold logic functions were also presented.

A generalized analysis methodology for arbitrary CDD structures and time varying excitations was presented. Outstanding features of the analysis are:

1. Arbitrary geometries can be handled.
2. Various combinations of bias modes are automatically incorporated. Whereas previous work assumed point source current excitation of the base structure, the presented analysis will solve for the potential function of structures having arbitrary current source distributions anywhere in the base region or on its boundary, and any realizable voltage boundary conditions.
3. The related dual systems, the distributed RC structure and Electro-Thermal systems, are simultaneously solved by a simple parameter transformation.
4. A particularly interesting feature of the mathematical formulation is, with little extra computation, the generation of the indefinite admittance matrix of the n-port system.

5. Also, as discussed by Louw [1975], the formulation yields pole location information suitable for synthesis work.
6. Finally, arbitrary collector structures can be analyzed. This adds a greater flexibility to CDD design and philosophy not present in previous work.

Recommendations for Further Work

CDD's provide an interesting source for further work in the general areas of synthesis, applications, and domain formation and control.

The means for general structure analysis has been presented. This should be examined to formulate synthesis guidelines that will aid in the specific creation of the transfer relations desired. Collector contact placement and the use of buried layer will add significantly to the set of obtainable device behaviors.

A combination of domain action and ETC technology will result in a greater flexibility in heater design. This application merits investigation.

Prior to the development of the MOS-bipolar structure, a composite lateral pnp, vertical npn design was considered but not followed through due to the lack of an adequate lateral pnp process at The University of Arizona in the Solid State Engineering Laboratory. The structure offered the interesting possibility of spatial feedback that would enhance the domain action. The concept of spatial feedback should be investigated.

In this dissertation, we intended to demonstrate domain phenomena in generalized structures. Therefore, we did not seek the limits to domain formation. Effects due to high level injection and to outward diffusion of the concentration of the carriers have not been considered. Studies on these problems will provide an understanding of limitations to the domain idea.

The operation of many devices, because they are indeed distributed structures, demonstrate facets of domain phenomena. We have previously mentioned "emitter crowding" as one manifestation of carrier domain. Another interesting demonstration can be found in the operation of I^2L circuits. In order to understand certain device behavior, it may be necessary to perform a distributed analysis as we have presented in this work.

APPENDIX A

ANALYSIS OF TWO-REGION BASE STRUCTURE

In the body of this dissertation, we chose to approximate the effect of the emitter by using an effective width in the aspect ratio. For long structures this will result in negligible error and is the simplest treatment. We now present the analysis of a struture that has two regions of different conductivity as shown in Fig. A-1. For simplicity, we place the distributed sources in region I only noting that superposition allows the simple extension for sources simultaneously in both regions.

As shown in Chapter 2, the d-KPDE for each region separately is

$$- \nabla^2 \phi(x,y) = F(x,y) = f(x) \ \delta(y) \tag{A.1}$$

Using Green's identity, we write

$$\left\langle g, - \nabla^2 \phi \right\rangle = \left\langle - \nabla^2 g, \ \phi \right\rangle - \int_S \left(g \frac{\partial \phi}{\partial n} - \phi \frac{\partial g}{\partial n} \right) dS \tag{A.2}$$

In region I, the potential function must satisfy

$$\phi_I(o,y) = \phi(a,y) = 0 \tag{A.3a}$$

$$\left. \frac{\partial \phi_I}{\partial y} \right|_{y=o} = 0 \tag{A.3b}$$

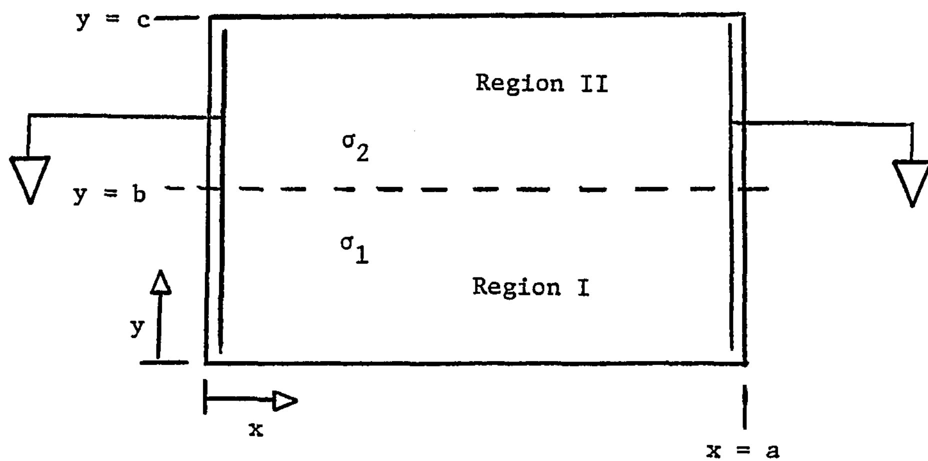

Fig. A.1 Base Structure Composed of Two Conductivity Regions

Selection of the boundary conditions

$$g(x,y|o,y') = g(x,y|a,y') = 0 \tag{A.4a}$$

$$g(x,y|x',b) = 0 \tag{A.4b}$$

$$\left.\frac{\partial g}{\partial y'}(x,y|x',y')\right|_{y'=o} = 0 \tag{A.4c}$$

for g simplifies Eq. (A.2) to

$$\iint_{R_1} g(x,y|x',y')\ F(x',y')\ dx'dy' = \phi_I(x,y) + \int_o^a \phi_I(x',b)\ \left.\frac{\partial g}{\partial y'}(x,y|x',y')\right|_{y'=b} dx' \tag{A.5}$$

By the procedure shown in Appendix C, the Green's Function is found to be

$$g(x,y|x',y') = \frac{2}{a}\sum_{n=1}^{\infty}\frac{\sin\left(\frac{n\pi x}{a}\right)\sin\left(\frac{n\pi x'}{a}\right)\cosh\left(\frac{n\pi y_<}{a}\right)\sinh\left[\frac{n\pi}{a}(b-y_>)\right]}{\frac{n\pi}{a}\cosh\left(\frac{n\pi b}{a}\right)} \tag{A.6}$$

For Region II, the distribution can be expressed in an eigenfunction expansion

$$\phi_{II} = \sqrt{\frac{2}{a}}\sum_{n=1}^{\infty}\phi_{II,n}\ \sin(k_n x)h_n(y) \tag{A.7}$$

where

$$k_n = \frac{n\pi}{a}$$

and

$h_n(y)$ = an unknown function of y

Substitution of Eq. (A.7) into Eq. (A.1) with the forcing function set to zero produces

$$\sqrt{\frac{2}{a}} \sum_{n=1}^{\infty} \left(\frac{\partial^2}{\partial y^2} - k_n^2 \right) \sin (k_n x) \; h_n(y) = 0 \tag{A.8}$$

which, by the orthogonality property of the basis functions becomes the total differential relations

$$\left(\frac{d^2}{dy^2} - k_n^2 \right) h_n(y) = 0 \tag{A.9}$$

The insulating boundary along y = c requires the solution to Eq. (A.9) to be proportional to cosh $[k_n (c-y)]$. Therefore, we write Eq. (A.7) as

$$\phi_{II}(x,y) = \sqrt{\frac{2}{a}} \sum_{n=1}^{\infty} \frac{\phi_{II,n} \sin k_n x \cosh k_n (c-y)}{\cosh k_n (c-b)} \tag{A.10}$$

Across the common boundary at y = b, the voltage function must be continuous. This implies that

$$\phi_1(x,y) = \sqrt{\frac{2}{a}} \sum_{n=1}^{\infty} \frac{\sin(k_n x)\, \sinh[k_n(b-y)]\, f_n}{k_n \cosh(k_n b)}$$

$$+ \sqrt{\frac{2}{a}} \sum_{n=1}^{\infty} \frac{\phi_{II,n} \sin(k_n x) \cosh(k_n y)}{\cosh(k_n b)} \quad (A.11)$$

where

$$f_n = \sqrt{\frac{2}{a}} \int_0^a f(x) \sin(k_n x)\, dx,$$

the Fourier Sine expansion coefficient of f(x). The normal current density must also be continuous. This requires

$$\sigma_1 \left.\frac{\partial \phi_I(x,y)}{\partial y}\right|_{y=b} = \sigma_2 \left.\frac{\partial \phi_{II}(x,y)}{\partial y}\right|_{y=b} \quad (A.12)$$

Combining Equations (A.10), (A.11) and (A.12) allows the resolution of the unknown coefficients $\phi_{II,n}$.

$$\phi_{II,n} = \frac{\sigma_1 f_n / \cosh(k_n b)}{\sigma_1 k_n \text{Qanh } k_n b + \sigma_2 k_n \text{Qanh } [k_n(C-b)]} \quad (A.13)$$

Substituting this result into Eq. (A.10) yields the potential distribution in region II, and the distribution in region I is obtained by substitution (A.12) into (A.11).

APPENDIX B

NONDIMENSIONALIZING THE d-KPDE

If an equation is cast into a dimensionless form, interpretation and generalization of the solution may be enhanced. Constants are lumped together and can usually be identified as characteristic scalars suitable for normalizations. Good examples of such numbers are the time constants of lumped RC networks and diffusion lengths that naturally emerge from the diffusion equations. The family of solutions related by scaling is obtained instead of the particular situation examined. This appendix shows the process of removing the dimensions of Eq. (2.13), the d-KPDE, and its associated boundary conditions (Eq. 2.14), are repeated here for easy reference.

$$- \nabla_{xy}^{2} \; \phi(x,y) = \rho_s' J_y^{\ell}(x) \; \delta(y-b) \tag{B.1}$$

$$\phi(o,y) = V_A \tag{B.2a}$$

$$\phi(a,y) = V_B \tag{B.2b}$$

$$\left.\frac{\partial\phi(x,y)}{\partial y}\right|_{y=o} = 0 = \left.\frac{\partial\phi(x,y)}{\partial y}\right|_{y=b} \tag{B.2c}$$

We choose the dimensionless variables, X, Y, and Φ, such that

$$aX = x \tag{B.3a}$$

$$bY = y \tag{B.3b}$$

$$V_o\Phi = \phi \tag{B.3c}$$

where the units of the left hand side of these relations are contained in the constants a, b, and V_o, and

a = length of base in the x-direction

b = length of base in the y-direction

V_o = a reference voltage - KT/q is a useful reference and is used herein.

Application of the chain rule to introduce the new variable set, (X,Y,Φ), transforms Eq. (B.1) into

$$\left(\frac{1}{a^2}\frac{\partial^2}{\partial X^2} + \frac{1}{b^2}\frac{\partial^2}{\partial Y^2}\right) V_o\Phi = - \rho_s' J_y^{\ell} \ (aX) \ (bY-b) \tag{B.4}$$

where

$$o \leq X \leq 1$$

$$0 \leq Y \leq 1$$

Multiplication of (B.4) by a^2 and using the definition

$$\delta[f(x)] = \frac{\delta(x - x_o)}{|f'(x_o)|} \tag{B.5}$$

where x_o is the location of the zero for the monotonic function, f(x) [Friedman, 1956], we obtain

$$\left(\frac{\partial^2}{\partial X^2} + R^2 \frac{\partial^2}{\partial Y^2}\right) \Phi(X,Y) = -\rho_s' \frac{a}{b} \frac{aJ_y^{\ell}(x)\ \delta(Y-1)}{V_o} \tag{B.6}$$

$$R = \frac{a}{b}\ \text{, aspect ratio}$$

For the special case where a constant current density is injected along the side y=b, Eq. (B.6) simplifies to

$$\left(\frac{\partial^2}{\partial X^2} + R^2 \frac{\partial^2}{\partial Y^2}\right) \Phi(X,Y) = \frac{-R_{ab}\ I_{MOS}\ \delta(Y-1)}{V_o} \tag{B.7}$$

where

$R_{ab} = \rho_s' \frac{a}{b}$ = end to end base resistance

I_{MOS} = Total bias current supplied by the MOS transistor

Equation (B.7) is the desired dimensionless d-KPDE.

APPENDIX C

DERIVATION OF GREEN'S FUNCTION

A powerful method of solution of linear boundary value problems employs Green's Functions, which are solutions to point source excitations. The boundary value problem is solved by taking a superposition integral of the forcing function with the Green's Function, the latter weighting the effect of the distributed source at the observation point. For this reason, it has been known as the influence function.

The Green's Function satisfies

$$\left(\frac{-\partial^2}{\partial x^2} - R^2 \frac{\partial^2}{\partial y^2}\right) g(x,y|x'y') = \delta(x-x')\ \delta(y-y') \tag{C.1}$$

and the boundary conditions

$$g(x,y|x',y')\Big|_{x=0} = 0 \tag{C.2a}$$

$$g(x,y|x',y')\Big|_{x=1} = 0 \tag{C.2b}$$

$$\frac{\partial g}{\partial t}(x,y|x',y')\Big|_{y=0} = 0 \tag{C.2c}$$

$$\frac{\partial g}{\partial y}(x,y|x',y')\Big|_{y=1} = 0 \tag{C.2d}$$

The functions

$$u_n(y) = \sqrt{\varepsilon_n} \cos (n\pi y) \qquad (C.3)$$

where

$$\varepsilon_n = \begin{cases} 1 & n = 0 \\ 2 & n \neq 0 \end{cases}$$

$$n = 0, 1, 2, \ldots$$

obtained by solving the eigenfunction equation with Neumann boundary conditions

$$-\frac{d^2}{dy^2} u_n(y) = \lambda_n(y) \qquad (C.4)$$

form an orthonormal basis suitable for expanding the Green's Function

$$g(x,y|x',y') = \sum_{n=o}^{\infty} b_n(x) \sqrt{\varepsilon_n} \cos (n\pi y) \qquad (C.5)$$

$$0 \leq y \leq 1$$

Substituting Eq. (C.5) into Eq. (C.1) and interchanging the operator with the summation (which can be done by virtue of the operator being self adjoint), we obtain

$$\sum_{n=o}^{\infty} \sqrt{\varepsilon_n} \left[\frac{-d^2}{dx^2} + (Rn\pi)^2 \right] b_n(y) \cos n\pi y = \delta(x-x')\delta(y-y') \tag{C.6}$$

We now use the orthogonality property of the expansion functions. Taking the inner product of Eq. (C.6) with $\sqrt{\varepsilon_m}$ cos ($m\pi y$), we obtain

$$\left[\frac{-d^2}{dx^2} + (Rm\pi)^2 \right] b_m(x) = \sqrt{\varepsilon_m} \cos m\pi y' \; \delta(x-x') \tag{C.7}$$

This equation can be solved by following the procedure in Friedman [1956], which results in

$$b_n(x) = \frac{\sqrt{\varepsilon_n} \; \cos(n\pi y') \; \sinh(n\pi R x_<) \; \sinh[n\pi R(1-x_>)]}{Rn\pi \; \text{Sinh}(Rn\pi)} \tag{C.8}$$

where

$$x_< = \min\ (x,x')$$

$$x_> = \max\ (x,x')$$

Substitution of Eq. (C.8) into Eq. (C.5) results in the desired Green's Function.

$$g(x,y|x'y') = \sum_{n=o}^{\infty} \frac{\varepsilon_n \; \cos(n\pi y') \; \cos(n\pi y) \; \sinh(n\pi R x_<) \; \sinh[n\pi R(1-x_>)]}{n\pi R \; \sinh(n\pi R)} \tag{C.9}$$

APPENDIX D

LISTING OF CDD BASE ANALYSIS PROGRAM

The listing that follows is of a program that performs the numerics required to obtain the two-dimensional potential distribution of a uniform rectangular base region with constant edge bias current. A particular structure is selected by specifying the aspect ratio R in the main control program of "Domain". The resolution desired is controlled by selecting NPX and NPY, the number of grid points in the x and y directions, respectively.

```
      PROGRAM DOMAIN (INPUT,OUTPUT)
      COMMON /DATA/ R,VA,VB,NPX,NPY
      COMMON /NX/ NX
C   NPX,NPY LESS THAN 50 UNLESS SYM SOL  THEN NPX LESS THAN 100
      NPX = 25
      NPY = 6
      R = 15
      VA=0.0
      VB = 0.0
      NX = NPX + 1
     IF(.NOT.((VA .EQ. 0.) .AND. (VB .EQ. 0.)))GOTO 40
C       THIS PORTION EXCERCISED ONLY IF THE SOLUTION IS SYMMETRUC IN
C  X *** ONLY HALF THE STRUCTURE IS THEN ANALYSED
C     NX IS THE NUMBER OF POINTS TO BE TAKEN IN THE X DIRECTION
C    IT IS CHECKED FOR SYMMETRY AND MODIFIED IF APPROPRIATE
C    THEN PASSED ONTO ARRAY, PLOT, AND PRINT
      ANX = FLOAT(NX)/2.
      NX = ANX + .5
      PRINT 45, NX, NPX
45    FORMAT(1H1, 3X,*SOL SYM  NX, NPX *,2(I5,2X))
40      CONTINUE
      CALL ARRAY
      CALL PRINT
      CALL PLOT
      CALL PROF
      STOP
     END


      SUBROUTINE ARRAY
C    FILL IN THE ELEMENTS OF V(J,K) --- CALLS SUB GREEN
      COMMON /DATA/ R,VA,VB,NPX,NPY
      COMMON /VOLT/ V(51,51)
      COMMON /NX/ NX
```

```
      NY = NPY+1
     DO 6 J= 1,51
     DO 6 K = 1,51
6      V(J,K) = 0.0
      DO 10 K = 1,NY
      DO 20 J=1,NX
C   AT THIS POINT, X AND Y ARE DEFINED    CALL GREEN
      CALL GREEN(J,K)
20    CONTINUE
10    CONTINUE
      RETURN
     END


      SUBROUTINE GREEN(J,K)
      COMMON /DATA/ R,VA,VB,NPX,NPY
      COMMON /VOLT/ V(51,51)
      COMMON /P/ P,NP,Y,X
      COMMON /PI/ PI
      REAL NP
      VO(X,Y) = X*(1.-X)
      X = FLOAT(J-1)/FLOAT(NPX)
      Y = 1. - FLOAT(K-1)/FLOAT(NPY)
C   INITIALIZE V TO THE VALUE FOR N=0
      V(J,K) = VO(X,Y)
      PI = 3.141592654
      DO 30 I = 1,50
      NP = FLOAT(I)*PI
      P = NP*R
      ADD = FADD(I)
     V(J,K) = ADD + V(J,K)
     ADV = ABS(ADD)
      ABV = ABS(V(J,K))*(.00010)
      IF (ADV .LT. ABV) GOTO 32
```

```
      IF (ADV .EQ. ABV) GOTO 32
30    CONTINUE
32    CONTINUE
       V(J,K) = V(J,K) + VA + (VB - VA)*X
      IFLAG = 0
      IF (I .EQ. 50) IFLAG = 1
      IF (IFLAG .EQ. 1) GO TO 40
      RETURN
40     PRINT 45, J, K
45     FORMAT (1H1, * CONVERGENCE POOR FOR J,K OF  *,2(I5,5X))
      RETURN
      END


      FUNCTION FADD(I)
      COMMON /P/ P,NP,Y,X
      COMMON /PI/ PI
      REAL NP
      ANG = NP*Y
5     CONTINUE
      IF (ANG .LT. 2.*PI) GOTO 10
      ANG = ANG - 2. * PI
      GO TO 5
10    CONTINUE
      V1 = 2.*(-1.)**I * COS(ANG)/P**2
      XM = 1.-X
      IF (P .GT. 50.) GOTO 100
      V2 = FSINH(P,XM)*(FCOSH(P,X) - 1.)
      V3 = FSINH(P,X) * (1 - FCOSH(P,XM))
      FADD = V1*(V2 - V3)/FSINH(P,1.)
      RETURN
100   CONTINUE
      IF (P*XM .GT. 50) GOTO 200
        PX = P*(X-1.)
```

```
      V2 = FSINH(P,XM) * EXP(PX)
      V3 = EXP(PX) * (1. - FCOSH(P,XM))
      FADD = V1*(V2-V3)
       RETURN
200    CONTINUE
      FADD = V1
      RETURN
      END



      SUBROUTINE PRINT
      COMMON /DATA/ R,VA,VB,NPX,NPY
      COMMON /VOLT/ V(51,51)
      COMMON /NX/ NX
      NY = NPY/7 + 1
      PRINT 1, R, VA, VB
1     FORMAT(1H1,*DOMAIN II*,/1X,*R = *, F7.2,*   VA = *,
     1 F7.2, *   VB = *,F7.2)
      DO 20 K=1,NY
      DO 10 J=1,NX
      LM = (K-1)*7 + 1
      LS = LM + 6
      PRINT 100, J, (V(J,L), L=LM,LS)
100   FORMAT(1HO, I2, 3X, 7(E15.7,3X))
10    CONTINUE
      PRINT 400
20    CONTINUE
400   FORMAT (1H1)
      RETURN
      END
```

```
      FUNCTION FSINH(P,X)
      R = P*X
      ISGN = 0
      IF (R .LT. 0.) ISGN = 1
      R = ABS(R)
      FSINH = .5 * EXP(R)
      IF (R .GT. 20.) GOTO 200
      FSINH = FSINH - .5 * EXP(-R)
200    IF (ISGN .EQ. 1) FSINH = -FSINH
      RETURN
     END


      FUNCTION FCOSH(P,X)
      R = ABS(P*X)
      FCOSH = .5*EXP(R)
      IF (R .GT. 20.) RETURN
      FCOSH = FCOSH + .5 * EXP(-R)
      RETURN
     END


      SUBROUTINE PLOT
      COMMON /DATA/ R,VA,VB,NPX,NPY
      COMMON /VOLT/ V(51,51)
      COMMON /NX/ NX
      COMMON /VMAX/ VMAX
      DIMENSION F(60)
      INTEGER F
      PRINT 1, R, VA, VB
1     FORMAT(1H1,*DOMAIN II*,/1X,*R = *, F7.2,*   VA = *,
     1 F7.2, *   VB = *,F7.2)
```

```
      V MAX = 0.0
      DO 2 J=1,51
      IF (V(J,1) .LT. VMAX) GOTO 2
      XJ = J-1
      XMAX = XJ/FLOAT(NPX)
      VMAX = V(J,1)
      PRINT 500,  J
500   FORMAT(1H , * J =  *, I3)
2     CONTINUE
      PRINT 100, XMAX, VMAX
100  FORMAT(1H ,* XMAX = *, F7.3,*   VMAX = *,E12.5,///)
      DO 20 J=1,60
20    F(J) = (1. - FLOAT(J-1)/NPY)*1000
      J = 0
      PRINT 30, J, (F(J),J=1,20)
30    FORMAT(1H0, I4,1X,20(I4,2X),/)
      NY = NPY/20 + 1
      DO 40 K = 1,NY
      DO 50 J = 1,NX
      JX = (FLOAT(J-1)/NPX)*1000
      DO 60 L = 1,20
      LL = (K-1)*20 +L
      F(L) = ABS(V(J,LL)/VMAX)*1000.
60      CONTINUE
      PRINT 30, JX, (F(I),I=1,20)
50      CONTINUE
      PRINT 1000
1000   FORMAT(1H1)
      LM = K*20 + 1
      LS = LM + 19
      IF (K .EQ. NY) GO TO 250
      PRINT 30,K,(F(I),I=LM,LS)
250   CONTINUE
40      CONTINUE
```

```
      RETURN
     END

      SUBROUTINE PROF
C      TO CALCULATE VOLT PROFILE
C     V(X,YO) = V/(X,YO) - IK(X-.5)
      COMMON /DATA/ R , VA, VB, NPX, NPY
      COMMON /VOLT/ V(51,51)
      COMMON /VMAX/ VMAX
      COMMON /NX/ NX
      DIMENSION FL(9)
      DIMENSION F(101)
C    Y = 1-(JY - 1)/NPY  X = JX-1)/NPX
      PRINT 101
101    FORMAT(1H1)
      KY = 1
      JCK1 = FLOAT(NX)/2. + .5
      JCK2 = FLOAT(NX)/2.
      KEVE = 0
      IF (JCK1 .GT. JCK2) KEVE = 1
      KXM = 2*NX - KEVE
      DO 1 KX = 1,NX
      F(KX) = V(KX,KY)/VMAX
      KXMM = KXM - (KX-1)
      F(KXMM) = V(KX,KY)/VMAX
1      CONTINUE
     NXX = NPX + 1
     DO 2 JX = 1,NXX
      X =(FLOAT(JX) - 1.)/FLOAT(NPX)
      DO 3 K = 1,9
      FK = FLOAT(K-1)*.25
      FL(K) = F(JX) - 2.*FK*(X-.5)
3      CONTINUE
```

```
      PRINT 50, JX, (FL(K), K=1,9)
50      FORMAT(1H0, I3, 3X, 9(E10.4,3X))
2      CONTINUE
      RETURN
     END
```

LIST OF REFERENCES

Ali, M. T. "Three-Dimensional Analysis of Electrothermal Integrated Circuits," Ph.D. Dissertation, Electrical Engineering Department, The University of Arizona, Tucson, Arizona, 1975.

Arfken, G. Mathematical Methods for Physicists, 2nd Ed., Academic Press, Inc., London, 1970.

Friedman, B. Principles and Techniques of Applied Mathematics, John Wiley and Sons, Inc., New York, 1956.

Gray, P. R. "Computer Simulation of Integrated Circuits in the Presence of Electrothermal Interactions," IEEE Journal of Solid State Circuits, VSC-11, No. 6, Dec. 1976.

Grove, A. S. Physics and Technology of Semiconductor Devices, John Wiley and Sons, Inc., New York, 1967.

Gilbert, B. "Monolithic Analog READ-ONLY Memory for Character Generation," IEEE Journal of Solid State Circuits, Vol. SC-6, No. 1, February 1971.

________. "Translinear Circuits: A Proposed Classification," Electronic Letters, Vol. 11, No. 1, January 9, 1975a.

________. "A New Technique for Analog Multiplication," IEEE Journal of Solid State Circuits, Vol. SC-10, No. 6, December 1975b.

Hamilton, D. J., F. A. Lindholm, and A. H. Marshak. Principles and Applications of Semiconductor Device Modeling, Holt, Rinehart and Winston, Inc., New York, 1971.

Harrington, R. F. Field Computation by Moment Methods, The MacMillan Company, New York, 1968.

Hauser, J. R. "The Effects of Distributed Base Potential on Emitter-Current Injection Density and Effective Base Resistance for Stripe Transistor Geometries," IEEE Trans. on Electron Devices, Vol. ED-11, May 1964.

Lindholm, F. A., and D. J. Hamilton. "A Systematic Modeling Theory for Solid State Devices," Solid State Electronics, 7, No. 11, November 1964.

Louw, W. J. "The Design of Linear Electrothermal Integrated Circuits," Ph.D. Dissertation, Electrical Engineering Department, The University of Arizona, 1975.

Macneal, R. H. "An Asymmetrical Finite Difference Network," Quarterly of Applied Mathematics, October 1953.

Seidel, D. B. "Aperture Excitation of a Wire in a Cavity," Ph.D. Dissertation, Electrical Engineering Department, The University of Arizona, 1977.

Smith, J. "Carrier Domain Electronics: A Spatially Distributed Approach to Functional Integrated Circuits," Ph.D. Dissertation, University of Florida, 1974.

________. "A Second-Generation Carrier Domain Four-Quadrant Multiplier," IEEE Journal of Solid State Circuits, Vol. SC-10, No. 6, December 1975.

Sze, S. M. Physics of Semiconductor Devices, Wiley Interscience, New York, 1969.